DTIC
S ELECTE
JAN 0 6 1993
E
D

OPEN AND FILLED HOLE STATIC TENSILE
STRENGTH CHARACTERIZATION OF
METAL MATRIX COMPOSITE SCS-9/ß21s

THESIS

Jacob T. Roush
Palace Acquire Intern, DOD

AFIT/GAE/ENY/92D-12

93-00121

93   1 04 007

OPEN AND FILLED HOLE STATIC TENSILE STRENGTH
CHARACTERIZATION OF METAL MATRIX COMPOSITE
SCS-9/β21s

THESIS

Presented to the Faculty of the School of Engineering

of the Air Force Institute of Technology

Air University

In Partial Fulfillment of the

Requirements for the Degree of

Master of Science in Aeronautical Engineering

Jacob T. Roush

Palace Acquire Intern, DOD

December 1992

DTIC QUALITY INSPECTED 5

Approved for public release; distribution unlimited

Preface

The purpose of this study was to characterize the tensile behavior of a metal matrix composite with open and filled holes. To accomplish this, unnotched tensile behavior also had to be investigated. The research was performed at three temperature regimes: room temperature, 482° Celsius, and 650° Celsius.

Metal matrix composites are strong candidates for elevated temperature applications where high strength and low density are necessary. The metal matrix under investigation is SCS-9/β21s. SCS-9 is a silicon carbide fiber and β21s is a Titanium based alloy. Both cross-ply and quasi-isotropic laminates with a specimen width to hole diameter ratio of six were analyzed.

In performing the experimentation and writing this thesis, I have had a great deal of advice and support from others. To personally thank each individual who offered suggestions and counselling would not be possible. In particular, I would like to thank Dr. S. Mall whose guidance throughout this undertaking has been immensely appreciated and my sponsor Lt. Col. James Hansen of the Materials Laboratory for supplying material and advice from the onset of this task. I would also like to formally acknowledge the assistance of Mark Derriso and Capt. Brian Sanders. And finally to my family who set standards for morality and ethics that extend beyond the family unit.   Jacob T. Roush

ii

Table of Contents

iv

List of Figures

vii

List of Tables

Abstract

Success of systems such as the Advanced Tactical Fighter (ATF) and the Integrated High Performance Turbine Engine Technologies program (IHPTET) are dependent on continued research into the material characterization of metal matrix composites. SCS-9/ß21s has a reduced gauge thickness, in comparison with other potential metal matrix composites, due to a smaller diameter fiber. This reduced gauge thickness makes it an attractive candidate for the skin of hypersonic vehicles.

Static tensile testing of cross-ply and quasi-isotropic metal matrix composite SCS-9/ß21s displays pronounced notch sensitivity at room temperature. While the material is mildly notch sensitive at $482^{\circ}C$, it becomes completely insensitive to the effect of a hole at $650^{\circ}C$. The ultimate unnotched strength of the $[0/90]_{2s}$ laminate is 906 MPa at room temperature and decreases by 25% and 55% at elevated temperatures of $482^{\circ}C$ and $650^{\circ}C$, respectively. The ultimate unnotched strength of the $[0/\pm45/90]_s$ laminate is 777 Mpa at room temperature and exhibited the same magnitude of reductions in strength at elevated temperature as in the cross-ply configuration. A characteristic bi-linear stress strain curve, in both notched and unnotched tensile testing, results from the release of residual stresses and break down of the fiber-matrix interface, not from micro-plasticity.

Analytical work was completed to predict material

properties, elastic and plastic stress concentration factors, stresses around the periphery of the notch, failure loads, and residual stresses. Damage progression was documented in the form of fiber-matrix debonding, fiber failure, matrix cracking, and plasticity. Acetate edge replication, in conjunction with optical and scanning electron microscopy, proved to be a powerful tool in defining the stages of damage progression.

OPEN AND FILLED HOLE STATIC TENSILE STRENGTH

CHARACTERIZATION OF METAL MATRIX COMPOSITE

SCS-9/ß21S

INTRODUCTION

Materials have been combined to produce composites for thousands of years. Mud bricks, reinforced with straw, and laminated woods were used as building blocks for hundreds of years B.C. Early history reported that the Mongols made bows from cattle tendons, wood, and silk bonded together with adhesives (1:1-2). A composite is defined as a combination of two or more constituent elements to form a bonded quasi-homogeneous structure that produces synergistic mechanical and physical property advantages over that of the base elements (2:395-403). A recent addition in the field of composites are the continuous fiber reinforced metal matrix composites, which have evoked great interest among engineers concerned with structural applications. They are particularly desirable to the aerospace industry due to their high stiffness and strength to density ratios.

Success of current programs such as the Advanced Tactical Fighter (ATF) and the Integrated High Performance Turbine Engine Technologies program (IHPTET) are dependent on continued research into the material characteristics of continuous fiber metal matrix composites.

Although composite types are sometimes difficult to distinguish, they can generally be placed into one of three

categories: particulate based, whisker/flake filler, or continuous fiber system (2:395-396). Each of the aforementioned types have advantages and disadvantages depending upon the specific application. It is advantageous to briefly introduce the three forms of composites and examine some of the physical and material characteristics typically inherent to that type.

Particulate composites are distinguished from filamentary types by the fact that the fillers have no primary dimension, all dimensions of the fillers are approximately the same size. The particle size can range from several microns to several hundred microns and the volume fraction of fillers is larger than 25 percent. Due to the random dispersion of particles, the composite generally behaves isotropic in nature.

Whisker/flake composites are the second common form of composite. The fillers generally have a large length to width or length to diameter ratio. Elementary studies in fracture mechanics, performed by Griffith, (3:163-197) show that as a fiber diameter decreases the size and number of surface flaws also decrease. As the thickness of the fiber approaches zero the strength grows exponentially to the modulus divided by ten. Whisker/flake composites implement small diameter constituents attempting to approach crystalline perfection in the fillers. Both particulate and whisker composites are advantageous where complex geometries make continuous fiber reinforced composites an unacceptable alternative.

Continuous fiber reinforced composites usually introduce fibers with high strength and stiffness into a softer matrix material. The orientation of these fibers dictate directionality of the mechanical properties; the composite can be tailored to meet the requirements of a specific application. They are also attractive for elevated temperature applications since many fibers: silicon carbide, boron, graphite, etc. maintain a large amount of their strength and stiffness with increased temperature.

The composite under investigation in this research is a continuous fiber reinforced metal matrix composite. The composite, SCS-9/ß21s, is manufactured by Textron Specialty Materials. Figure 1 contains a photograph of the cross section of a SCS-9 fiber surrounded by matrix material. ß21s is the designation given to the ß phased titanium matrix with constituents, by weight percent, Ti-15Mo-2.6Nb-3Al-0.2Si (4). The fiber and foils of matrix material were consolidated via a hot isostatic press (HIP) procedure.

The coefficients of thermal expansion (CTE) of the matrix and the fiber are usually significantly different in metal matrix composites. During the manufacturing process, elevated temperatures are introduced which cause the matrix to behave as a visco-plastic material. This is necessary to insure the matrix material will flow properly and consolidation of the composite will be complete. It is standard practice when attempting to quantify the residual stresses to choose a
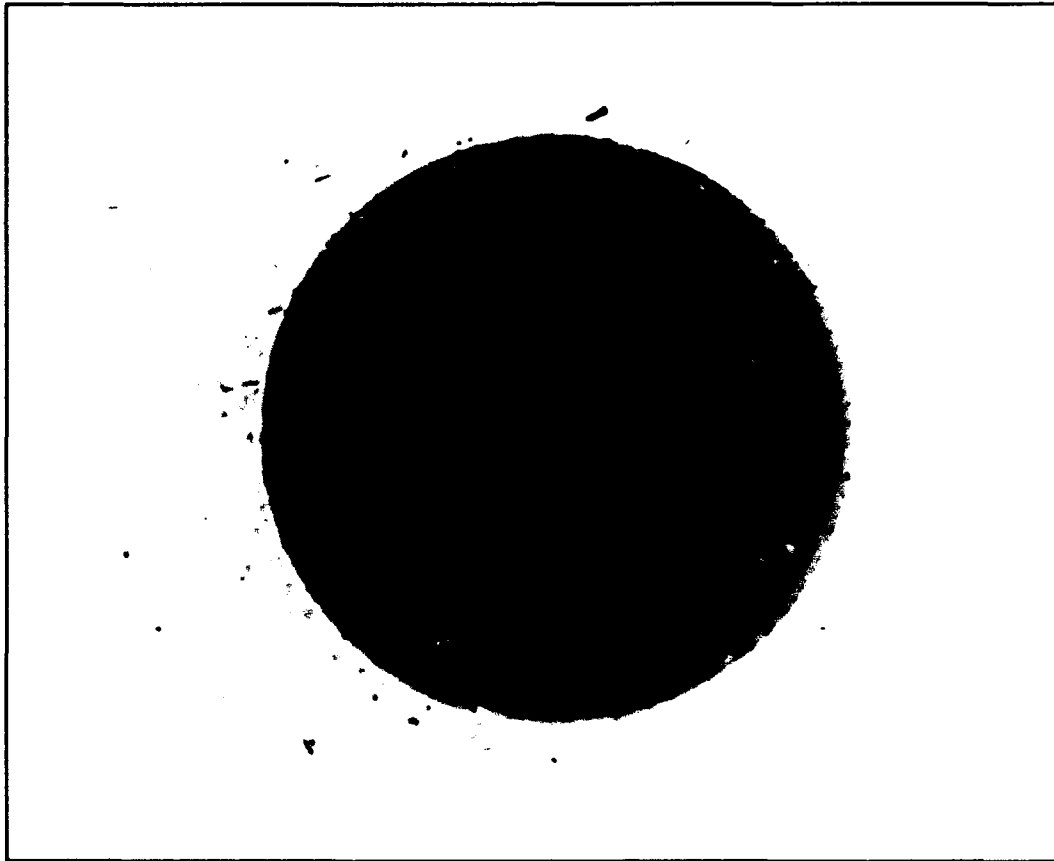
Figure 1 SCS-9 Silicon Carbide Fiber

temperature, depending on the matrix material, where the residual stresses will be negligible. A manufacturing cool down from this temperature is then implemented in conjunction with a micro-mechanical analysis to predict the residual stresses in the composite due to the difference in CTEs of the matrix and the fiber. Typically large compressive and radial stresses build up at the interface between the matrix and the fiber; the axial and circumferential stresses in the matrix are both tensile in nature (5).

4

The existence of off-axis plies, plies with fibers not oriented in the load direction, in continuous fiber reinforced metal matrix composites generally attribute to a characteristic bi-linear stress-strain curve, displayed in Figure 2. Usually there exists an initial linear portion, a secondary linear portion, a knee separating the two linear regions, and possible a nonlinear region. The strength of the interface between the fibers and matrix has been shown by others to be weak, and it is believed that this interface fails and is manifested as a knee in the stress-strain curve. Realize that it is not generally useful to simply make the interface as strong as possible or as weak as possible. The interface, like the total composite, should be carefully designed for the ultimate application of the composite. The interfacial failures of off-axis plies may be beneficial in serving as a type of mechanical fuse, recognizable by nondestructive evaluation, to prevent catastrophic failure (6:271-279). Inelastic deformation, usually attributed to the matrix material, combined with damage gives rise to the final macroscopic nonlinear response evident in the stress-strain curve (7).

Metal matrix composites reinforced with continuous fibers exhibit numerous modes of damage. Damage in MMCs consist primarily of fiber breakage, matrix cracking, matrix plastic deformation, delamination, and fiber-matrix debonding. The sequence and combinations of the failure mechanisms depend on
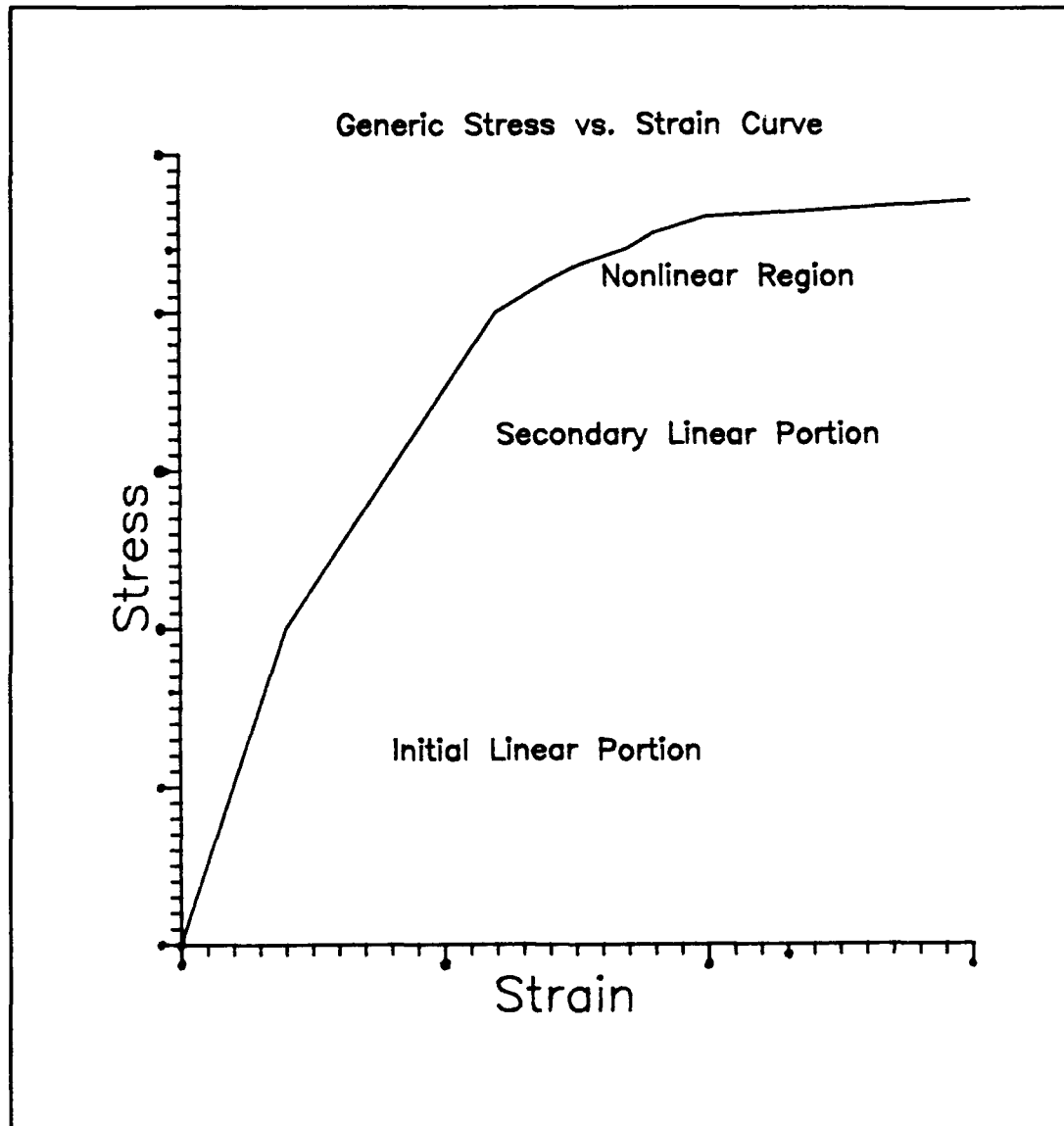
Figure 2 Characteristic Bi-linear Stress-Strain Curve

many variables including constituent properties, fabrication process, loading conditions, specimen geometries, and heat treatments (8:1-29). Due to the complexity (introduced by combining constituent elements to form a composite) of the material behaviors and failure progressions, experimental

6

investigation is almost always necessary to fully characterize a metal matrix composite.

This study is concerned with the tensile characterization of MMC SCS-9/ß21s. A similar MMC, namely SCS-6/ß21s, has been characterized quite extensively. SCS-9 is unique in that its fiber diameter is 45 percent smaller then the SCS-6 fiber. Introducing this smaller diameter fiber yields a reduced thickness of the quasi-isotropic laminate, $[0/\pm45/90]_s$, by 42 percent in comparison with SCS-6/ß21s. The development of this smaller diameter fiber was necessary in order to achieve minimum gauge laminates for hypersonic vehicle fuselage structures. Unnotched testing on SCS-9/ß21s has been completed by others on unidirectional, $[0/90]_{2s}$, and $[0/\pm45/90]_s$ laminates. The focus of this study is the characterization of $[0/90]_{2s}$ and $[0/\pm45/90]_s$ SCS-9/ß21s laminates with open and filled holes. There has been no work completed by the engineering community to characterize notched SCS-9/ß21s laminates. The width-to-diameter of the notch in all specimens will be six, and both Mar-m-246 and 7075-T6 materials will be implemented for the pins. Determination of the notch sensitivity of the laminates will be addressed. Analytical work will be completed to predict material properties, elastic and plastic stress concentration factors, failure loads, and residual stresses. Damage progression will be documented in the form of fiber-matrix debonding, fiber failure, matrix cracking, delamination, and plasticity.

Theory/Background/Literature Review

Theoretical work is often necessary while attempting to experimentally characterize any material. Characterizing metal matrix composite SCS-9/ß21s with open and filled holes is no exception. Attempting to predict experimentally observed material response also provides a valuable check on the validity of a particular theory for a specific material. This section will address standard composite laminate nomenclature, Classical Laminate Plate Theory, and the difference between micromechanical and macromechanical theory. Background on the computer program METCAN and a literature review is also included.

Definitions and Nomenclature

A laminae is defined as a single arrangement of unidirectional fibers surrounded by matrix material which typically supports the fibers, provides a means for load distribution, and usually increases the strength. The term laminae and ply are used interchangeably. Three principal material directions exists within a laminae: 1 is along the fiber direction, 2 is transverse to the fiber direction, and 3 is through the thickness. Figure 3 displays the principal material directions within a laminae. Load would be applied in the X direction for a standard uniaxial tension test. An angle theta is taken as positive from the X axis to the 1 axis. A laminate is any number of laminae stacked and consolidated together with the orientation of the principal

8
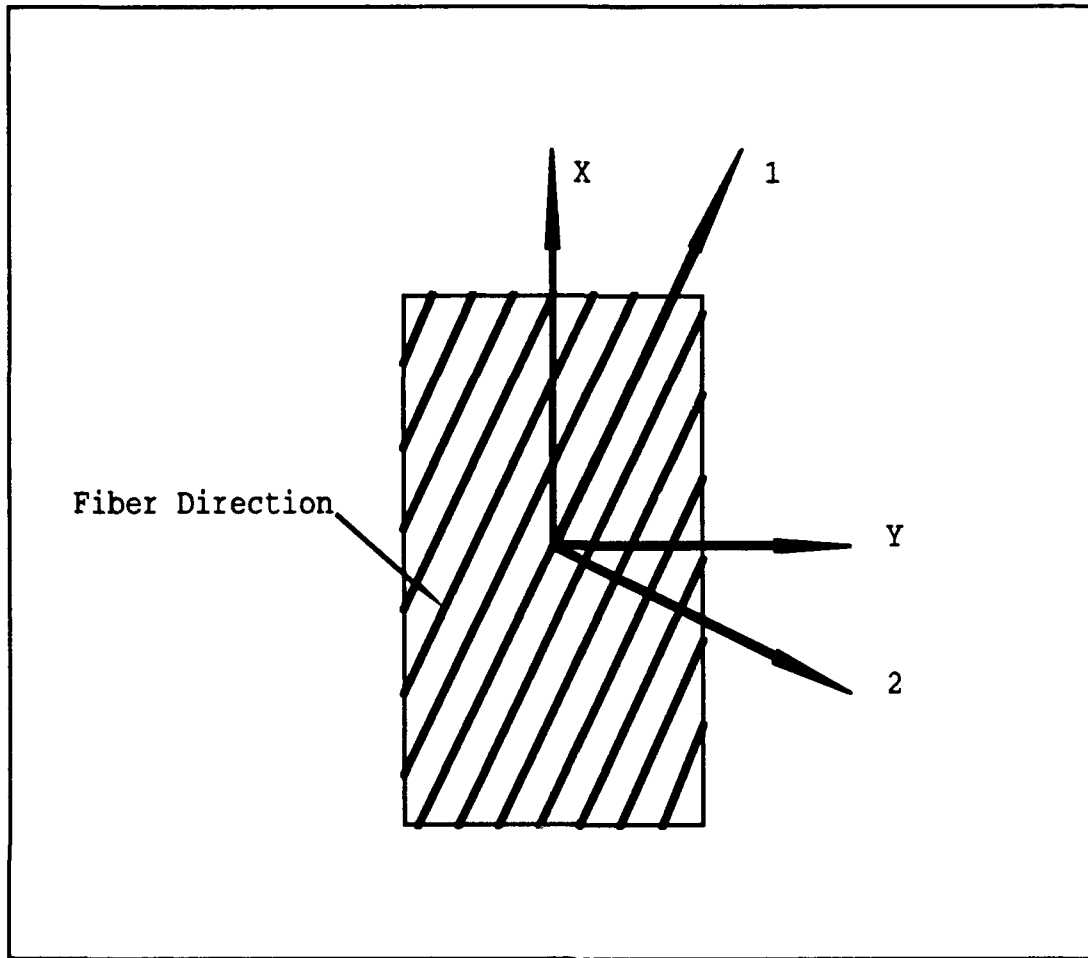
Figure 3 Principal Material Directions Within a Laminae

material directions of the individual laminae dependent upon the specific design application.

Standard nomenclature for defining a laminate with equal thickness plies consists of specifying the orientation of the 1st principal material direction within a ply with respect to a reference direction, which is typically an anticipated unidirectional load direction. The two laminates under investigation in this study are $[0/90]_{2s}$ and $[0/\pm45/90]_s$,

```
Cross-ply                    Quasi-isotropic

  0 Ply                          0 Ply

 90 Ply                         +45 Ply

  0 Ply                         -45 Ply

 90 Ply       Symmetry at        90 Ply

 90 Ply       Midplane           90 Ply

  0 Ply                         -45 Ply

 90 Ply       Thickness / 2     +45 Ply

  0 Ply                          0 Ply
```

Figure 4 Cross-sectional View of $[0/90]_{2s}$ and $[0/\pm 45/90]_s$ Laminates

where the subscript s stands for symmetrical about the midplane and subscript 2s stands for 2 times symmetrical about the midplane. Figure 4 displays a cross-sectional, through the thickness, view of these laminates. Laminate $[0/90]_{2s}$ is also referred to as a cross-ply laminate in literature for obvious reasons. Laminate $[0/\pm 45/90]_s$ is referred to as a quasi-isotropic laminate. This laminate can be stressed along any of the fiber orientations and exhibit the same material response. Stressed at an angle other than 0, 45, or 90

10

degrees it behaves only slightly different than the response in a principal material direction. The composite behaves in a quasi-isotropic fashion.

Classical Laminate Plate Theory

Classical Laminate Plate Theory (CLPT) enables prediction of laminate response to applied forces and moments. The basic building block for CLPT is the laminae. The strain-stress relations for the principal material coordinates of a laminae is given by the system of Equations 1. [S] is defined as the

$$
\begin{bmatrix} e_1 \\ e_2 \\ \gamma_{12} \end{bmatrix} = \begin{bmatrix} S_{11} & S_{12} & 0 \\ S_{12} & S_{22} & 0 \\ 0 & 0 & S_{66} \end{bmatrix} \begin{bmatrix} \sigma_1 \\ \sigma_2 \\ \tau_{12} \end{bmatrix}
\tag{1}
$$

compliance matrix, and the terms S_{ij} are easily obtained from engineering constants E_1, E_1, G_{12}, and ν_{12} (9:47-53). Equation 1 is invertible providing a stress-strain relationship of the form shown in Equation 2, where again Q_{ij}, the stiffness

$$
\begin{bmatrix} \sigma_1 \\ \sigma_2 \\ \gamma_{12} \end{bmatrix} = \begin{bmatrix} Q_{11} & Q_{12} & 0 \\ Q_{12} & Q_{22} & 0 \\ 0 & 0 & Q_{66} \end{bmatrix} \begin{bmatrix} e_1 \\ e_2 \\ \gamma_{12} \end{bmatrix}
\tag{2}
$$

matrix, is obtained via engineering constants. Transformation of these equations for any orientation of the principal material directions can be performed via application of a transformation matrix. These transformed equations can be

11

thought of as the stress-strain relations for any particular laminae of a laminate.

An assumption of perfectly bonded laminae, no delamination, infinitesimally thin bonds, continuous displacements across the laminae boundaries, and thin laminates is inherent to CLPT. Kirchhoff hypothesis for plates incorporates a number of other assumptions necessary in the formulation of this theory. This is explained in detail by Jones (9:147-157). The resultant governing system of equations of CLPT are of the form shown in Equation 3.

$$
\begin{bmatrix} N_x \\ N_y \\ N_{xy} \\ M_x \\ M_y \\ M_{xy} \end{bmatrix} = \begin{bmatrix} A_{11} & A_{12} & A_{16} & B_{11} & B_{12} & B_{16} \\ A_{12} & A_{22} & A_{26} & B_{12} & B_{22} & B_{26} \\ A_{16} & A_{26} & A_{66} & B_{16} & B_{26} & B_{66} \\ B_{11} & B_{12} & B_{16} & D_{11} & D_{12} & D_{16} \\ B_{12} & B_{22} & B_{26} & D_{12} & D_{22} & D_{26} \\ B_{16} & B_{26} & B_{66} & D_{16} & D_{26} & D_{66} \end{bmatrix} \begin{bmatrix} e_x^0 \\ e_y^0 \\ e_{xy}^0 \\ k_x \\ k_y \\ k_{xy} \end{bmatrix}
\tag{3}
$$

A_{ij} is called the extensional stiffness matrix because it relates N_i, axial force per unit width, to the middle surface strains ϵ_i^0. B_{ij} is termed the coupling stiffness matrix because its presence implies coupling between extension and bending. D_{ij} is called the bending stiffness matrix. All the terms for the above matrices are obtainable from knowing the engineering constants, orientation of the individual plies, and geometry of the laminate. All laminates which are symmetrical in orientation and geometry possess a B_{ij} matrix

equal to zero, meaning that there is no coupling between bending and extension. This decouples Equation 3 into two separate equations, one which governs the response of the laminate to applied moments and the second which governs the response of the laminate to applied axial loads. For a symmetrical laminate under axial loading there exists no bending and the strain vector through the thickness of the laminate is equivalent to the midplane strain vector. The governing equations for static tensile testing of symmetric laminates $[0/90]_{2s}$ and $[0/\pm45/90]_s$ simplifies to Equation 4.

$$
\begin{bmatrix} N_x \\ N_y \\ N_{xy} \end{bmatrix} = \begin{bmatrix} A_{11} & A_{12} & A_{16} \\ A_{12} & A_{22} & A_{26} \\ A_{16} & A_{26} & A_{66} \end{bmatrix} \begin{bmatrix} \epsilon_x \\ \epsilon_y \\ \gamma_{xy} \end{bmatrix}
\tag{4}
$$

From this equation, laminate stiffness's in the load direction and transverse to the load direction, E_x and E_y, can be predicted. Analytical values for Poisson's ratio, ν_{xy}, and the shear modulus, G_{xy}, can also be obtained. Figure 5 represents the positive in-plane forces on a flat laminate. Moments are not included on this diagram because the concern of this investigation was the evaluation of a continuous fiber reinforced composite subjected to static tensile loads.

Classical Laminate Plate Theory, described in the preceding paragraphs, can also be employed in conjunction with laminae failure criteria such as: Maximum Stress Theory, Maximum Strain Theory, Tsai-Hill Theory, and Tsai-Wu Tensor
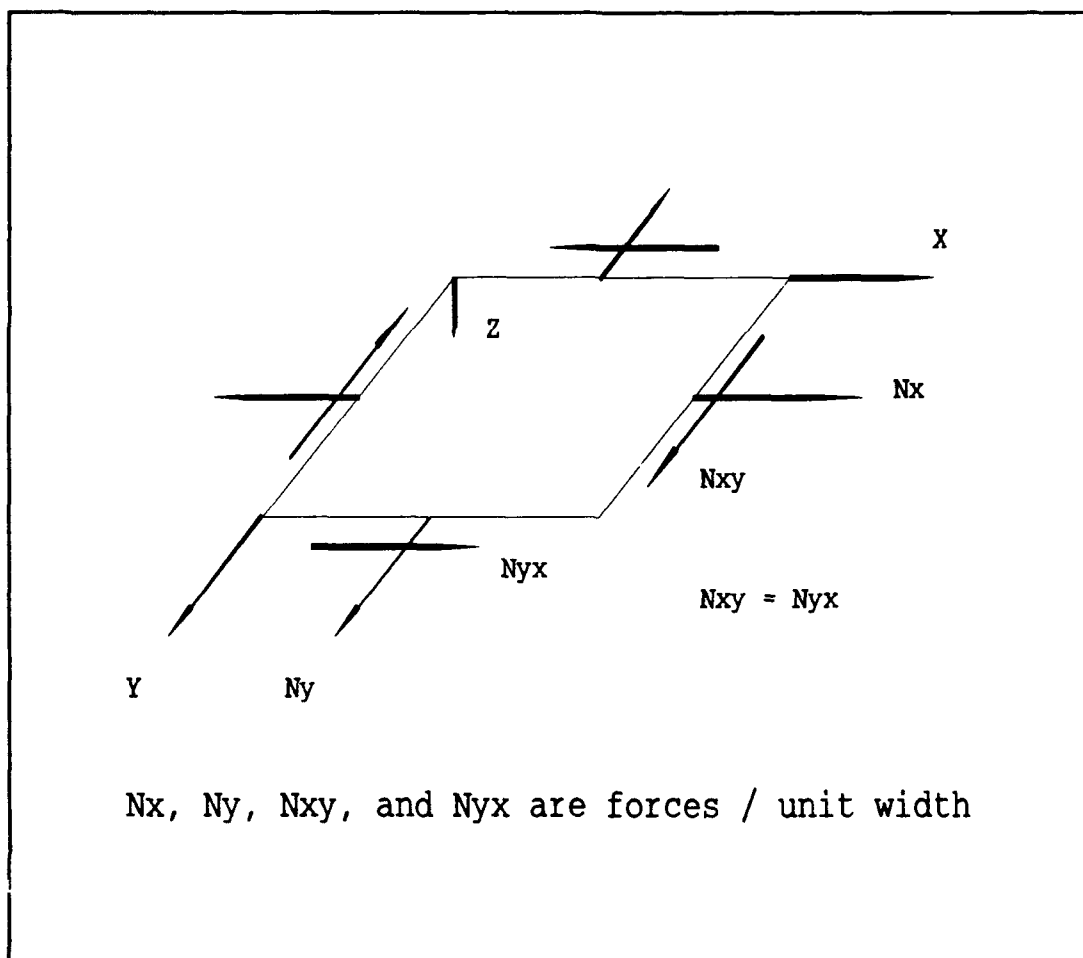
Figure 5 In Plane Forces on a Flat Laminate

Theory to predict the failure strengths of unnotched laminates. Limited and total discount methods can be implemented in an attempt to match experimental findings with analytical predictions. This will be discussed in further detail in Chapter 4, the Results and Discussion Chapter, as they are implemented.

Micromechanical vs. Macromechanical Analysis

Classical Laminate Plate Theory, described in the previous

section, is a macromechanical analysis. The constituent elements, namely the fiber, the matrix, and the interface, are treated as a conglomerated unit, the laminae. CLPT assumes that the engineering constants of the laminae are known values. Micromechanical analysis differs from macromechanical analysis in that the interaction between the constituent elements is examined in an attempt to predict material properties in terms of these constituent elements.

There are two basic approaches to micromechanics of composite materials. The first is a mechanics-of-materials approach or strength-of-materials approach. This approach typically implements equilibrium, compatibility, and constitutive laws to define the mechanical system. The second is the elasticity approach, which is at least three approaches: boundary principles, exact solutions, and approximate solutions (9:85-86).

Extensive work is being done by the engineering community to model composite materials on the micromechanical level. It is beyond the domain of this research to document existing micromechanical models since the focus of this research is primarily on the macromechanical approach. Rather, the micromechanical theory and equations used in this research will be discussed in the Results and Discussion Chapter as they are implemented, namely Rule of Mixtures and Halpin-Tsai equations.

METCAN

Metal Matrix Composite Analyzer (METCAN) is a Fortran program that was developed at the NASA Lewis Research Center to perform nonlinear analysis of fiber reinforced metal matrix composites. METCAN implements micromechanical equations, described in (10), which are derived based on a mechanics-of-materials formulation assuming a square array unit cell model of a single fiber surrounded by matrix and an interface, shown in Figure 6. "Application is made of the principles of displacement compatibility and force equilibrium as defined in elementary mechanics-of-materials theory and Fourier's law for heat conduction from thermodynamics" (10:4). Additional assumptions are that fibers are continuous and parallel, properties of all fibers are identical, complete bonding exists between constituents, and the constituents are isotropic or transversely isotropic. METCAN's model incorporates three subregions (A, B, and C), displayed in Figure 6, to characterize the through-the-thickness nonuniformity of the constituent micro-stresses. Although METCAN utilizes a unidirectional micromechanical model, it can be implemented to analyze a composite laminate with any stacking sequence. METCAN is a powerful tool for defining the residual micro-stresses accumulated in the composite during the processing cool down. Figure 7 displays typical METCAN micro-stresses for the unit cell model.

METCAN utilizes a resident databank for the constituent (fiber, matrix, and interface) properties which can be
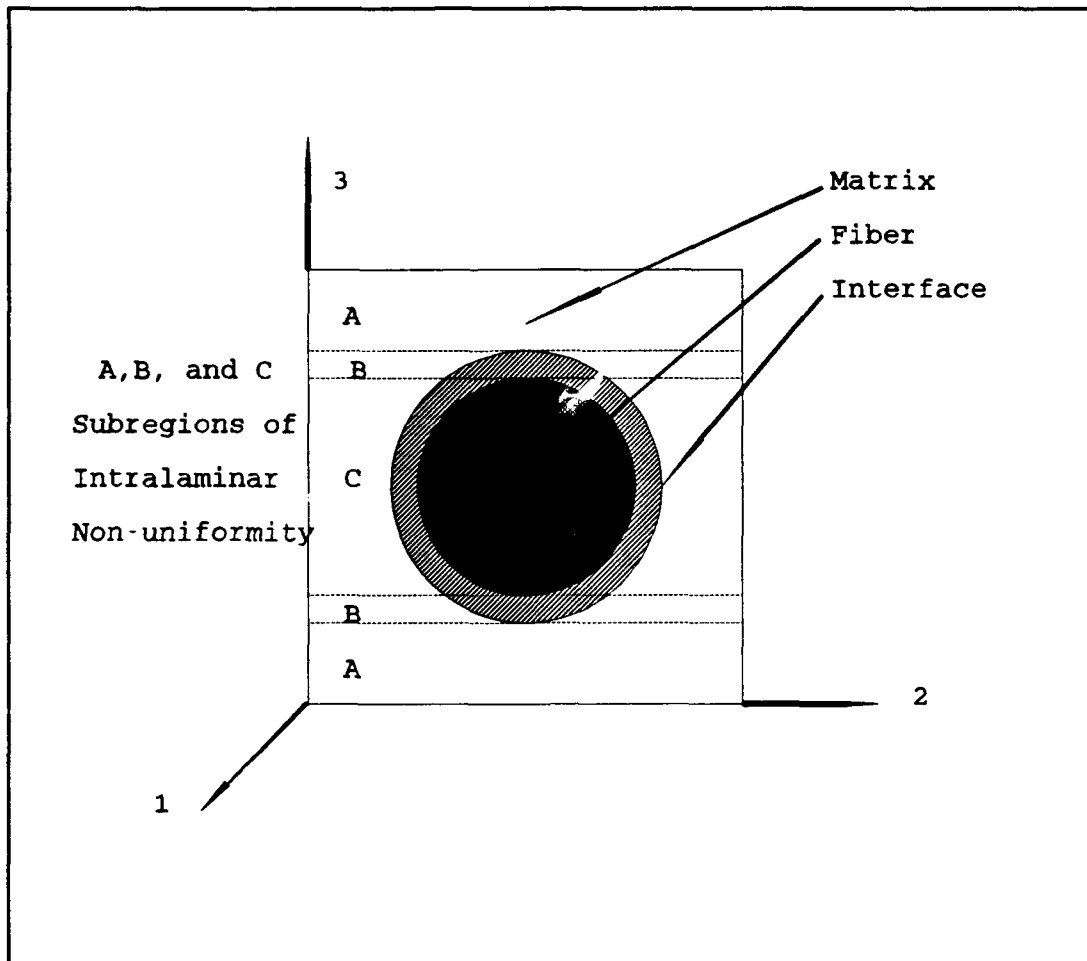
Figure 6 METCAN Square Unit Cell Model

tailored for any particular composite, relieving the user of repetitive inputing. Through an input file, the user specifies the fiber, matrix, and interface materials via the assigned code from the resident databank. The user also specifies geometry, ply orientation, load profiles, temperature profiles, and desired output format. A users guide is available to potential users (11).
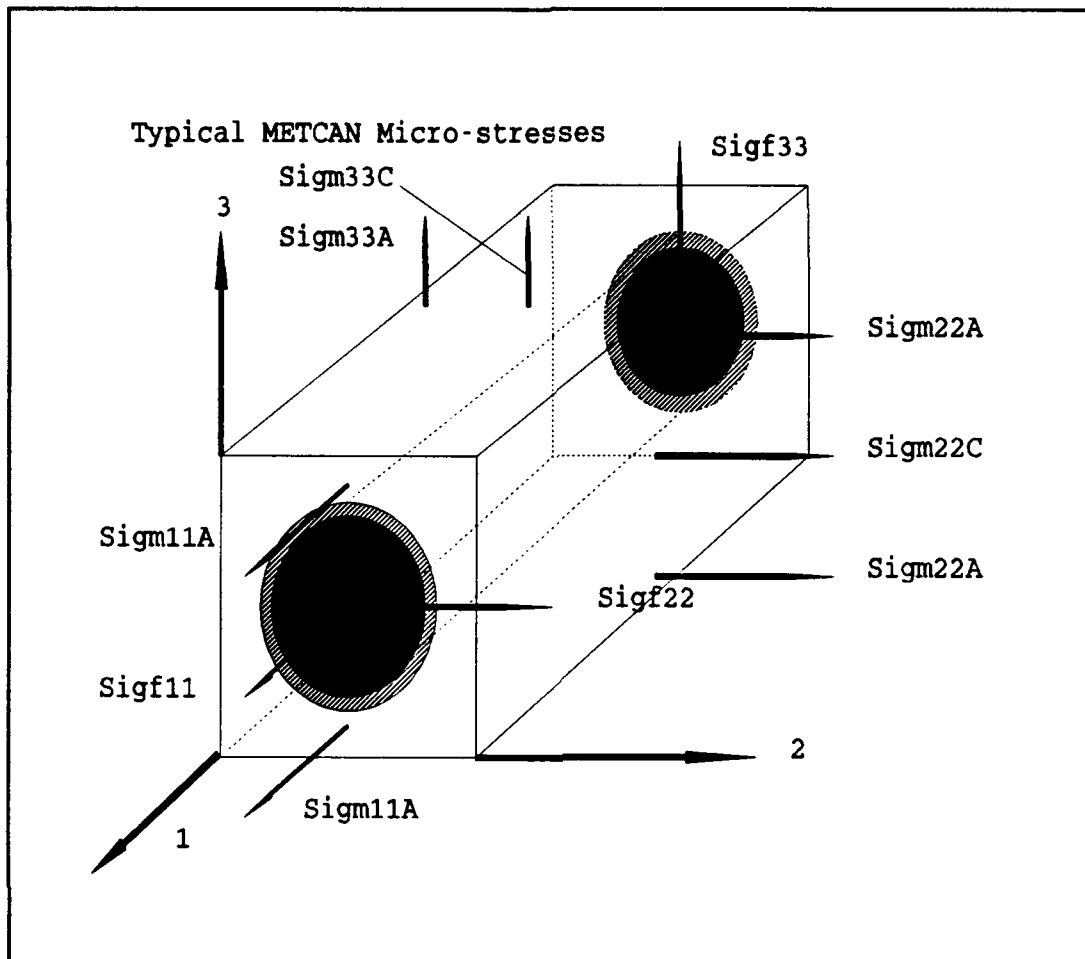
Figure 7 Typical METCAN Micro-stresses

Literature Review

This section addresses research completed by others which provides valuable information pertinent for the completeness of this study. Much of the literature addresses the response of metal matrix composites SCS-6/ß21s and SCS-6/Ti-15-3, similar composites with larger fibers, to various static and fatigue loads. This literature, although not specific to SCS-

9/β21s, is definitely applicable as general knowledge since the composites are similar. Very little work has been completed on the SCS-9/β21s composite system due to its recent introduction into the engineering community.

Gayda and Gabb (12) examined the effect of heating method and specimen design on the response of metal matrix composites to isothermal fatigue testing. The composite used was an eight ply unidirectional SiC/Ti-15-3 composite. They concluded that there is little, if any, significant change in the isothermal fatigue life between inductive and radiantly heated specimens. Providing a uniform temperature field exists in the specimen gauge area, this result can be extended to elevated temperature static tensile tests and allow for comparison between data obtained implementing both heating methods.

Pindera (13) outlined the elements of experimental and analytical methods for accurate shear characterization of unidirectional composites with attention to metal matrix composites. It was found that acceptable shear characterization methods are the 10 degree off-axis tension test, the $[\pm45]_s$ laminate test and the Iosipescu test. Of these, the first two are definitely most applicable since they do not require additional apparatus beyond that of a standard tensile test.

Saltsman and Lerch (14) tested SCS-6/Ti-15-3 unnotched composite specimens under static tensile loads at room

temperature and 427°C. The matrix material, Ti-15-3, is similar to β21s except it has lower oxidation resistance, about 30 percent lower stiffness, and about 25 percent lower ultimate strength. $[0]_8$, $[0/90]_{2s}$, $[\pm30]_{2s}$, $[\pm45]_{2s}$, $[90]_8$, and $[\pm60]_{2s}$ laminates were investigated. The strengths of the laminates are listed in decreasing order above. They found that the degree of non-linear behavior increased as the strength decreased. The nonlinear behavior of the $[0]_8$ laminate could be analytically predicted through matrix plasticity. No constituent cracking could be observed prior to failure for this laminate. Fiber/matrix debonding was evident in all laminates containing off-axis plies. All laminates with off-axis plies contained a second linear portion in the stress-strain curves; the secondary stiffness modulus was always significantly less then the initial modulus.

Newaz and Majumdar (5,15) investigated $[0]_8$ and $[90]_8$ SCS-6/Ti-15-3 laminates subject to tensile loading. A number of composite specimens were subject to a loading-unloading profile in an attempt to document failure progression. They found that the inelastic deformation of the 0 degree laminate is primarily due to plasticity and the inelastic deformation of the 90 degree laminate is due to both damage and plasticity. They found that the location of fiber fracture in the 0 degree laminate was highly influenced by the molybdenum ribbon which is used to hold the fibers in place during the

consolidation process. Formation of extense shear bands along the fibers in the 90 degree laminate is hypothesized to be the reason for a significantly lower strain to failure of this laminates in comparison to the strain to failure of the matrix material.

Johnson (16) provides background on present experimental procedures and techniques for detecting damage in metal matrix composites. Useful parameters for defining failure progression are defined and evaluated. Johnson also predicted the residual stresses in a unidirectional SCS-6/Ti-15-3 laminate. He assumed that any stresses that would develop during the manufacturing process at temperatures greater than one half the melting point of the matrix would be relieved due to creep. Using the predicted residual stresses he was able to show that an applied tensile load of approximately 135 Mpa would be necessary to overcome the residual stresses in a 90 degree ply. This stress level correlated very well with a knee evident in the stress-strain curve for this laminate.

Johnson and Pollock (17) characterized unnotched SCS-6/Ti-15-3 under strain controlled testing. A neat panel of Ti-15-3 was investigated along with $[0]_8$, $[0/90]_{2s}$, $[0_2/\pm45]_s$, and $[0/\pm45/90]_s$ laminates at room temperature and 650°C. At temperatures around 650°C they found a significant amount of time-dependent deformation associated with the matrix material; this was negligible at lower temperatures. They found that at room temperature only the unidirectional

laminate had a tensile strength that was significantly greater than the matrix material alone. On the other hand, at 650°C the matrix yield strength is so low that all laminates tested exhibited ultimate strengths significantly greater than that of the matrix alone. This is a major reason why fiber reinforcement is necessary for elevated temperature applications. Failure surfaces of all laminates tested under monotonic loads exhibited void coalescence associated with ductile failure. Stiffness loss due to interfacial failures was obscured by matrix yielding at 650°C.

Johnson, Bakuckas, and Bigelow (18) investigated [0/90]$_s$ with center holes under fatigue loading at room temperature. In general, fatigue damage consisted of fiber matrix debonding in the 90 degree plies and matrix cracking from the debonded surfaces. The initiation of the matrix cracks occurred at approximately 60 to 75 degrees from the load direction at the edge of the center hole, not at 90 degrees the point of maximum stress concentration. The matrix cracks were bridged by the 0 degree fibers; the matrix cracks propagated around the fibers, not through them. Fiber matrix debonding in the 0 degree fibers was observed near the center hole of the specimens tested.

Johnson and Naik (19) characterized fatigue damage initiation and growth of SCS-6/Ti-15-3 specimens with center holes and double edge notches at room temperature. [0]$_8$, [0/90]$_{2s}$, [0/±45/90]$_s$, and [0/90/0] laminate configurations

22

were tested. They found that fiber matrix debonding and matrix cracking greatly reduces the stress concentrations around the notches. Elastic stress concentration factors for the [0/90]$_{2s}$ and [0/90/0] laminates were calculated to be 3.60 and 3.62. They also found that these predicted elastic stress concentration factors are at least 25 percent too high once local, near the hole, fiber matrix debonding occurs.

Rattray and Mall (20) investigated the static tensile behavior of quasi-isotropic composite SCS-6/ß21s with central holes at room temperature and 650°C. The specimens had width-to-diameter ratios ranging from 2.5 to 10. The primary objectives of the study were to define the failure mechanisms and to determine the notched strength as a function of hole diameter. They found that the unnotched and notched strengths at 650°C were approximately one half the strength of the specimens at room temperature. The laminate was notch sensitive at both room and elevated temperature. The failure mechanism involved fracture of a small number of fibers near the hole at the point of maximum stress concentration at approximately 50 percent of the failure strength. Due to this damage the stress concentration was significantly reduced and fracture of the remaining fibers occurred just prior to final failure of the specimen.

Harmon, Saff, and Graves (21) developed a routine, MMCLIFE, to predict notched and unnotched composite strength, stiffness, crack growth, residual strength, and cyclic life.

23

They implement the theory developed by Lekhnitskii (22:171-186) to calculate the stress distribution around the periphery of a circular or elliptical opening in an orthotropic plate. Once the periphery stress distribution is known, an elastic stress concentration factor can be predicted. The routine also allows for determination of the stress concentration gradient through the net section of the notched laminate. A shear lag model was introduced to model matrix yielding in the 0 degree plies enabling the calculation of a plastic stress concentration factor for these plies. The MMCLIFE routine was not used by this author but a significant portion of the theory behind it was utilized in the analysis of SCS-9/ß21s.

Newaz and Majumdar (23) analyzed crack initiation around holes in a unidirectional, SCS-6/Ti-15-3, metal matrix composite under monotonic and fatigue loading. An analytical analysis similar to the approach taken by Harmon, Saff, and Graves was implemented to predict stresses around the notch. They found that continuous, through the thickness, cracks emanated at the periphery of the hole at 65 to 72 degrees from the load axis under fatigue loading. The shear stress was found to have a maxima within this range, suggesting that shear stress has a large influence on the initiation of fatigue cracks. In monotonic tensile tests, fracture occurred at 90 degrees from the load axis at the point of maximum stress concentration. They found that there are actually two competing mechanisms for failure of circular notched specimens

under monotonic loading. "As the specimen is loaded, yielding initiates at the four symmetric locations (65-72 degrees). ... However, because of absence of cyclic loading, the slip is unable to intensify and lead to crack formation at those locations. On the other hand, as the load is increased, the fiber at the 90-degree location experiences larger and larger tensile stresses. Ultimately, a point is reached where the fiber fails because its tensile strength is exceeded. This finally sets off failure of the composite."

Lee and Mall (24) investigated a quasi-isotropic graphite /epoxy composite laminate with a reinforced hole. Experimentally they used adhesive bonded and snug-fit plugs, employing three different types of material, in conjunction with multiple specimen hole sizes. This was completed in an attempt to address the effect of various reinforcements on the strength and failure mechanism of the composite laminate. They concluded that the reinforcement material should have the same stiffness as the base laminate, forcing the plug and laminate to deform compatibly as load is applied. They also found no improvement due to bonded reinforcements, since failure initiated at the interface between the plug and adhesive or the laminate and the adhesive, nullifying any effect the adhesive obtained.

Experimental Equipment and Procedure

This chapter will discuss the manufacturing of the material, specimen form and preparation, experimental equipment, experimental procedure, and post-test specimen evaluation. In order to evaluate the tensile characteristics of metal matrix composite SCS-9/ß21s with holes, both notched and unnotched specimens had to be examined. Unnotched specimen testing was necessary to obtain base-line tensile data to compare notched specimens with. Testing was completed on two laminates, $[0/90]_{2s}$ and $[0/\pm45/90]_s$, also referred to as cross-ply and qu? ; isotropic. The material was investigated at three temper .cures: room temperature, $482^\circ C$, and $650^\circ C$. In order to obtain some necessary material properties for a thorough analysis, a number of tests were completed on $[16]_{16}$ and $[\pm45]_{2s}$ laminates. Tensile test data, along with discussion of the failure mechanisms, is presented in the Experimental Results and Discussion Chapter. This chapter will be divided into numerous sub-sections, each explaining distinct steps that were necessary for the acquisition of reliable data required to form an integral analysis.

Manufacturing and Material Identification

The composite under investigation in this research is the continuous fiber reinforced metal matrix composite, SCS-9/ ß21s. SCS-9, illustrated in Figure 1, is a silicon carbide fiber with nominal diameter of 81 μm. The inner core is a monofilament pure carbon substrate. Pryrolytic graphite is

deposited to smooth the substrate and enhance electrical conductivity. Chemical vapor deposition (CVD) is implemented with silane and hydrogen gases. Silane decomposes to form ß silicon carbide (ßSiC) continuously on the substrate. By altering the gas flow in the tubular reactor, the outer surface is coated with a carbon rich layer approximately 3 μm thick (2:395-398). ß21s is the designation given to the ß phased titanium matrix with constituents, by weight percent, Ti-15Mo-2.6Nb-3Al-0.2Si (4). The fiber and foils of matrix material were consolidated via a four step hot isostatic press (HIP) procedure. In the first step the temperature was ramped up to 760°C at 1.9°C/min (max) while the pressure was simultaneously ramped to 862 kPa ± 517 Kpa. In the second step the temperature was increased further to 300°C while the pressure was ramped to 103 Mpa ± 3.4 Mpa. This profile was then held at the pressure and temperature for 2 hours. Finally the consolidated composite was allowed to cool in the HIP vessel to 200°C. This procedure is described in further detail in references (25,26).

Specimens were identified by a numbering scheme from 1 to 90 so they could be traced to the specific panel from which they were cut, namely: B910583, B910584, B910592, B910597, B910598, and B910604 (serial numbers necessary to obtain individual panel manufacturing data). The orientation and specimen numbering for each of the six panels is displayed in Table 1. Cross-ply and quasi-isotropic laminates were

Table 1: Specimen Identification

Panel	Specimens	Orientation
B910583	1-6	$[0/\pm45/90]_s$
B910584	62-77	$[0/\pm45/90]_s$
B910592	7-12	$[0/\pm45/90]_s$
B910597	84-89	$[16]_{16}$
B910598	13-24	$[0/90]_{2s}$
B910604	49-61 & 78-83	$[0/90]_{2s}$ & $[\pm45]_{2s}$

Note: 25-48 are tensile bearing coupons which were not tested as part of this study

implemented for the bulk of this research. $[\pm45]_{2s}$ and $[16]_{16}$ laminates were used to determine the shear modulus and shear strength of the SCS-9/ß21s laminae.

Cutting and Polishing

All specimens were cut via high speed diamond impregnated blades, all holes were ultrasonically drilled, and selected specimens were polished. Specimens obtained from plates B910583, B910592, and B910598 were supplied in already sized form by the Materials Laboratory, WPAFB. The length of these specimens were reduced from 254 mm to 190.5 mm to accommodate the vacuum heat treatment oven. Specimen edges were then examined using optical microscopy to check for damage introduced during the cutting process. If matrix or fiber damage was excessive the specimens were ground down with 45 micron diamond suspension on a Metlap® #8 wheel using a Buehler Maximet® Specimen Preparation System. A number of specimens were then polished to 3 microns using Perfmat®

cloths and decreasing sized diamond suspension in order to remove visible matrix damage under high magnification. These specimens were used in an acetate/acetone replicating technique which will be discussed later.

Manufacturing Flaw Detected

Plates B910584 and B910604 were nondestructively evaluated via CSCAN inspection to check for damage. The CSCAN results of both panels failed to reveal damage that may have initiated during consolidation. But upon examination of polished specimen edges, it was noted that the fibers were contorted along the planar polished edge. Figure 8 displays an optical photograph of a typical polished edge of a $[0/90]_{2s}$ specimen prior to any applied load. Note how the 0 degree fibers, oriented horizontally, are weaving into and out of the matrix, not desirable in a continuous fiber MMC. Figure 9, another optical photograph at higher magnification of a specimen edge prior to an applied load, exhibits an adverse effect of the molybdenum material, lighter colored material, which is used to hold the SCS-9 fibers in place during the manufacturing process. The molybdenum ribbon, alternatively moly-weave, has caused these fibers to deform out-of-plane.

Photographs of the face section of a specimen polished and etched down to the first set of 0 degree fibers offers additional proof of the out-of-plane deformation exhibited by the fibers. Figure 10, a photograph of a face polished specimen, proves that the fibers deform out-of-plane across
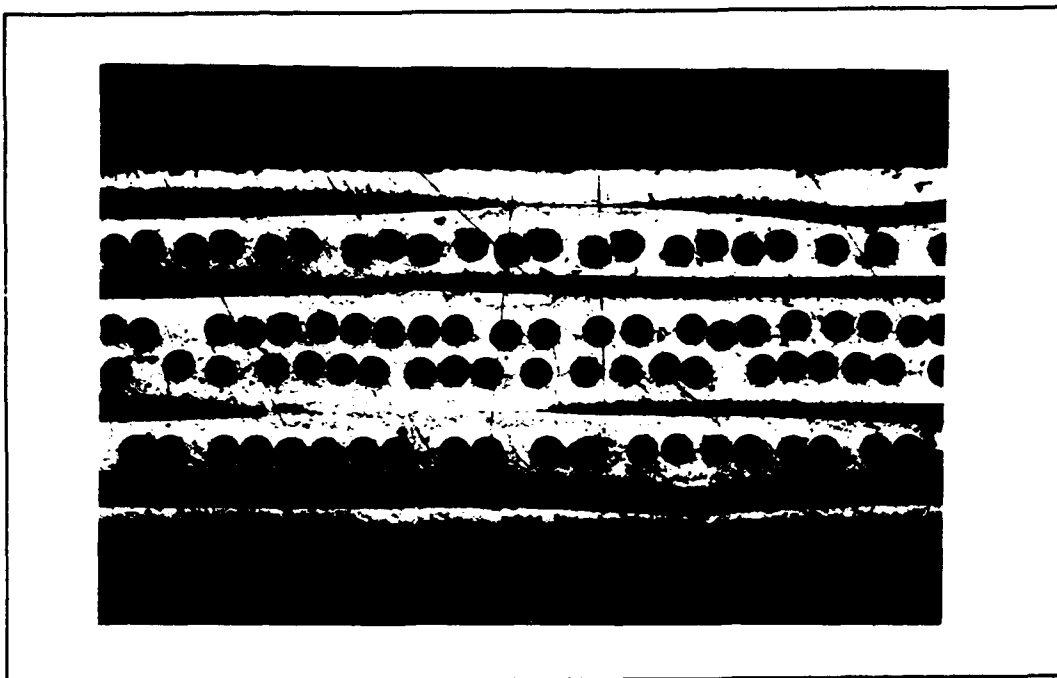
Figure 8 Initial Polished Edge [0/90]$_{2s}$ Specimen
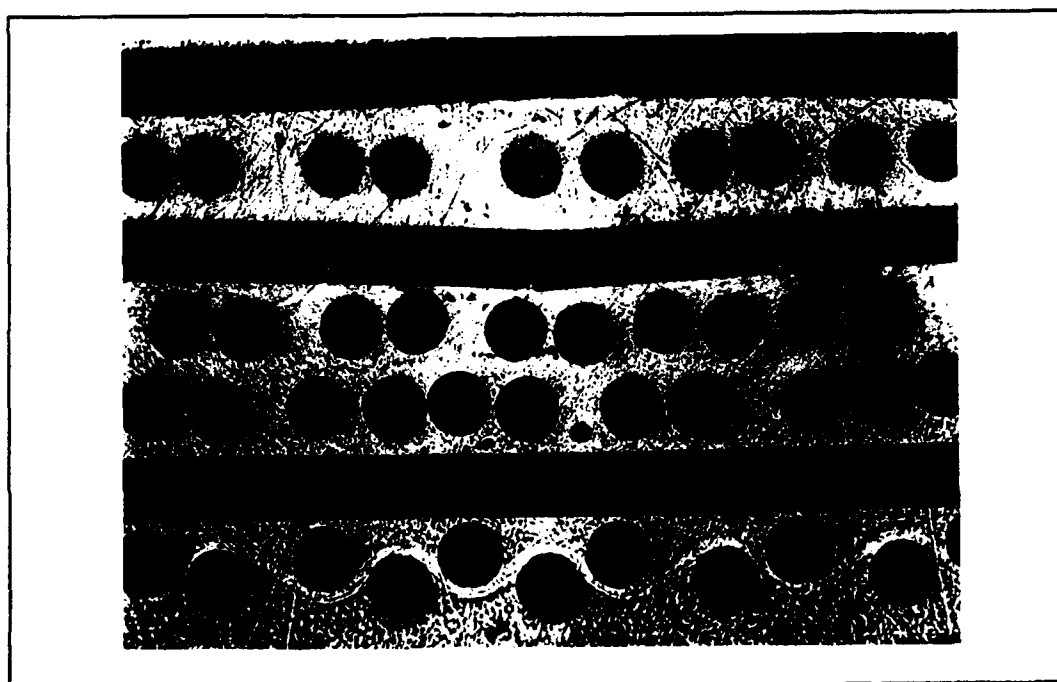
Figure 9 Initial Polished Edge [0/90]$_{2s}$ Specimen
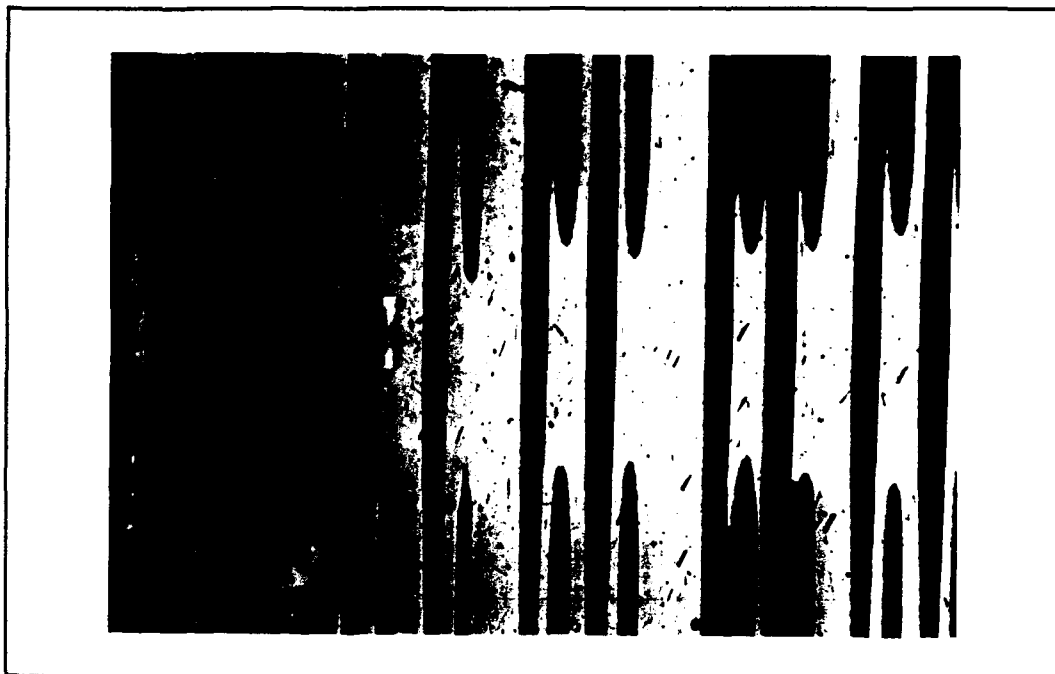
Figure 10 Polished Face Section [0/90]$_{2s}$ Specimen

the width of the specimen at the lightly colored rectangular areas, the moly-weave. An important question left to ask is how many, if any, of these fibers have experienced failure due to this out-of-plane stress induced during consolidation. The matrix material of untested sections of both [0/90]$_{2s}$ and [0/±45/90]$_s$ laminates was removed down to the first 0 degree ply using Kroll's etchant. The specimens were then carbon coated to allow for Scanning Electron Microscopy (SEM). Figure 11 displays a SEM photograph of a [0/90]$_{2s}$ specimen with the matrix material etched away. SCS-9 fibers are very brittle and the out of plane shear has caused not only out-of-plane fiber deformation but also fiber failures along the

Figure 11 Face Section of Etched $[0/90]_{2s}$ Specimen

moly-weave prior to any loading condition.

Using the SEM, a simple statistical analysis was completed to arrive at an estimate of the amount of fiber failures. In the analysis, the total number of fibers was counted across the width of a specimen and the number of broken fibers at a moly-weave was tallied. This was completed for multiple moly-weaves and an average was taken. The $[0/90]_{2s}$ specimen exhibited an average of 16 percent broken fibers across the width of the specimen at any particular moly-weave. The $[0/\pm45/90]_s$ laminate exhibited an even higher percentage of broken fibers at 25 percent. It has been recently published by others that all the panels supplied should show evidence of

the same effect of manufacturing damage as discussed above.

Heat Treatment

The choice of heat treatment has significant effects on the physical microstructure and resulting microhardness values. Lerch and Castelli (4) tested multiple heat treatments on ß21s at 650°C and found that a metastable condition appears to exist at this temperature. They suggest that a secondary precipitate reaction is occurring and additional aging, up to 100 hours, does not produce significant microstructural and hardness changes. Guidelines have been set by the NIC Steering Committee for ß21s which recommends a vacuum age at 621 C for eight hours followed by a vacuum furnace cool to room temperature (27). Their recommendation correlates well with the findings of Lerch and Castelli. To maintain consistency and enable comparison with data from others, this standard heat treatment was implemented in this research.

Specimen Dimensions

The specimen width, thickness, length, hole diameter, and pin diameter had to be measured prior to testing. Specimen dimensions were measured by a micrometer with an accuracy of ±.00127 mm. The typical thickness of a 8 ply laminates was approximately .95 mm while the standard width was close to 19 mm. All specimens tested were 177.8 mm to 190.5 mm long, which is longer than the ASTM standard 152.4 mm. Longer specimens were necessary to accommodate the testing apparatus.

The holes had a nominal diameter equal to 3.175 mm, generating a width to diameter ratio of approximately six. Guidelines outlined in the Consortium Testing Specifications (CTS) Materials and Structures Augmentation Program (28) state that for filled hole tensile testing of MMCs the tolerance between the pin diameter and hole diameter must not exceed .0254 mm. The guidelines also specify the pin material to be Mar-m-246. Mar-m-246 pins with diameters of 3.175 mm and 4.7625 mm were purchased through Satec Systems Incorporated. The 4.7625 mm pins were then ground down to appropriate diameters and measured using a micrometer. Pins made of 7075-T6 aluminum were also implemented in this research. Hole diameters were measured within .0127 mm via precision pins. The specified tolerance between the pin and hole diameter was therefore accomplished.

Final Preparation for Room Temperature Tests

This section will discuss the application and purpose for applying tabs and strain gauges to room temperature specimens. The position of an extensometer, also used to measure strain, will also be defined. The main purpose of the application of a tab is to redistribute the local stresses caused by the grips and to preserve the specimen from damage from the actual teeth of the grip. Tabs are unnecessary at elevated temperature due to the fact that the application of heat is a dominant effect over the localized stresses at the grips and therefore the specimen will fail in the gauge area. The tab

material was a continuous glass fiber crossweave in a phenolic sheet. The tab length was 38.1 mm and the thickness was 1.6 mm. The portion of the tab to be positioned towards the center of the specimen was beveled at approximately 45 degrees to further distribute the local stresses. Tabs were affixed to the specimens using epoxy EPON® resin 828 and curing agent V-40. No specimen exhibited failure at the grip, therefore this is a recommended procedure. Two strain gauges, remote and local, were applied to the room temperature specimens by standard methods. The position of the strain gauges is extremely relevant to discussion in subsequent sections. The remote strain gauge used was a CEA-06-250UN-350 and the local strain gauge used was a CEA-06-032UW-120. The remote strain gauge, measuring longitudinal strain, was applied at least five hole diameters away from the hole; it is assumed that the specimen basically behaves as if it were unnotched at this distance from the hole. The local strain gauge, also measuring longitudinal strain, was mounted at 90 degrees to the hole, along the periphery. The backing surface of this gauge was trimmed to allow the placement of the gauge to be less than .5 mm from the actual periphery. This gauge measured the accumulated strain at the point of maximum stress concentration. A 12.7 mm ceramic rod extensometer was then mounted either locally, encompassing the hole, or remotely, at least five hole diameters away. Figure 12 displays the location of the strain gauges, the tabs, and the extensometer
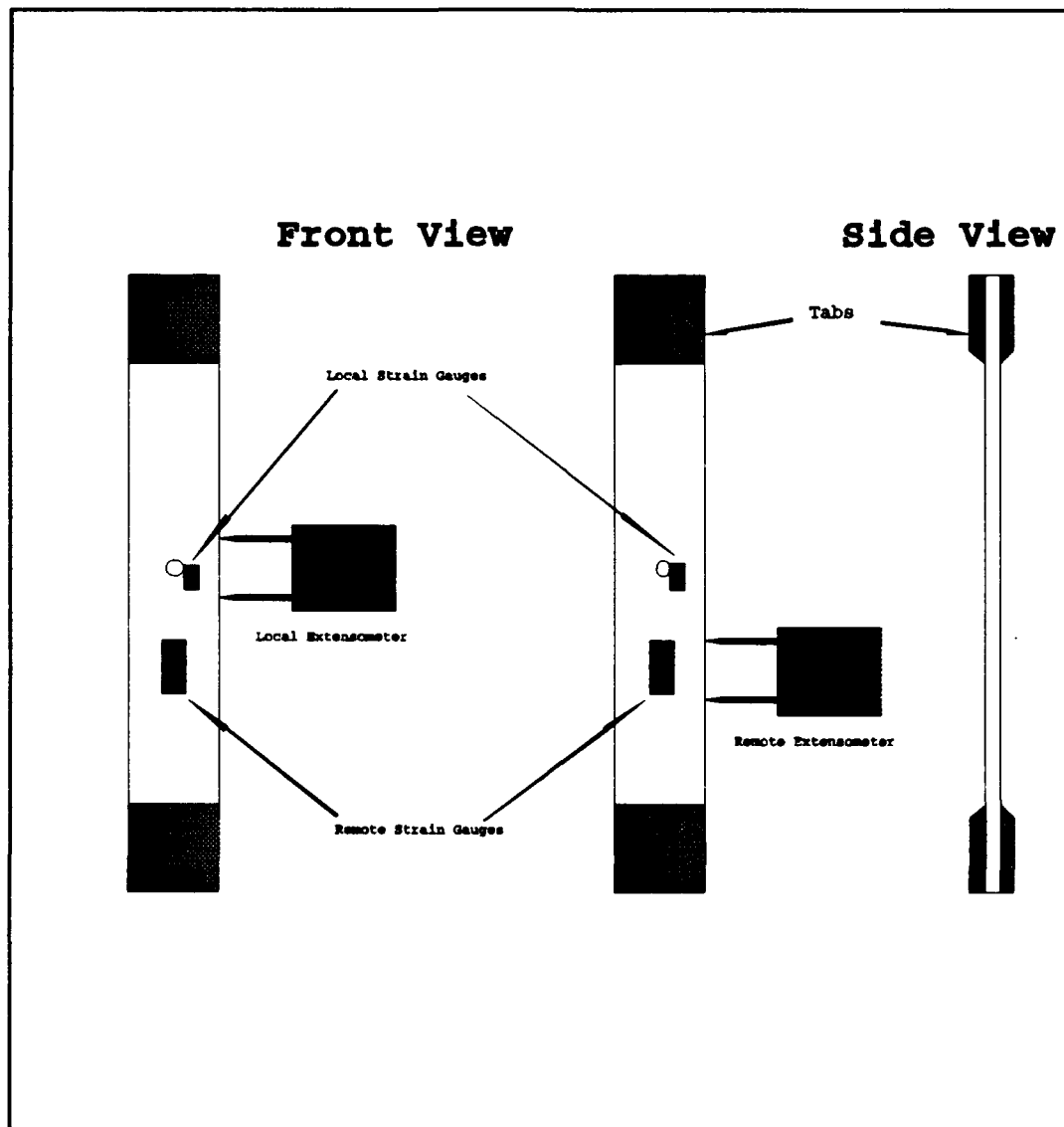
Figure 12 Strain Gauge, Tab, and Extensometer Placement

for a typical room temperature test. Strain gauges could not be implemented during specimen evaluation at elevated temperature due to the fact that they cannot withstand the heat. A local or remote extensometer was the only source of strain data at elevated temperature.

36

Test Equipment

Major test components included a 110 kip servo-hydraulic Materials Test System (MTS), a high temperature MTS 12.7 mm extensometer, a Micricon 823 process control system, a Rockland series 2000 filter, strain gauge conditioning amplifiers, and a Zenith personal computer (PC) with data acquisition capabilities. The integration of the components enabled collection of pertinent data necessary for subsequent analysis. The following paragraphs will describe in limited detail the functions of the aforementioned components.

The MTS, displayed in Figure 13, is a system with the capability to control the testing via transducers, a microprofiler, a function generator, a 458.20 MicroConsole with digital display, DC output voltages that correspond to load, displacement, and strain, and hydraulic grips. The load and displacement transducers output a specific voltage per given physical occurrence. The MicroConsole, via calibration, converts the voltages received from the transducers to an actual engineering quantity which is displayed digitally. It also maintains the capability of outputing the transducer DC voltages directly to a Quatech analog to digital (A/D) board. The function of the microprofiler is to enable the user to define the type of load or displacement profile required in a particular test. The hydraulic grips can be adjusted to apply an appropriate pressure on the specimen.

The 12.7 mm high temperature extensometer, simply another
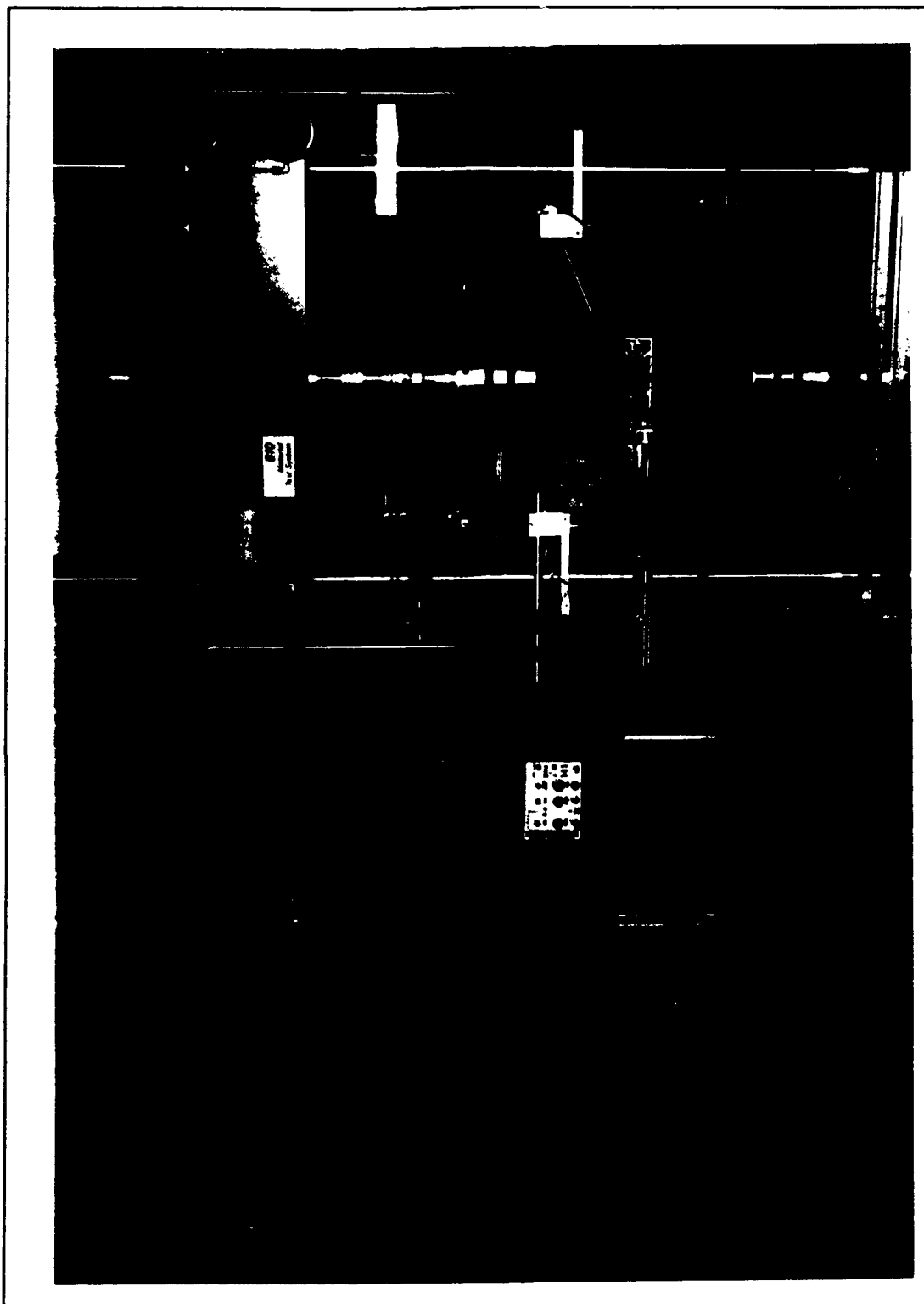
Figure 13 Photograph of the Materials Test System

38

transducer, outputs voltage, the magnitude depending on the gain setting, per unit displacement of the ceramic rods. Through calibration the strain is calculated as a function of voltage. The ceramic rods of the extensometer, ground to a point using a diamond wheel, are positioned on the edge of a specimen and held in place through pressure applied via the mounting apparatus. The distance between the points of the extensometer's ceramic rods, set by the manufacturer, defines the gauge length, which in this research is 12.7 mm.

A Rockland series 2000 filter was implemented for the later part of the research to filter out undesirable noise in the system. The filter incorporates a low pass filter which was adjusted to filter out frequencies over 200 Hz.

Strain gauge conditioning amplifiers were necessary to amplify output voltages from the strain gauges to levels compatible with the data acquisition system. Gain and offset variables enable the user to maximize the resolution of the amplifier to meet the particular test requirements.

A Zenith 286 PC with data acquisition capabilities was employed for the collection of data. Data acquisition was accomplished through a Quatech A/D board which receives output voltages from the MicroConsole and amplifiers. Software converts these input voltages to physical quantities, using calibration equations, and generates output data files.

The Micricon process control system was used in conjunction with radiant heaters to attain elevated

temperatures in the specimen gauge area. The Micricon controller employs a three mode controller or "PID" system: Proportional, Integral, or Derivative factors which are adjusted to achieve a smooth temperature profile in the specimen. The system received feedback from two Nickel-Chromium vs. Nickel-Aluminum type K thermocouples. Two additional type K thermocouples were also implemented to monitor the temperature and insure a uniform temperature gradient throughout the gauge area of the specimen. Each of the two radiant heaters contained two active General Electric 1000 Watt 120 Volt quartzline strip lamps.

Test Procedures

The previous sections explained the material type, form, and integrity. Cutting, polishing, and heat treatment has been discussed. Strain gauging and extensometer application was covered. The equipment necessary for the acquisition of data was also discussed. This section will systematically discuss the procedure involved in a typical tensile test.

Strict specimen alignment and precise thermocouple placement is of extreme importance for the collection of valid data. The specimen was aligned in the grips using a rectangular aluminum block held against the specimen edge in conjunction with a small level. For elevated temperature tests, thermocouples were tack welded to the specimen. The placement of the thermocouples is dependent upon whether local or remote strain data is to be collected, refer to Figure 14.
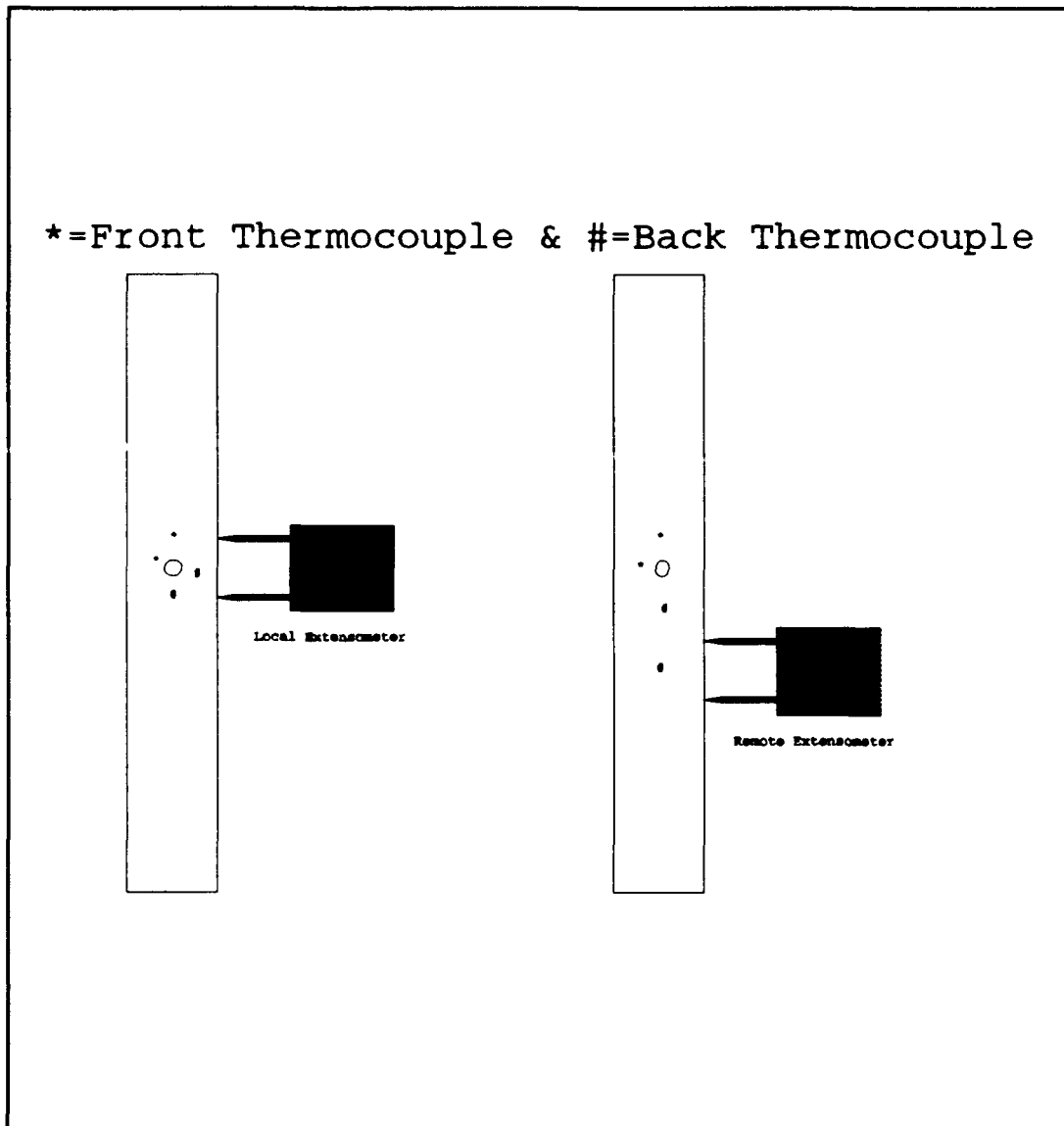
Figure 14 Thermocouple Locations for Remote and Local
Extensometer Positions

Realize that when collecting local data, the gauge area of the
specimen can be no smaller than the gauge length of the
extensometer, which encompassed the hole. When collecting
remote data the specimen must exhibit uniform temperature in

the area of the notch and also in the gauge area of the extensometer, which is mounted five hole diameters away. Figure 14 displays thermocouple placement for local and remote data acquisition that proved to be adequate in insuring uniform heating throughout the gauge area. Thermocouples 1 and 2 were used to control the feedback, while additional thermocouples 3 and 4 were used to monitor temperatures at prescribed locations.

Prior to applying load, the extensometer had to be installed, amplifiers adjusted, prescribed temperature maintained, and heat lamps positioned. The extensometer was mounted on the specimen and zeroed (output voltage equal to zero at gauge length of extensometer). Strain gauges were wired to amplifiers and bridges were balanced under zero load. The microprofiler was programmed for a monotonically increasing, constant slope load rate of 22.2 Newtons per second. The Micricon was then programmed for a constant slope temperature ramp of 2.7 to $3.6^{\circ}C$ per second. Care was taken to adjust the gain, rate, and reset values accordingly to insure that an overshoot in temperature did not exceed 2.0 percent. The specimen was then held at the prescribed temperature for 3 to 5 minutes before the load was applied; this amount of time proved adequate for stabilization of the specimen's temperature. Figure 15 displays the specimen in the grips with the thermocouples attached, the extensometer mounted, and the back radiant heat lamps in position.
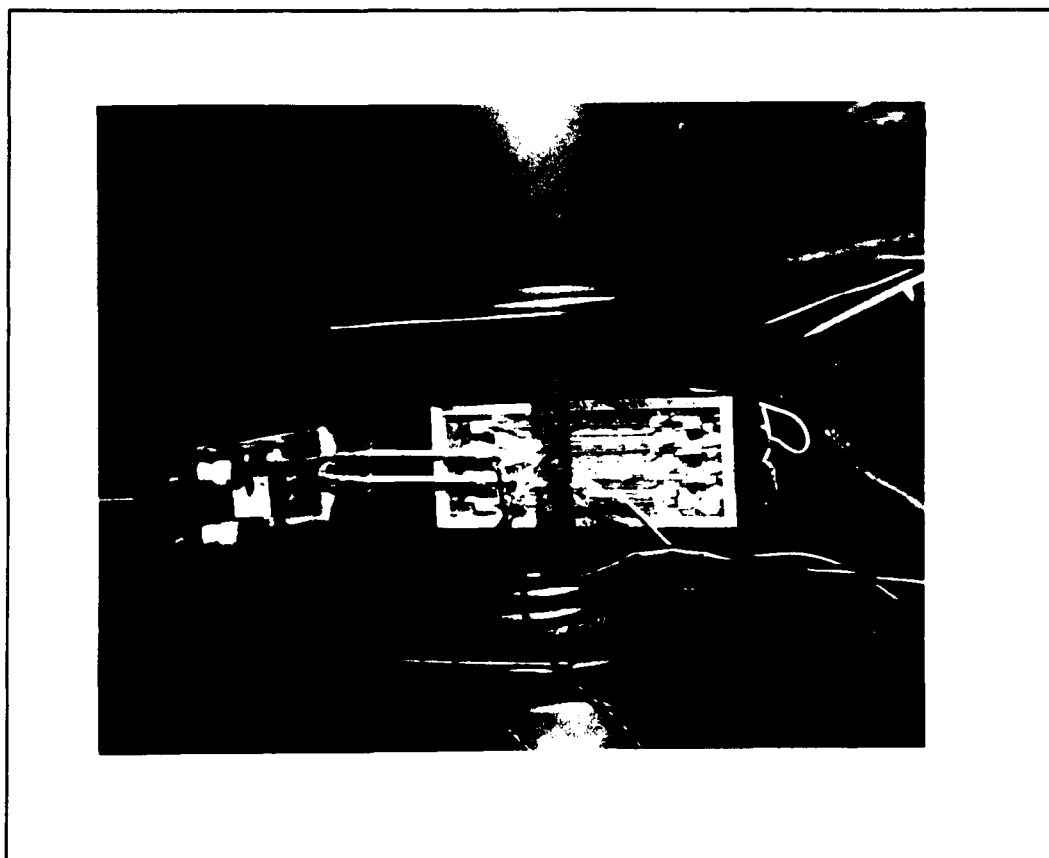
Figure 15 Specimen in Grips

Acetate replication was performed, locally and remotely, for both laminates at room temperature and elevated temperature. For room temperature replication the tensile test was put on hold at prescribed loads and acetone/acetate replication was performed via standard techniques. For elevated temperature tensile tests, the test was put on hold at prescribed loads and the temperature was allowed to cool to room temperature maintaining this load. The standard replication was then performed at room temperature. The heat

43

was reapplied and the specimen was allowed to stabilize at the test temperature prior to loading to the next prescribed load. The ultimate failure loads of tensile tests with replication was within the experimental deviation expected in ultimate strength.

Post-test Specimen Evaluation

Examination of replicas and failed specimens is essential for characterization of metal matrix composites. Prior to optical and scanning electron microscopy specimen preparation was necessary.

Replicas were examined optically to look for matrix cracking, delamination, fiber cracking, etc. The replicas were then carbon coated for SEM evaluation which proved to be a powerful tool in investigating fiber/matrix debonding.

Substantial specimen preparation is necessary prior to microscopy. Specimens were cut/sectioned using a Buehler low speed sectioning saw with a diamond impregnated blade. Some specimens were cut in a fashion such that both longitudinal and transverse microscopy could be performed. The specimen could also be sectioned adjacent to the fracture surface. The sectioned specimens were cleaned with alcohol and acetone to remove contaminates. Ultrasonic cleaning also proved to benefit in the removal of any remaining contaminates. Some sectioned specimens were mounted in Epomet® molding compound and ground down to 3 microns as described previously. They were then placed on a Buehler Vibromet and polished to 1

44

micron, then to .5, and finally to .06 microns. A number of specimens were loaded to a prescribed percentage of the ultimate failure strength and then etched with Kroll's etchant to determine failure progression near the notch. Carbon coating is recommended for all specimens to be examined via SEM.

Experimental Results and Discussion

This chapter will begin by employing the computer program METCAN, discussed in Chapter 2, to predict residual stresses and micro-stresses in a typical load profile. Unnotched specimen data is given and analytical work is presented to predict laminate properties and strengths. Open hole specimen data will then be presented and analyzed to address: damage progression, the mode of fracture, notch sensitivity, etc. Analytical work is then discussed to quantify the stresses around the periphery of the hole, elastic and plastic stress concentration factors, and prediction of notched laminate strengths. Finally, this chapter will conclude with the presentation and discussion of filled hole tensile data. The experimental results and discussion were obtained from static tensile tests of metal matrix composite SCS-9/β21s with $[0/90]_{2s}$ and $[0/\pm45/90]_s$ orientations. Acetate replication, metallography, and fractography will be used in conjunction with analytical methods to define the aforementioned material characteristics.

Residual stresses

Prior to examining the stress-strain data the residual stresses in the fiber and matrix will be quantified. METCAN is a computer program developed at NASA Lewis Research Center to perform linear and nonlinear analysis of fiber reinforced metal matrix composites. A linear analysis was performed on SCS-9/β21s. The interface was not modeled due to a lack of

pertinent constituent properties. Table 2 includes constituent properties for SCS-9 and ß21s used in this analysis; the properties are presented in METCAN's prescribed English unit system (S=Strength, D=Diameter, T=Tension, C=Compression)

Table 2
METCAN: Material Properties

Fiber

Property	Units	SCS-9
D_f	Mils	3.100
ρ_f	lb/in^3	0.110
Tempm$_f$	Deg F	2700.
E_{f11} & E_{f22}	Mpsi	48.00
ν_{f12} & ν_{f23}	in/in	0.260
G_{f12} & G_{f23}	Mpsi	24.24
α_{f11} & α_{f22}	ppm/F	2.083
K_{f11} & K_{f22}	Btu/hr/in/F	0.750
C_f	Btu/lb	0.290
$S_{f11T}, S_{f11C}, S_{f22T}, S_{f22C}$	Ksi	418.0

Matrix

Property	Units	ß21s
ρ_m	lb/in^3	0.178
E_m	Mpsi	16.19
ν_m	in/in	0.300
α_m	ppm/F	5.280
K_m	Btu/hr/in/F	0.814
C_m	Btu/lb	0.142
S_{Mt}	Ksi	166.5
S_{Mc}	Ksi	190.0

It was assumed that the residual stresses are zero or negligible at a temperature of 650°C. With known values for coefficient of thermal expansion: α_m=9.504 ppm/°C and α_f=3.749 ppm/°C, (*ppm is parts per million, converted to the metric system*) the residual stresses can be obtained for a

47

manufacturing cool down to 23°C. The residual stresses are:

$$Sigm11A=Sigm11C = 163 \text{ Mpa}$$
$$Sigm22A = 317 \text{ Mpa}$$
$$Sigm33A = 294 \text{ Mpa}$$
$$Sigm22C=Sigf22 =-142 \text{ Mpa}$$
$$Sigm33C=Sigf33 =-180 \text{ Mpa}$$
$$Sigf11 =-344 \text{ Mpa}$$

The orientation of these residual micro-stresses within a laminae are defined in Chapter 2, Figure 7. Also included in Chapter 2 is a diagram of the METCAN micromechanics model, Figure 6. Large compressive radial stresses have built up at the interface between the matrix and fiber. The axial and transverse stresses in the matrix are both tensile. Figure 16 is a representative sketch.
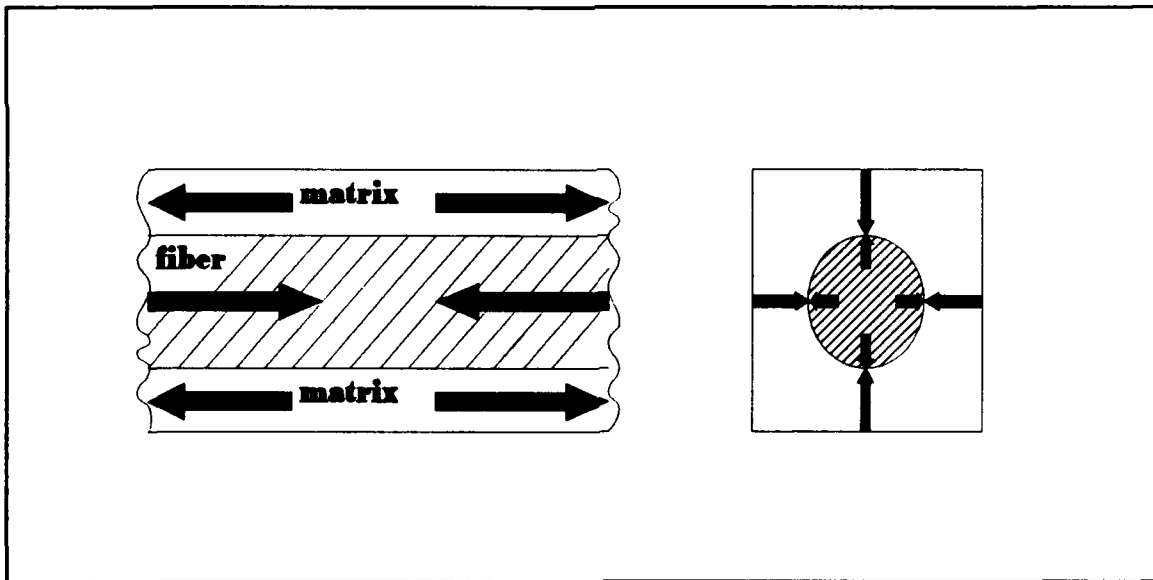
Figure 16 Residual Stresses in a Typical Ply

Unnotched Specimen Evaluation

Unnotched tensile data was obtained for cross-ply and

48

quasi-isotropic laminates at room temperature, 482°C, and 650°C. These tests were necessary to obtain a net strength line (or the baseline data) which could then be used to compare the notch sensitivity of both open and filled hole specimens. The original intention was to test three specimens at each temperature for each laminate. The quantity of tests was reduced to one data point at each temperature due to the fact that the unnotched ultimate strength of SCS-9/ß21s compared very well with results published by others; unnotched data is available but failure progression is not documented. The deviation was small enough to justify a single data point at each temperature. Ultimate strength, yield stress, elastic modulus, and mechanical failure strain results are presented in Table 3. The coefficient of thermal expansion was measured to be 7.31e-6/°C ± 0.80 for $[0/90]_{2s}$ and 6.59e-6/°C ±0.30 for $[0/\pm45/90]_s$. Yield strength is defined as a 0.2 percent

Table 3:Unnotched Tensile Data

Specimen Id.	Orientation	Temp. C	Ultimate MPa	Yield Mpa	ϵ_{ult} %
49	$[0/90]_{2s}$	R.T	906.2	-----	0.753
51	$[0/90]_{2s}$	482	680.6	640	0.679
50	$[0/90]_{2s}$	650	408.0	340	1.006
62	$[0/\pm45/90]_s$	R.T	776.9	680	0.901
63	$[0/\pm45/90]_s$	482	575.5	510	0.984
64	$[0/\pm45/90]_s$	650	339.7	272	1.739

-----: insufficient strain at failure to define .2% offset

offset from initial modulus. All the specimens were cut from panels in which the molybdenum cross-weave had damaged the fibers during the manufacturing process. This manufacturing flaw was discussed previously in Chapter 3, pages 29-32.

Figures 17 and 18 display the stress-strain response for laminates $[0/90]_{2s}$ and $[0/\pm45/90]_s$, respectively, employing the half inch extensometer. The knee in the initial stress-strain curve is indisputable for both laminates at room temperature and $482^{\circ}C$. Figures 19 and 20 show the initial portions of the stress-strain curves. It will be shown through a micro-mechanical evaluation, acetate replication, and fractography that this bi-linear response is due to the release of residual stresses and interfacial failures of the off-axis plies and not micro-plasticity. At $650^{\circ}C$ the stiffness loss due to interfacial failures is obscured due to matrix yielding. The yield strength of ß21s in tension drops 35% from 1066 Mpa at room temperature to 750 Mpa at $482^{\circ}C$ and drops an astounding 83% to 205 Mpa at $650^{\circ}C$. Due to this massive drop in yield strength a second linear portion of the stress-strain curve at $650^{\circ}C$ is not obviously visible, but the initial linear region is still evident.

Interfacial Failures / Linear Regions

METCAN can be used to analyze whether the knee is due to debonding of the 90 degree plies or micro-plasticity. An analysis of micromechanical material response was performed at room temperature to predict the applied load at which there

50
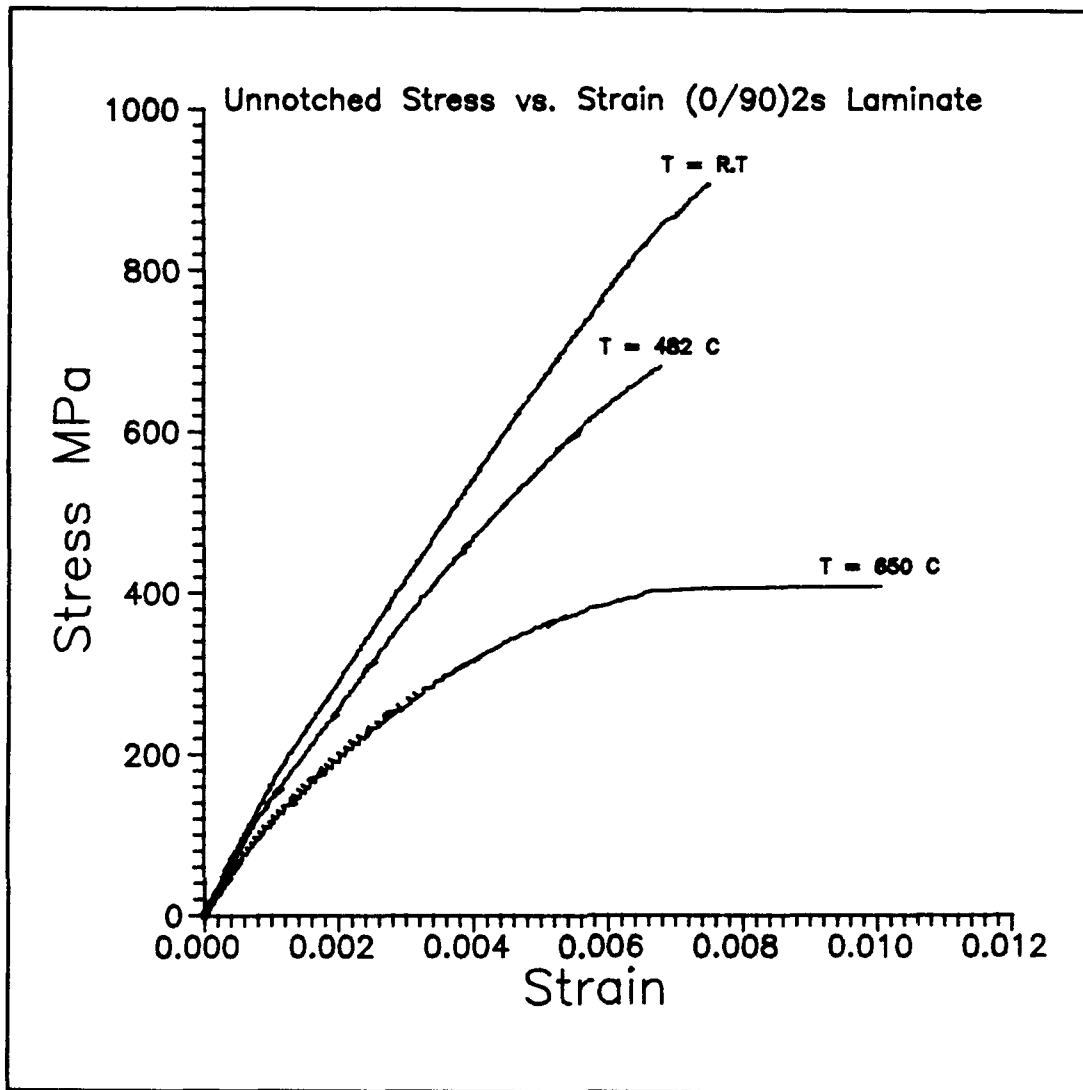
Figure 17 Unnotched Stress vs. Strain $[0/90]_{2s}$

exists a release of the initial residual stresses in the 90 degree plies. METCAN predicts that at an applied gross stress equal to 168 Mpa the micro-stresses at the interface of the fiber and matrix, namely Sigf22 and Sigm22C, change from compression to tension in the 90 degree ply, or the residual stresses at the interface have released. Realize that 22 is
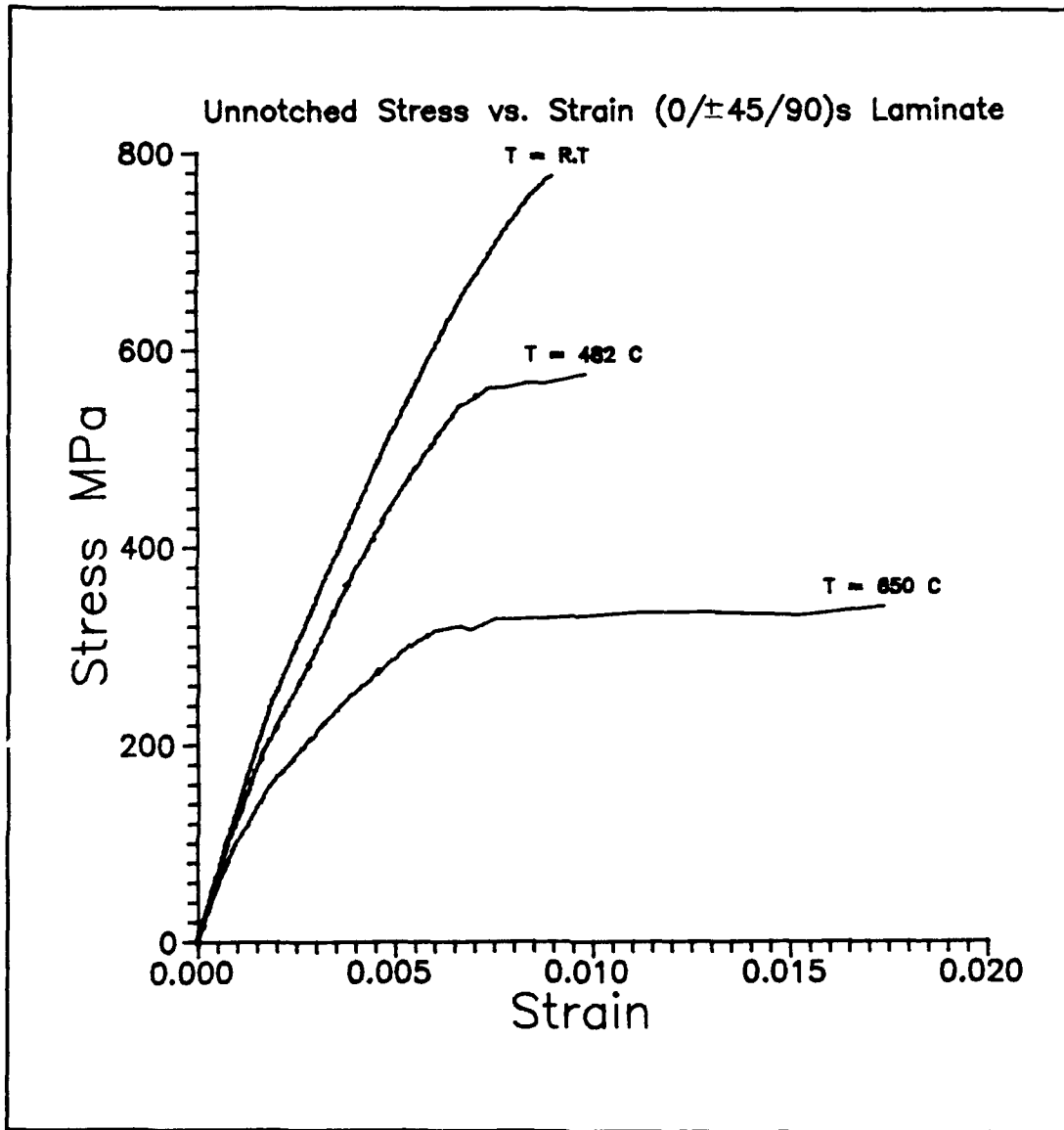
Figure 18 Unnotched Stress vs. Strain [0/±45/90]$_s$

the load direction in the 90 degree laminae and C is the area

of the unit cell model adjacent to the fiber, refer to Figures

6 and 7 in Chapter 2 pages 17-18. Referencing the

experimental results shown in Figure 17 it is found that the

knee occurs between 180 and 200 Mpa for the [0/90]$_{2s}$ laminate
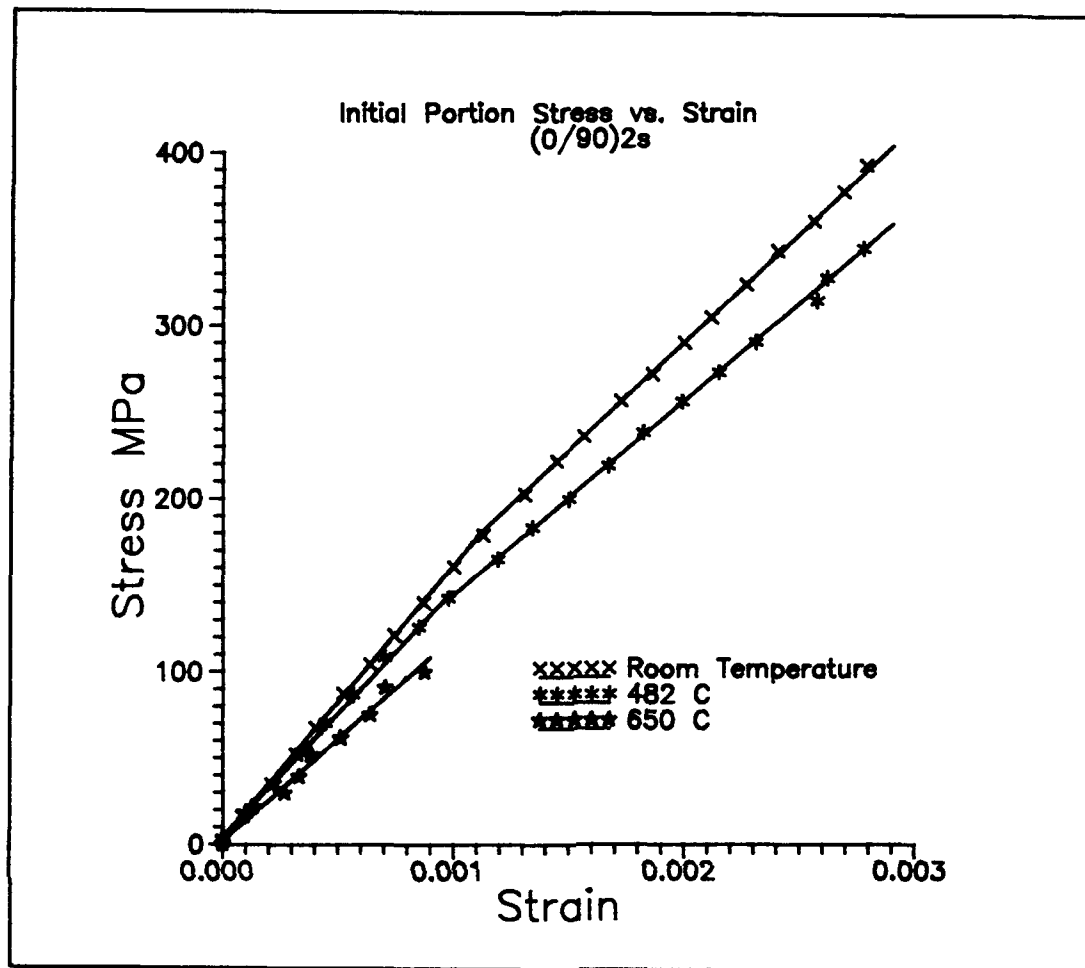
Figure 19 Initial Portion of Stress-Strain Curve [0/90]$_{2s}$

at room temperature. Therefore there is a correlation in the micro-mechanical model for release in residual stress and the knee in the stress-strain curve. The interface is very weak at room temperature. It should also be noted that the micromechanical stresses in the matrix are all well below the yield stress of β21s at an applied stress where the knee occurs, proving again that the knee is not due to micro-plasticity. Analysis of METCAN results at 650°C demonstrate

53
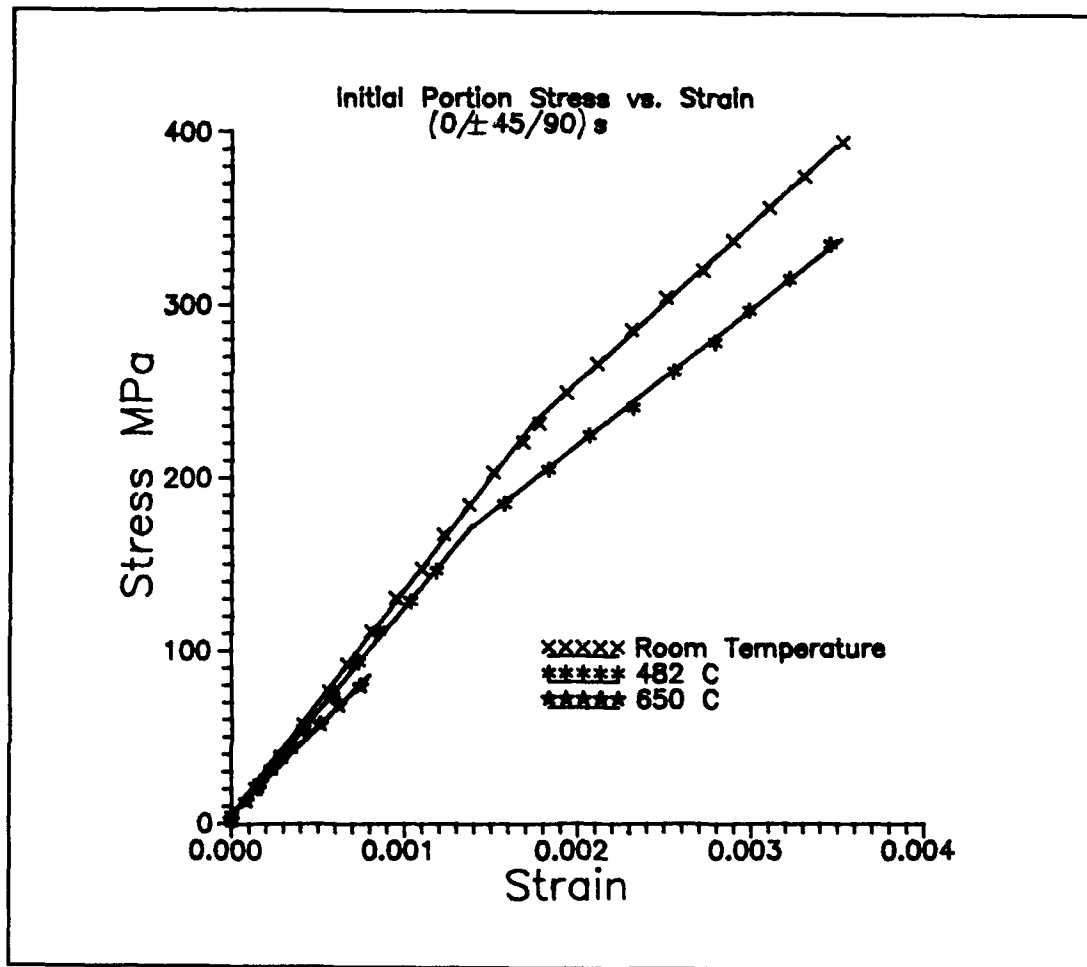
Figure 20 Initial Portion of Stress-Strain Curve
[0/±45/90]$_s$

that with a gross applied stress of 195 Mpa, the micromechanical stresses in the 90 degree plies approach the yield stress of 821s. This causes the second linear region of the characteristic bi-linear stress-strain curve to become obscured. Figure 17 demonstrates that at 650°C the knee occurs at approximately 80 Mpa where METCAN predictions of the micromechanical stresses are, as in the room temperature case,

below the yield strength of 821s. Therefore debonding of the 90 degree plies cause the knee in the stress-strain curve at elevated temperatures. It is believed that at elevated temperature the chemical strength of the interface is stronger than at room temperature. METCAN was not implemented to predict micro-stresses for a typical load profile at $482^{\circ}C$ since it is spanned by the room temperature and $650^{\circ}C$ analysis.

Acetate replication of a polished edge of a specimen during loading allows the progression of damage to be documented. Realize that replication of the remote area, at least five hole diameters away, of a notched specimen is analogous to replication of an unnotched specimen at equivalent loads. Replication was completed for both cross-ply and quasi-isotropic laminates at all temperature regimes. Figures 21-25 are SEM photographs of carbon coated replicas of a 90 degree fiber in a $[0/90]_{2s}$ laminate tested at $482^{\circ}C$. The load direction in all figures is vertical.

Figures 21 and 22 are both photographs of a representative fiber prior to any applied load. Figure 21 is a photo of a 90 degree fiber of an initially polished edge. From this figure it is seen that the fiber and matrix are free from any pronounced edge defects. The interface, visible as the black circular outer ring, the cai on rich layer, is obviously bonding the fiber and matrix. Figure 22 is a replica taken after the specimen was stabilized at the test temperature and

then allowed to cool back down to room temperature. From this photograph it is concluded that temperature alone, due to oxidation and environmental effects, has effect on the interface. This is not to be misconstrued as debonding for it is a surface phenomenon. Figure 23 is a representative fiber at 21 percent of the failure strength of the coupon. This corresponds to a stress lower than the knee on the stress-strain curve; no evidence of debonding can be seen from this photograph. Figure 24 is a replica taken at 38 percent of the failure strength, corresponding to a stress above the knee in the stress-strain curve. The fiber has definitely debonded. The acetone penetrates into the debonded interface, evident as a gap which has formed between the fiber and matrix . The 90 degree fibers also appeared to be protruding beyond the matrix. Figure 25 is a replica taken at 81 percent of the failure strength. Note the plastic deformation of the matrix adjacent to the fiber as it becomes oval in nature with its major axis oriented in the load direction.

Throughout the replicating process, no matrix cracks were detected up to approximately 85 percent of the ultimate failure stress and no delamination was observed. It was not possible to conclude debonding of the 45 degree fibers in the $[0/\pm45/90]_s$ laminate using replication techniques. This is probably due to the fact that the 90 degree fibers have protruded and the acetate/acetone viscous fluid mixture could not flow adequately to replicate the 45 degree plies.

Figure 26 is a SEM photograph of a typical initially polished edge prior to an applied load. Notice that the harder fibers are protruding slightly beyond the softer matrix, this is not to be confused with debonding but rather a function of the polishing technique. Figures 27 and 28 are SEM photographs of the polished edge of failed room temperature $[0/90]_{2s}$ and $[0/\pm45/90]_s$ specimens respectively. It is obvious from these two photographs that the 90 degree fibers have debonded and Poisson's effect in the matrix causes the fibers to protrude. The 45 degree fibers, seen in Figure 28, also exhibit debonding and are being pulled into the matrix in a scissor effect which is common for angle-ply laminates.
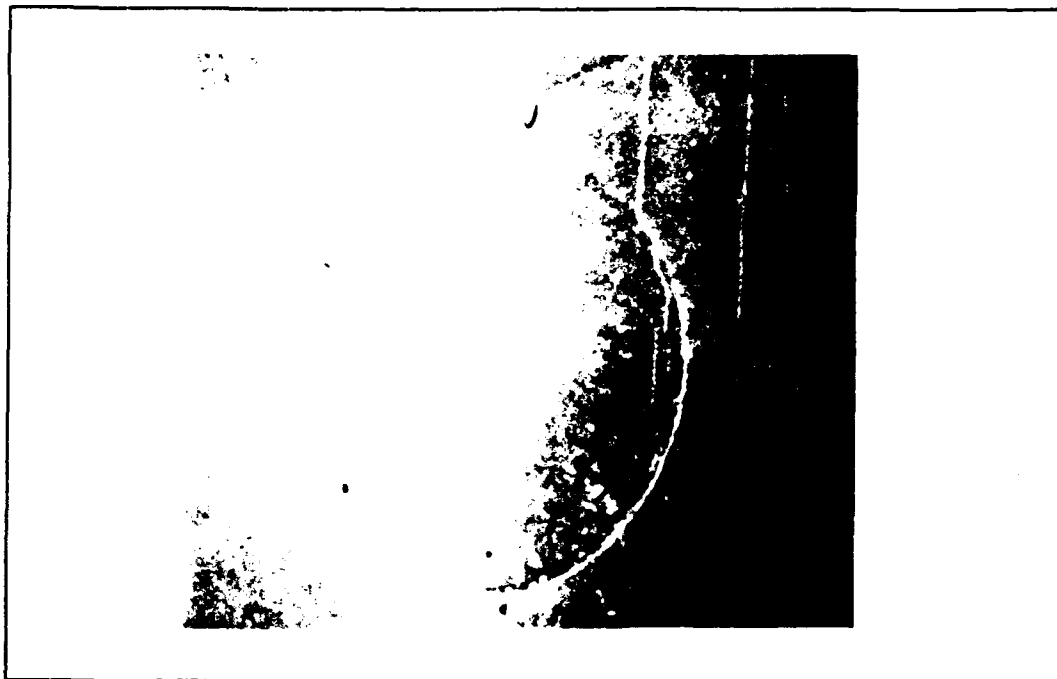
Figure 21 Initial Polished Edge
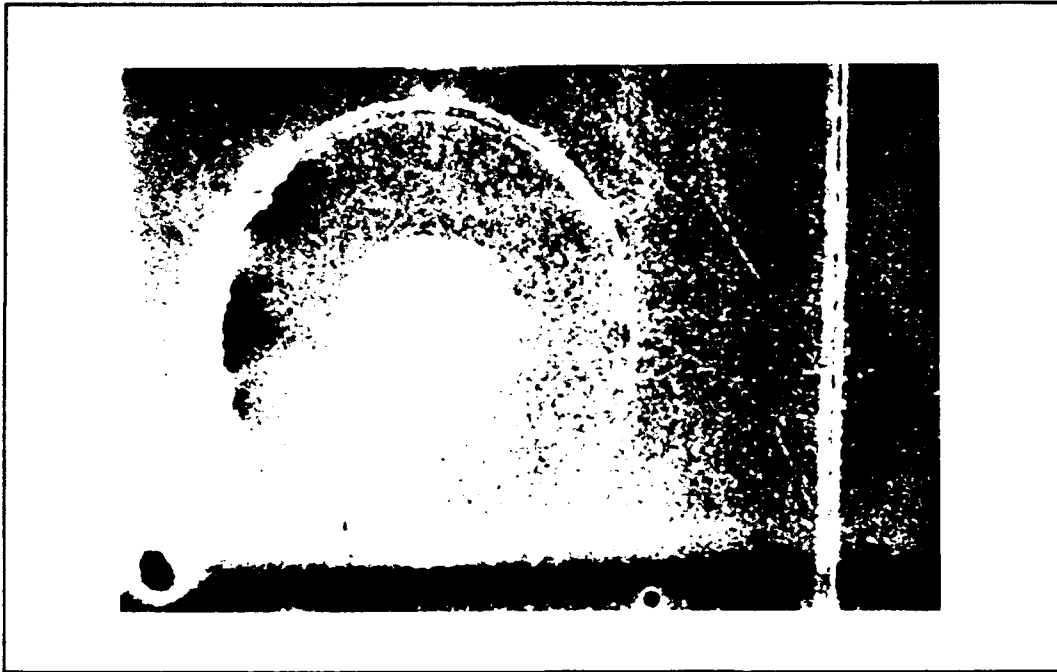
Figure 22 Initial Polished Edge After Heating

Figure 23 21% of Failure Strength
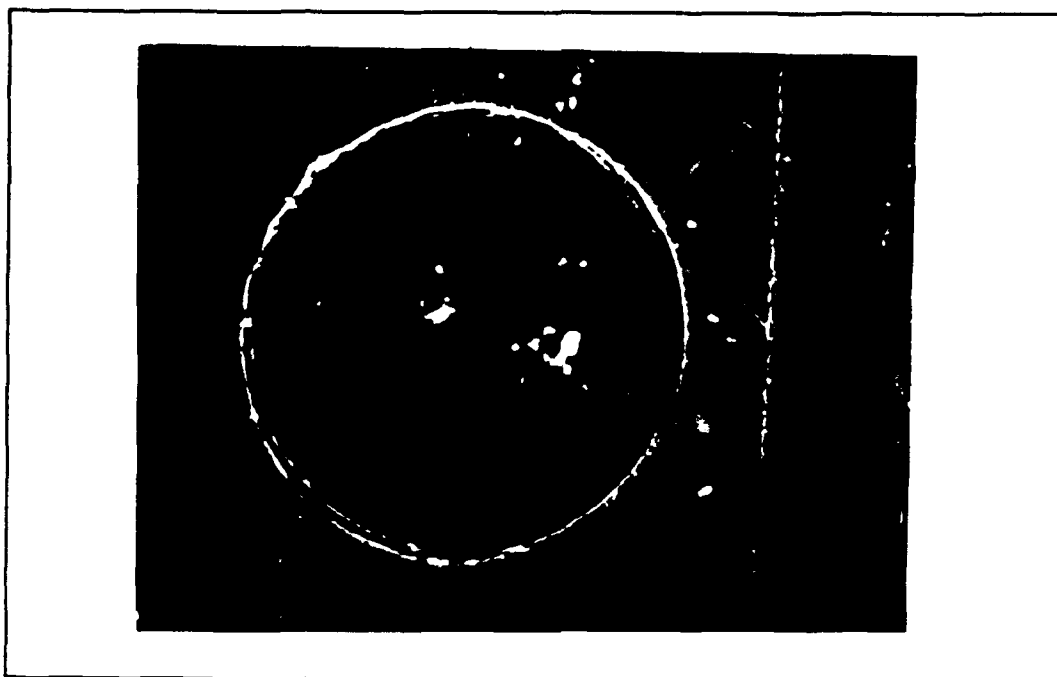
Figure 24 38% of Failure Strength
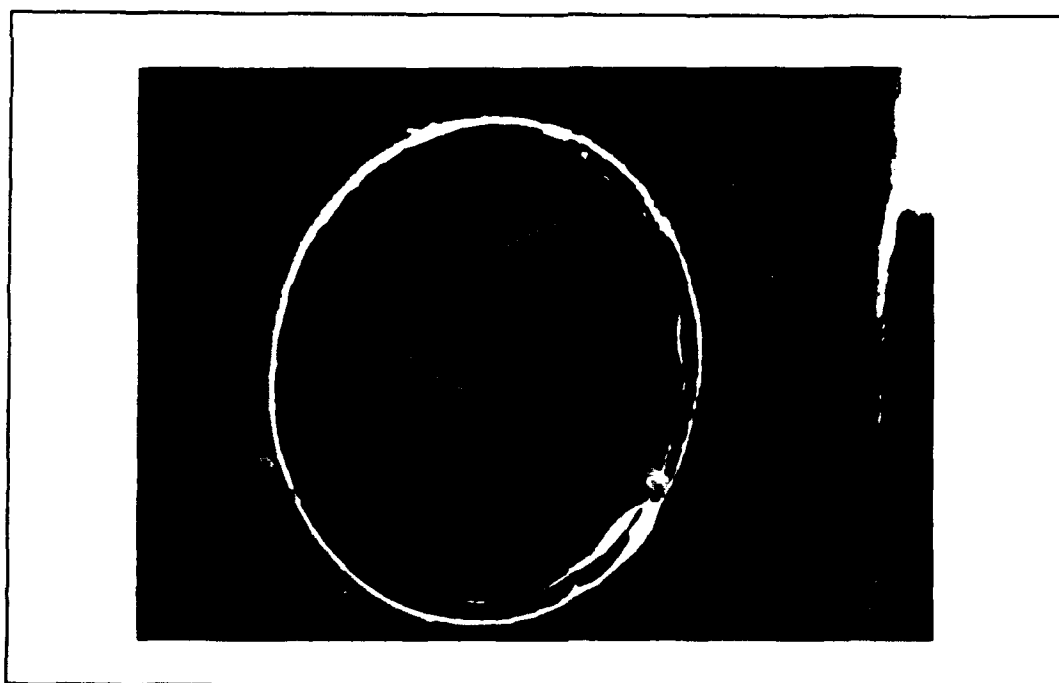
Figure 25 81% of Failure Strength

Figure 26 Initial Polished Edge

Figure 27 [0/90]$_{2s}$ Room Temperature

60
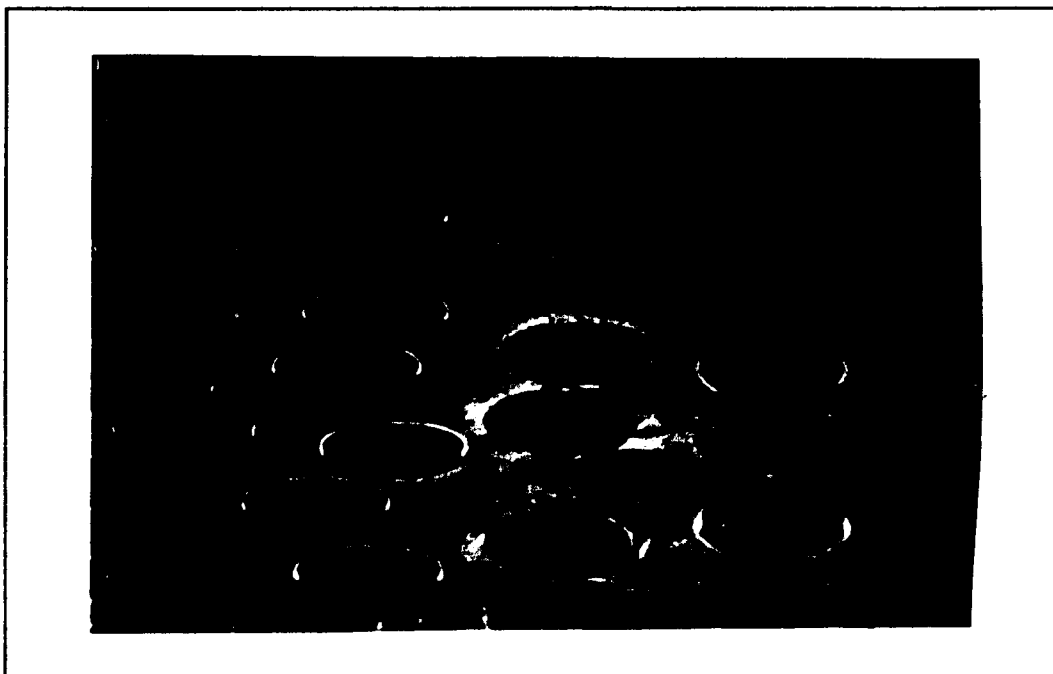
Figure 28 $[0/\pm45/90]_s$ Room Temperature

Failure Progression

$[0/90]_{2s}$ and $[0/\pm45/90]_s$ laminates at all temperatures display initial linear regions and a nonlinear response in the later portion of the stress-strain curves at all temperatures, visible in Figures 17 and 18. In the first linear region the stress-strain response for both laminates at all temperatures is governed by elastic behavior of the fiber and the matrix without damage. In tne second linear region the constituents of the laminates still behave elastically with damage in the form of off-axis ply interfacial failures, evident as a knee in the curves. Final laminate response is governed by nonlinear behavior. The fiber is basically elastic until

61

failure. Bearden found that a SCS-9/B21s unnotched 0 degree laminate exhibits nonlinear behavior at around .55 percent strain (30). Note that the stress-strain response in Figures 17 and 18 becomes nonlinear at approximately this value of strain. The matrix material, B21s, is elastic-perfectly plastic. The final nonlinear region is due to fiber failures, primarily in the 0 degree plies, and matrix plasticity. This type of failure progression is common for unnotched metal matrix composites under static tensile loads and is well documented (14-17,20,23).

Prediction of Laminate Properties

Composite properties E_x, E_y, G_{xy}, and ν_{xy} were predicted at room and elevated temperatures using Classical Laminate Plate Theory. Calculations for laminates $[0/90]_{2s}$ and $[0/\pm45/90]_s$ at room temperature are contained in Appendix A. The material properties of the fiber and matrix are known quantities. A volume fraction calculation for the laminate was performed. Micromechanics equations were implemented to predict laminae response, namely: Rule of mixtures, Halpin-Tsai, and a third criteria, which assumes no contribution from debonded fibers to the stiffness of the laminae. A criteria for determining the bonded and debonded properties of the laminate was arrived at that compared well with experimental data.

Volume fraction calculations were performed via optical methods. Photographs of a polished edge of several specimens were taken at known magnifications. The total number of

fibers, with mean diameter of 81 μm, in a known cross-section could be counted. The fiber volume fraction was calculated by dividing the sum cross-sectional area of the fibers by the total cross-sectional area. The average fiber volume fraction, V_f = .285, was then used for all subsequent calculations. The volume fraction of the matrix material is simply $V_m = 1 - V_f$.

Rule of Mixtures was used to calculate Young's modulus in the direction of the fibers and the Poisson's ratio for load in the 1 principal direction, Equations 5 and 6. Young's modulus and Poisson's ratio of the fiber are available through Textron manufacturing data (26). The modulus of ß21s was obtained from testing completed by Jalees Ahmad at the Wright Patterson Air Force Base Materials Laboratory (29). Poisson's ratio for Ti-15-3 was implemented for matrix material since ν is an unknown quantity for ß21s at the present time. For an elevated temperature application the corresponding matrix modulus is implemented while the fiber modulus is assumed constant, which is a very good assumption up to 650°C.

$$E_1 = E_f V_f + E_m V_m \qquad (5)$$

$$\nu_{12} = \nu_f V_f + \nu_m V_m \qquad (6)$$

An attempt was made to implement the Halpin-Tsai equations to calculate E_2 and G_{12}. A comparison can be made between the Halpin-Tsai predictions of the initial laminae moduli and results from testing completed by Bearden (30). Providing the deviation between experimentally obtained and analytically

63

predicted moduli is small, Halpin-Tsai equations can then be used to predict debonded properties by assuming that the moduli of the fiber, E_f and G_f, go to zero in the debonded ply. Halpin-Tsai can also be implemented to calculate elevated temperature properties E_2 and G_{12} by inputing the appropriate matrix property at a particular temperature and assuming that the fiber properties are constant at elevated temperature. These equations are of the following form

$$\frac{M}{M_m} = \frac{1 + \xi \eta V_f}{1 - \eta V_f} \tag{7}$$

where

$$\eta = \frac{(M_f/M_m) - 1}{(M_f/M_m) + \xi} \tag{8}$$

with
  M = composite modulus E_2 or G_{12}
  M_f = corresponding fiber modulus E_f or G_f
  M_m = corresponding matrix modulus E_m of G_m

The matrix is considered isotropic, therefore G_m was calculated using $G = E/(2+2\nu)$. ξ is a measure of the fiber reinforcement that depends on the fiber geometry, packing geometry, and loading condition. ξ has a theoretical limit from zero to infinity; when ξ is equal to zero the equations reduce to a series connection model and when ξ is equal to infinity the equations reduce to a parallel connection model.

To match experimental results for E_2, found by testing completed on $[90]_4$ SCS-9/β21s by Bearden (30), ξ would have to be equal -.92. Realize that Halpin-Tsai assumes a perfect bond between the fiber and matrix which is obviously not a

64

proper assumption for this material. Therefore Halpin-Tsai equations were abandoned for prediction of E_2 for bonded and debonded properties at room and elevated temperatures. In the analysis to predict the composite modulus an experimental value for E_2 was, therefore, employed.

Two room temperature tests were conducted on $[\pm 45]_{2s}$ laminates to obtain the experimental composite property G_{12}. Strains, ϵ_x and ϵ_y, were measured in the longitudinal and transverse directions. Figure 29 demonstrates the stress-strain response. From the linear portion of this curve, G_{12} was obtained by the following formula

$$G_{12} = \frac{\sigma_x}{2(\epsilon_x - \epsilon_y)} \tag{9}$$

The average experimental shear modulus at room temperature is 37.5 GPa. To fit experimental results ξ would have to be equal to -1.18, which is again theoretically impossible. Therefore, Halpin-Tsai equations were also abandoned for prediction of the shear modulus and experimental results were used. There exists a present inability to measure transverse strain at elevated temperature, due to the unavailability of high temperature strain gauges. Therefore, the shear modulus at elevated temperature was assumed to be 35.0 Gpa at $482^{\circ}C$ and 30.0 Gpa at $650^{\circ}C$.

Halpin-Tsai proved to be inadequate in predicting bonded properties, therefore it was assumed to be incapable of predicting debonded laminae properties. Instead it was assumed
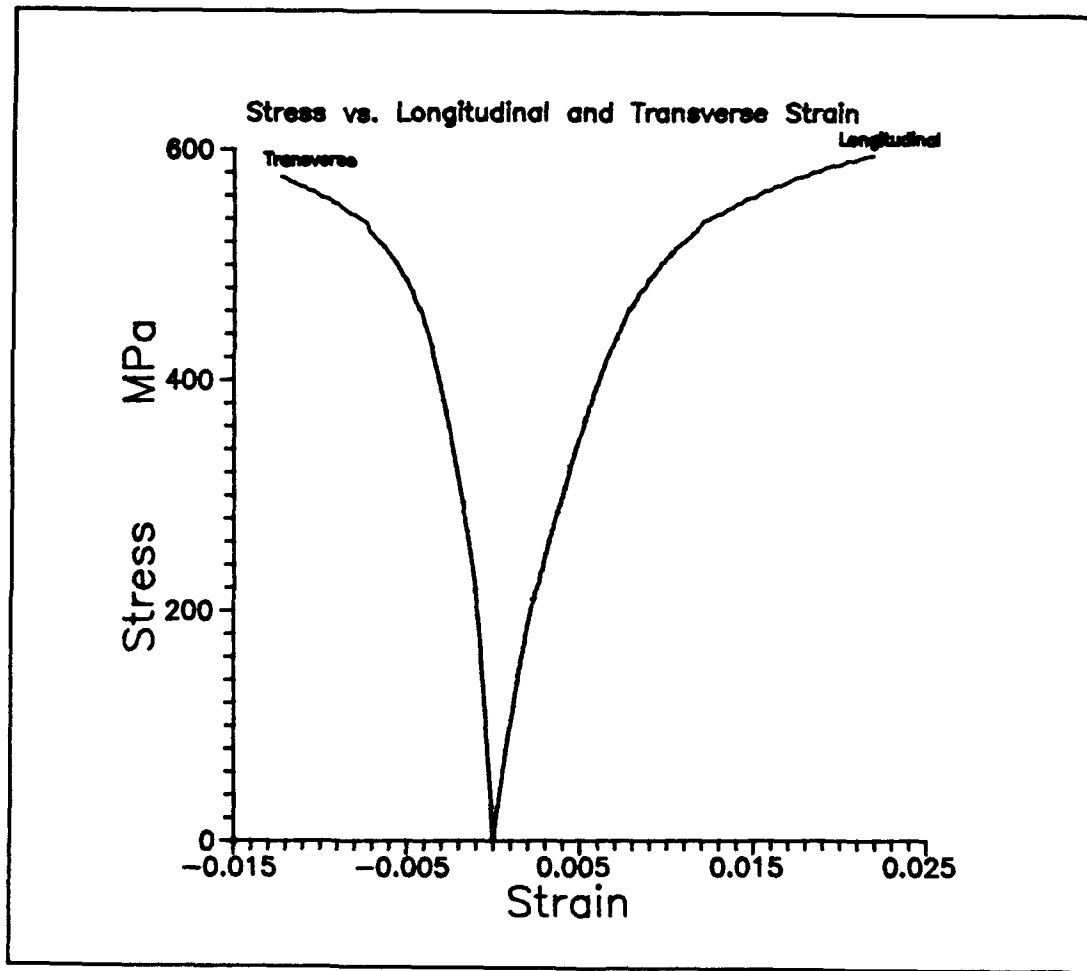
Figure 29 Stress vs. Strain for [±45]₂ₛ Laminate

that the debonded ply can be modeled as matrix material with an appropriate correction factor, namely the matrix volume fraction in the bonded ply. This is done by simply implemented Rule of Mixtures and assigning a zero value to the modulus of the fibers, E_f. This assumption implies that there is no contribution to the stiffness or strength of the laminae from the debonded fibers. Equations 10 through 13 are the mathematical representations of this assumption.

66

$$E_{1d} = V_m E_m \qquad\qquad (10)$$

$$E_{2d} = V_m E_m \qquad\qquad (11)$$

$$G_{12d} = V_m G_m \qquad\qquad (12)$$

$$\nu_{12d} = V_m \nu_m \qquad\qquad (13)$$

The above formulations proved to yield excellent correlation between the predicted and experimentally observed debonded laminate modulus, E_x, at room and elevated temperature. Table 4 incorporates both predicted and experimental values for initial (Ei) and secondary (Es) Young's modulus in the load direction. In Table 4, column A is the prediction of the initial modulus prior to any ply debonding. Column B is the prediction of the secondary modulus with the 90 degree plies debonded. Column C is the prediction of the secondary modulus with both the 90 and 45 degree plies debonded. Realize that the initial modulus in the transverse direction, E_y, is equivalent to E_x in both the cross-ply and quasi-isotropic laminates. Table 5 displays predicted room temperature composite properties ν_{xy} and G_{xy} which will be used in subsequent sections.

From Table 4 an important question can be addressed concerning the failure progression the quasi-isotropic laminates. Recall that acetate replication techniques proved inadequate in determining when the 45 degree plies actually debond. Observing Figure 18 it is evident that there exists two linear portions in a quasi-isotropic stress-strain

Table 4: Experimental and Predicted Properties

Laminate	Temp. C	Exp.Ei Gpa	Exp.Es GPa	Pred. A	Pred. B	Pred. C
[0/90]$_{2s}$	R.T	158.	123.	156.	131.	---
[0/90]$_{2s}$	482	146.	112.	142.	118.	---
[0/90]$_{2s}$	650	118.	77.	114.	99.	---
[0/±45/90]$_s$	R.T	132.	90.	134.	121.	98.
[0/±45/90]$_s$	482	125.	79.	127.	115.	85.
[0/±45/90]$_s$	650	101.	46.	100.	92.	67.

Table 5: Predicted Properties ν_{xy} and G_{xy}

Laminate	ν_{xy}	G_{xy} (GPa)
[0/90]$_{2s}$	0.322	37.50
[0/±45/90]$_s$	0.215	50.79

curve. Since a second knee is non-existent, the 45 degree plies either debond immediately after debonding of the 90 degree plies or they remain bonded until near failure of the composite, Figure 28 proves they are debonded at failure. Modeling the quasi-isotropic laminate with only the 90 degree plies debonded predicts Young's moduli which are 34, 46, and 100 percent higher than experimentally observed values at room temperature, 482°C, and 650°C respectively. Modeling the quasi-isotropic laminate with both the 90 and 45 degree plies debonded predicts values of Young's moduli within 9 percent and 8 percent for room temperature and 482°C. The predicted modulus at 650°C was 46 percent higher than the experimental

value. This deviation is expected due to the fact that matrix yielding obscures the second linear region. Once the 90 degree plies debonds, the 45 and 0 degree plies must assume more of the applied stress. This incremental increase in stress in the 45 degree ply causes it to debond immediately after the 90 degree plies debond.

Prediction of Unnotched Laminate Strengths

Unnotched laminate strengths were predicted via Classical Laminate Plate Theory. Due to the anisotropic and heterogeneous nature of composite materials, failure of one ply does not necessary imply failure of the laminate; but rather is usually manifested as a reduction in stiffness. In an attempt to match experimental ultimate strength values, total discount and limited discount methods were implemented. Both maximum stress and Tsai-Hill failure criteria were applied in the analysis. In maximum stress failure criteria, the stresses in the principal material directions for each ply of the laminate must be less than the respective strengths. Therefore, the maximum stress failure theory is actually three separate subcriteria with no interaction between modes of failure. Tsai-Hill failure theory is an extension of von-Mises isotropic yield criteria and unlike the maximum stress theory it reduces to an isotropic material result by assuming maximum octahedral shear stress theory. Tsai-Hill theory takes into account the interaction of different modes of failure: tensile, compressive, and shear. For plane stress in

the 1-2 plane of a unidirectional laminae with fibers in the 1 direction Tsai-Hill failure criteria can be represented in the form of Equation 14a.

$$\frac{\sigma_1^2}{S_1^2} - \frac{\sigma_1\sigma_2}{S_1^2} + \frac{\sigma_1^2}{S_2^2} + \frac{\sigma_{12}^2}{S_{12}^2} = 1 \qquad (14a)$$

In a total discount method, once a ply reaches its laminae failure stress in either shear, tension or compression that ply is assumed to contribute no stiffness or strength in the laminate. In a limited discount method, once the stresses in a particular ply reach laminae failure stresses that ply is assigned appropriate constituent properties depending upon the criteria chosen.

Constituent properties are necessary in order to obtain stresses in the principal material directions for each ply in the composite. The values of these properties, namely E_1, E_2, G_{12}, and ν_{12} were discussed in a previous section and are available in Appendix A. The fundamental laminae strengths are also necessary for this analysis. For a laminae stressed in its own plane, there are three fundamental strengths, S_1, S_2, and S_{12}. S_1 is the axial or longitudinal strength, S_2 is the transverse strength, and S_{12} is the shear strength. Experimental values for S_1 and S_2 were obtained through research completed by Bearden and Mall on tensile tests of $[90]_4$ and $[0]_4$ laminates (30). These values are presented in Table 6. An off-axis specimen strength result was used in

70

conjunction with Tsai-Hill failure criterion in order to estimate the shear strength. Two tests at room temperature, $482°C$, and $650°C$ were completed for $[16]_{16}$. The stress-strain (mechanical) response is graphically presented in Figure 30. The coefficient of thermal expansion for this laminate was calculated to be $5.87e-6/°C$ ±.30. With known failure strength, σ_x, known laminae strengths S_1 and S_2, and known angle θ, the shear strength was obtained through Equation 14b.

$$\frac{1}{\sigma_x^2} = \frac{\sin^4\theta}{S_2^2} + \left[\frac{1}{S_{12}^2} - \frac{1}{S_1^2}\right]\cos^2\theta\sin^2\theta + \frac{\cos^4\theta}{S_1^2} \qquad (14b)$$

All specimens failed in shear along the fiber longitudinal axis. The average experimental values for S_{12} are included in Table 6 for room temperature, $482°C$, and $650°C$.

Total discount failure criterion in conjunction with maximum stress failure theory was attempted for laminate $[0/90]_{2s}$ at room temperature. Failure of the composite was predicted to occur at an applied stress of 498.7 MPa. Actual specimen failure occurred at 906.2 MPa. Therefore, the total discount method was abandoned for all subsequent analysis.

In attempting to predict laminate strengths via limited discount, two methods were implemented. In the first, once a particular laminae failed it was assigned matrix properties, for example: $E_1 = E_m$, $E_2 = E_m$, $\nu_{12} = \nu_m$, and $G_{12} = G_m$. This

71
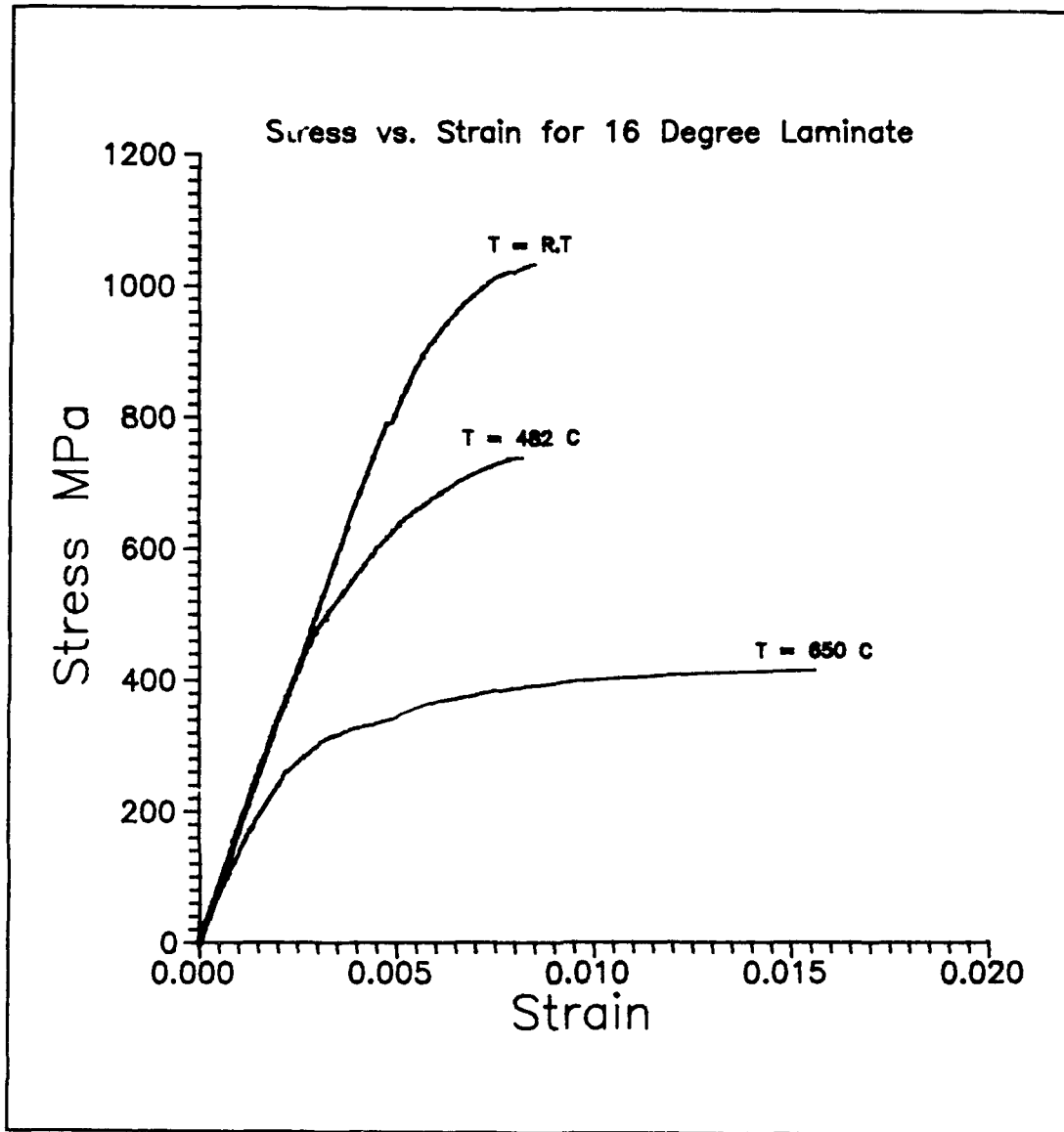
Figure 30 Stress vs. Strain Response of [16]$_{16}$

Table 6: Fundamental Laminae Strengths

Temp. C	S$_1$ MPa	S$_2$ MPa	S$_{12}$ MPa
R.T	1317	464	394
482	1129	342	235
650	636	123	122

method proved to overestimate the laminate strength. This is due to the fact that the failed ply cannot be modeled as homogeneous matrix material, disregarding the effect of off-axis fibers which still occupy a given volume but can no longer assume any of the applied load. In an attempt to correct for this, a second method was implemented which uses Equations 10 through 13 to model the failed laminate as matrix material with a correction factor. Intuitively this would seem more realistic since in the absence of delamination, which was never detected during acetate replication or observation of failed specimens, the matrix material of a failed ply is still consolidated to the adjacent plies. In Table 7 the predicted failure strengths, employing maximum stress theory, and experimentally observed failure strengths are displayed in MPa. Table 8 presents the results obtained implementing Tsai-Hill failure theory, again stress is given in MPa. Due to the acceptable deviations between predicted

Table 7: Laminate Strength Predictions Maximum Stress

Laminate	Temp. C	Exp. σ_{ult}	Pred. σ_{ult}	% Error
$[0/90]_{2s}$	R.T	906.2	888.2	2.0
$[0/90]_{2s}$	482	680.6	734.9	8.0
$[0/90]_{2s}$	650	408.0	396.9	2.7
$[0/\pm45/90]_s$	R.T	776.9	838.9	8.0
$[0/\pm45/90]_s$	482	575.5	542.8	5.7
$[0/\pm45/90]_s$	650	339.7	278.2	18.1

Table 8: Laminate Strength Predictions Tsai-Hill

Laminate	Temp. C	Exp. σ_{ult}	Pred. σ_{ult}	% Error
$[0/90]_{2s}$	R.T	906.2	897.6	0.9
$[0/90]_{2s}$	482	680.6	742.3	9.1
$[0/90]_{2s}$	650	408.0	391.1	4.1
$[0/\pm45/90]_s$	R.T	776.9	703.9	9.4
$[0/\pm45/90]_s$	482	575.5	535.4	7.0
$[0/\pm45/90]_s$	650	339.7	264.0	22.3

and experimental results, in spite of the elastic-plastic behavior of the laminate which cannot be modeled through CLPT, this method will be employed in subsequent sections where notched failure strength predictions are attempted.

Open Hole Specimen Evaluation

SCS-9/ß21s laminates of $[0/90]_{2s}$ and $[0/\pm45/90]_s$ lay-ups with open holes were investigated under static tensile loading. All specimens had a width to diameter ratio of approximately six. The same three temperature regimes analyzed for unnotched specimens were implemented for testing of notched specimens, namely room temperature, 482°C, and 650°C. Acetate replication, microscopy, and fractography were used to aid in the definition of failure progression. The notch sensitivity of both laminates at each temperature will be addressed. Theoretical elastic and plastic stress concentration factors were calculated and applied in an attempt to predict the notched laminate strength based on a

gross applied stress.

Room Temperature Response

Figures 31 and 32 are typical stress-strain curves for room temperature $[0/90]_{2s}$ specimens and $[0/\pm45/90]_s$ specimens. For a room temperature test three strains could be measured, discussed thoroughly in Chapter 3, using two strain gauges and a 1.27 cm extensometer which could be mounted locally or remotely. Throughout this discussion a local extensometer is defined as mounting the extensometer with the ceramic rods encompassing the hole; a remote extensometer is defined as mounting the extensometer at least five hole diameters away from the hole in the specimen. Both Figures 31 and 32 incorporate a remote extensometer which correlates very well with a remote strain gauge, as it should. Local strain is defined as a strain gauge mounted at 90 degrees along the periphery of the hole, refer to Figure 12, Chapter 3. In Figures 31 and 32 the ordinate represents a gross stress.

From these two figures three important points can be made regarding the effect of the hole in both laminates. First, the knee in the stress-local strain curve occurs at a stress level approximately 25 to 30 percent lower than the knee in the stress-remote strain curve. Second, the experimental values of the initial and secondary Young's modulus determined from the stress-remote strain curves are much higher than the modulus obtained from the stress-local strain curves. Figure 33 displays the initial portion of the stress-strain curves
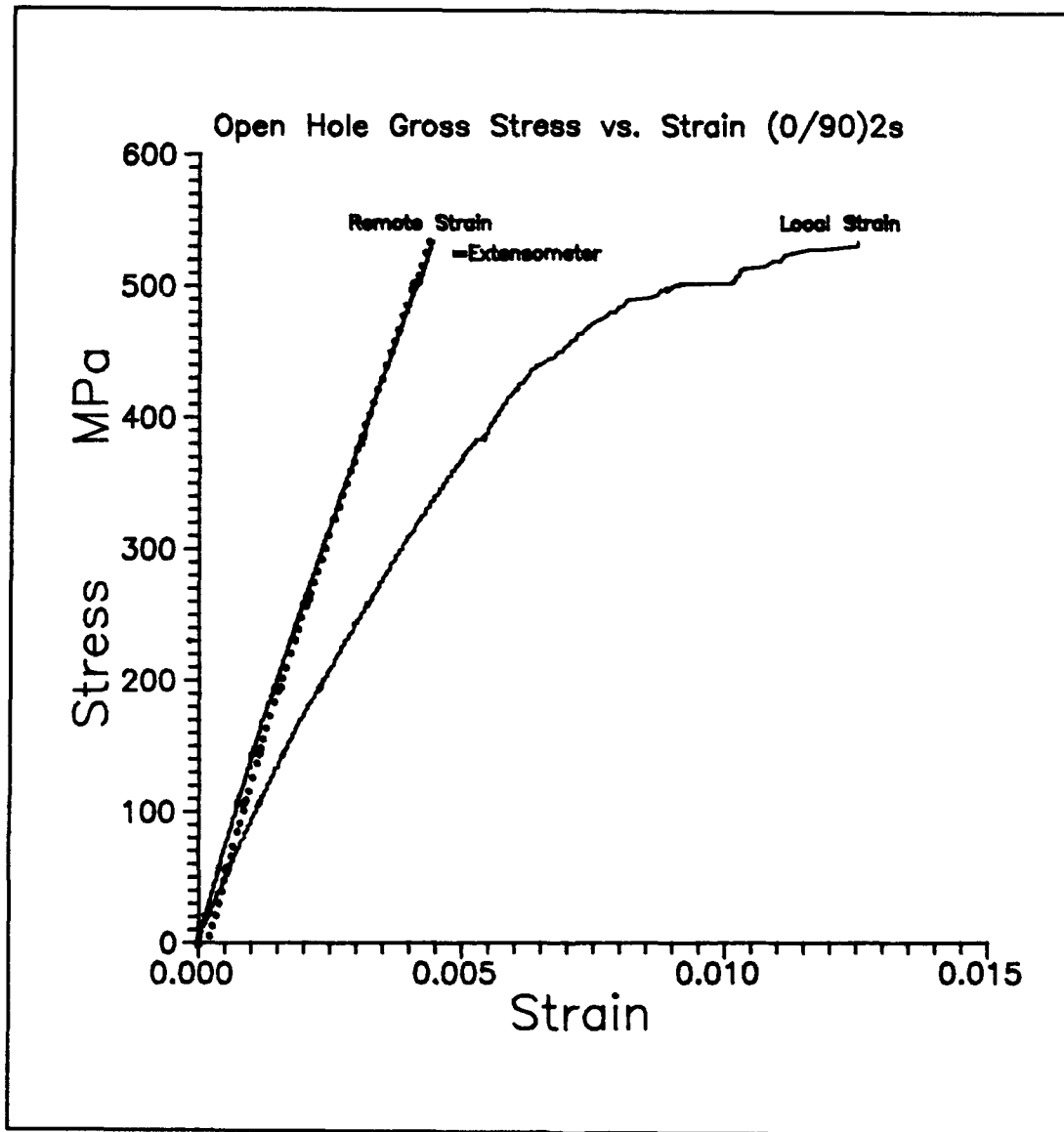
Figure 31 Open Hole Gross Stress vs. Strain $[0/90]_{2s}$ at Room Temperature

for the $[0/90]_{2s}$ laminate. The initial remote modulus is 38 percent higher than the initial local modulus. The secondary remote modulus is 41 percent higher than the secondary local modulus. Figure 34 displays the initial portion of the
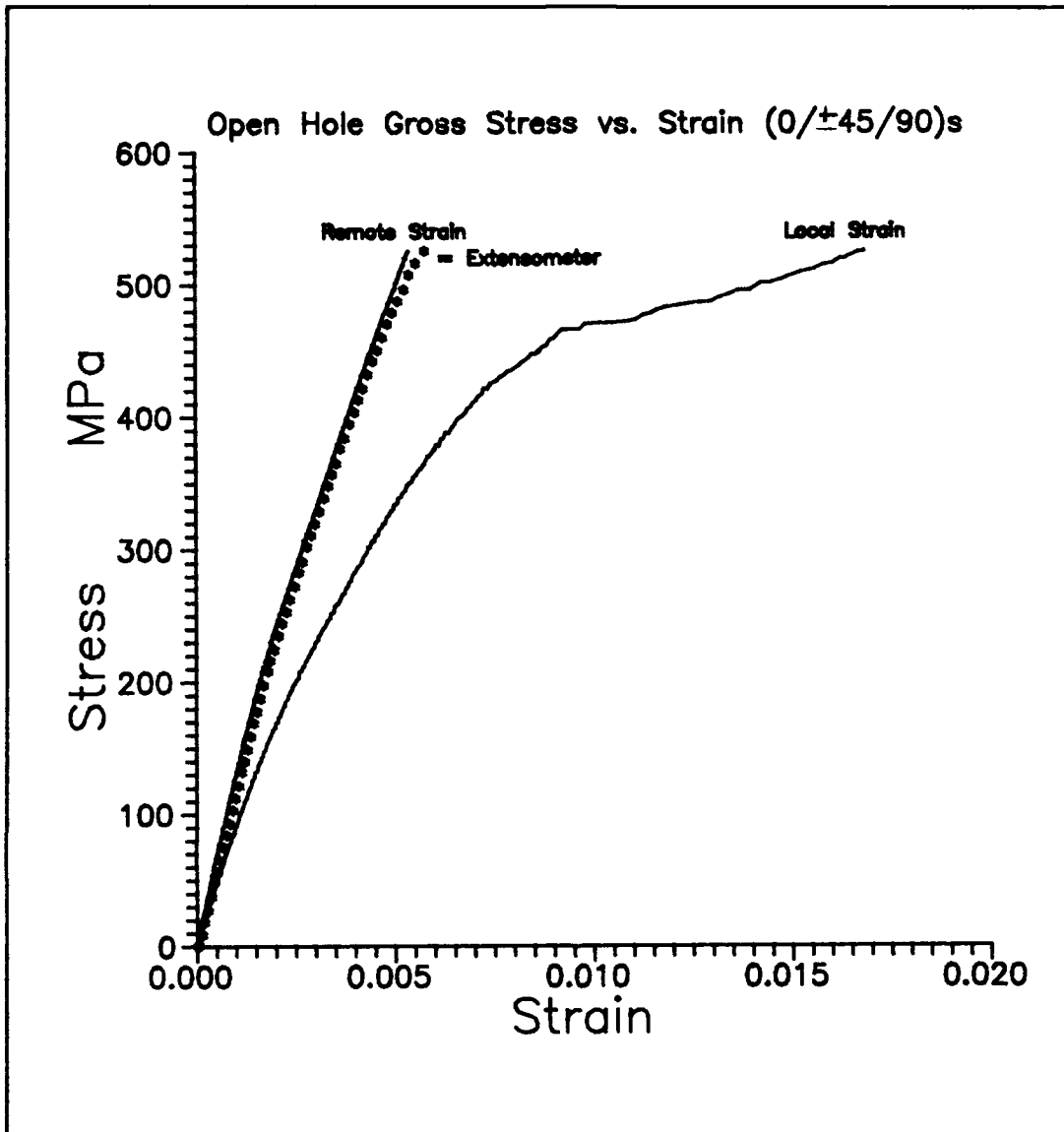
Figure 32 Open Hole Gross Stress vs. Strain [0/±45/90]$_s$ at Room Temperature

stress-strain curves for the [0/±45/90]$_s$ laminate. The initial remote modulus is 38 percent higher than the initial local modulus. The secondary remote modulus is 23 percent higher than the secondary local modulus. The initial remote
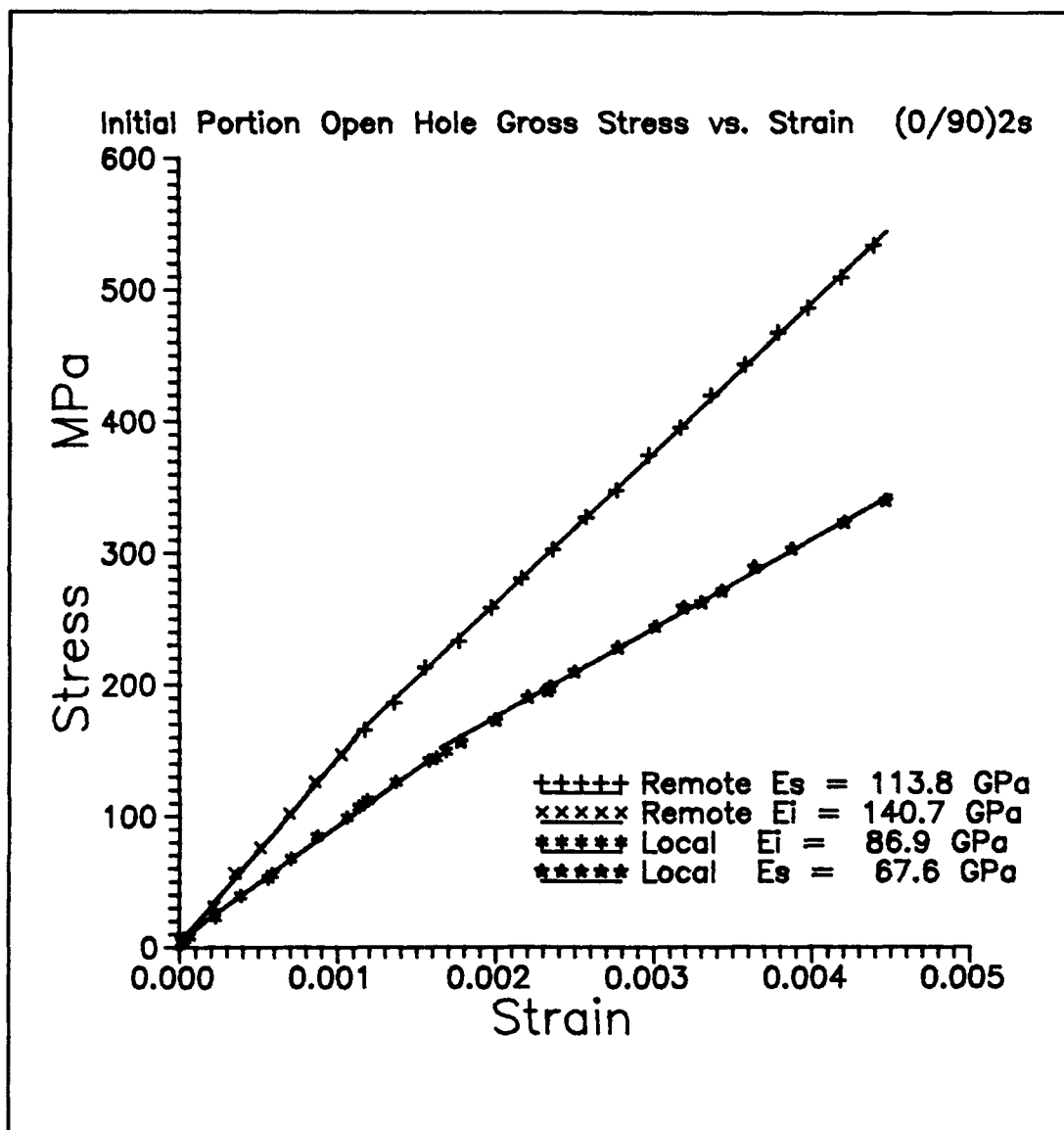
Figure 33 Initial Portion of Stress-Strain Curves
$[0/90]_{2s}$

modulus of the notched specimens was within 14 percent of the unnotched modulus in both laminates for all temperatures. This is an acceptable deviation considering the specimens were cut from different panels. And thirdly, the amount of
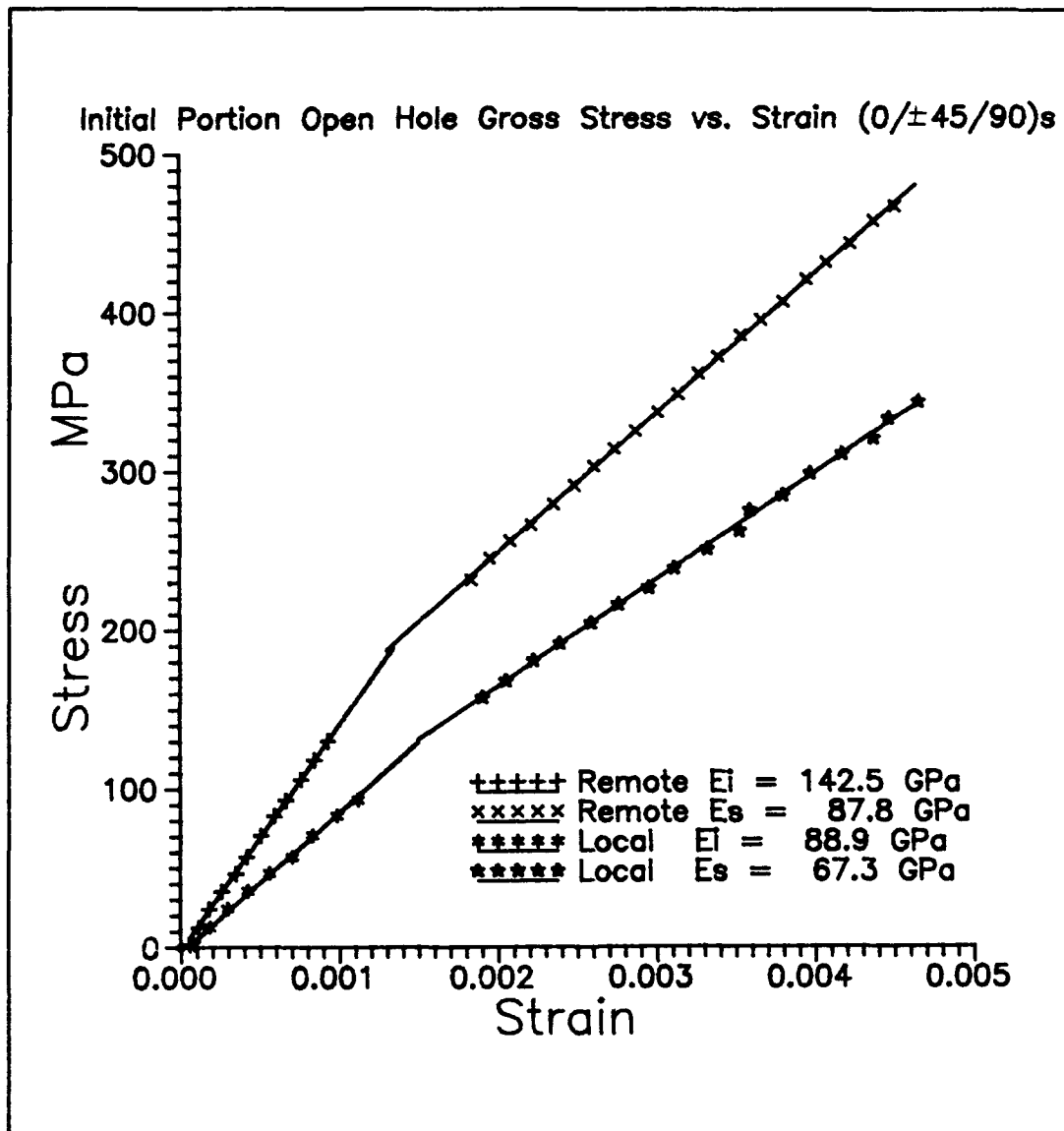
Figure 34 Initial Portion of Stress-Strain Curves
[0/±45/90]$_s$

accumulated strain prior to failure near the hole is extensive relative to the remote failure strain. In the cross-ply laminate the failure strain measured by the local strain gauge exceeds 1.25 percent. The quasi-isotropic laminate exhibited

local strains exceeding 1.68 percent. It is important to note that the yield strain of ß21s is approximately 1 percent at room temperature, below the local failure strains of both laminates, and the failure strain of the SCS-9 fibers is around one percent. Therefore, plasticity and damage should be expected to be evident near the hole and fracture surface. All three of the aforementioned points can be attributed to the existence of a stress concentration factor at room temperature. A theoretical attempt will be made to quantify the elastic and plastic stress concentration factors for both laminates in a subsequent section.

Elevated Temperature Response

In elevated temperature testing only the 1.27 cm extensometer was utilized for local and remote strain measurement and therefore local strain will now be defined as a local extensometer, refer to Figure 12 Chapter 3. The stress-local strain data must be analyzed separately from the stress-remote strain data in order to address the effect of the hole. Tables 9 and 10 contain the results from testing done on notched $[0/90]_{2s}$ and $[0/\pm45/90]_s$ laminates at room temperature, 482°C, and 650°C. The stress given in the tables is a gross stress. The thermal strain has been deducted out leaving an ultimate mechanical failure strain. The ultimate strain is either a remote strain or a local strain depending on the extensometer position, column 2 in the tables.

Table 9: Notched [0/90]$_{2s}$ Laminates W/D=6

Specimen Id.	Remote/ Local	Temp C	σ_{ult} MPa	ϵ_{ult}	Ei GPa	Es GPa
13	Remote	R.T	533.6	.0044	137.0	116.0
14	Remote	R.T	544.6	.0045	141.0	114.0
19	Local	R.T	581.7	.0055	117.0	107.0
20	Remote	482	443.0	.0045	131.0	99.0
21	Local	482	441.8	.0050	-----	-----
15	Local	650	293.0	.0092	121.0	77.0
16	Remote	650	253.6	.0047	-----	-----
18	Remote	650	265.5	.0042	101.0	82.0

----- : Modulus unattainable due to acetate replication

Table 10: Notched [0/±45/90]$_s$ Laminates W/D=6

Specimen Id.	Remote/ Local	Temp C	σ_{ult} MPa	ϵ_{ult}	Ei GPa	Es GPa
1	Remote	R.T	549.7	.0056	143.0	87.0
2	Local	R.T	525.5	.0054	130.0	92.0
10	Remote	482	437.4	.0051	130.0	79.0
5	Local	482	426.7	.0063	116.0	72.0
11	Remote	650	293.2	.0054	103.0	50.0
3	Local	650	272.4	.0137	116.0	77.0

Figures 35 and 36 present the cross-ply data in graphical form. Figure 35 displays data obtained with a remote extensometer while Figure 36 presents local extensometer data. A polynomial curve fit has been drawn through some data due to unavoidable noise in the system during a particular test. Again, the initial and secondary moduli, obtained from a remote extensometer in both [0/90]$_{2s}$ and [0/±45/90]$_s$ specimens,

81
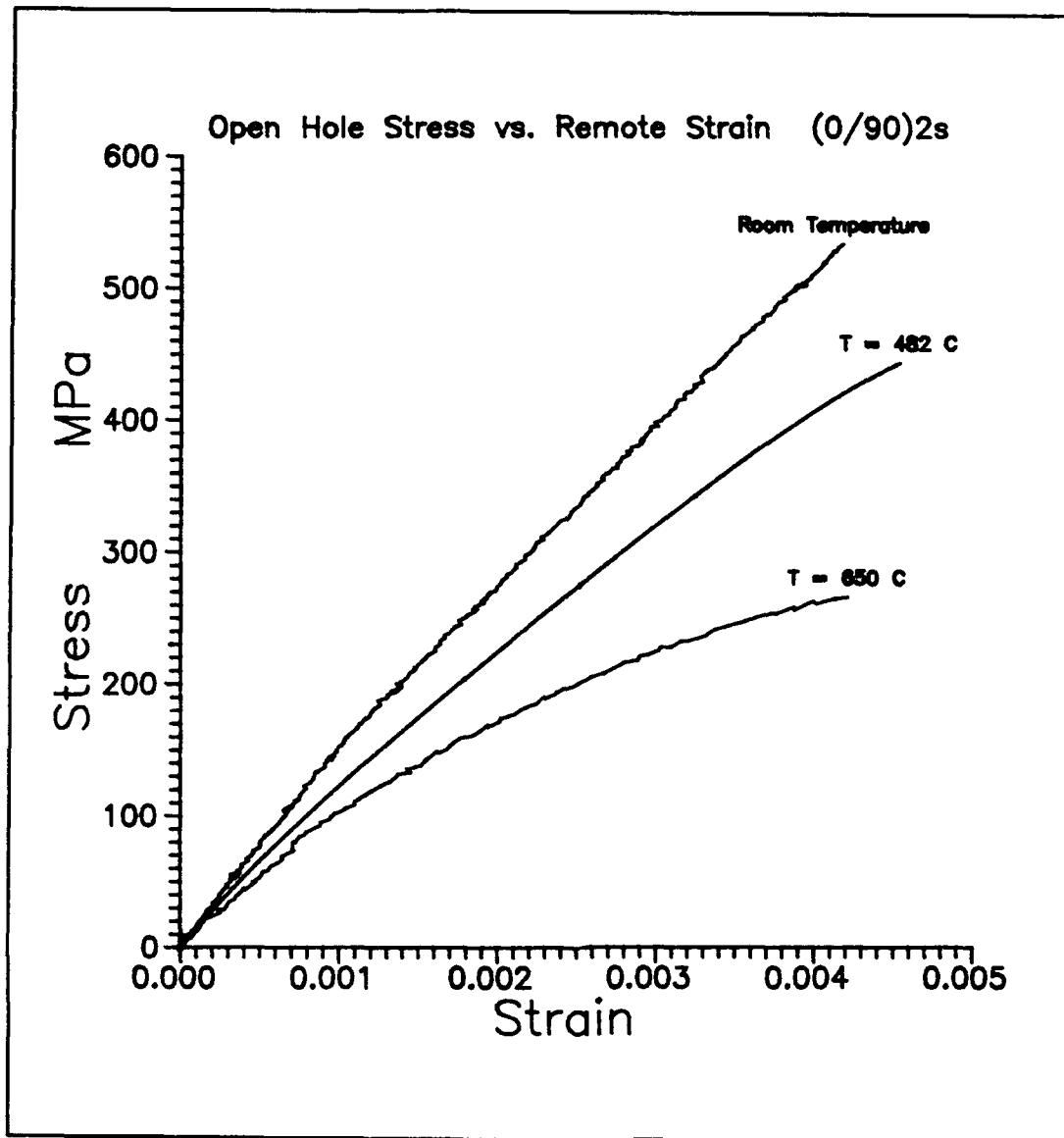
Figure 35 Open Hole Stress vs. Remote Strain $[0/90]_{2s}$

are within 15 percent of the unnotched specimen moduli. This is a relatively small experimental deviation considering the specimens were cut from different panels. Figure 37 displays the stress-strain curve for the $[0/\pm45/90]_s$ laminate while implementing a remote extensometer. Figure 38 presents local
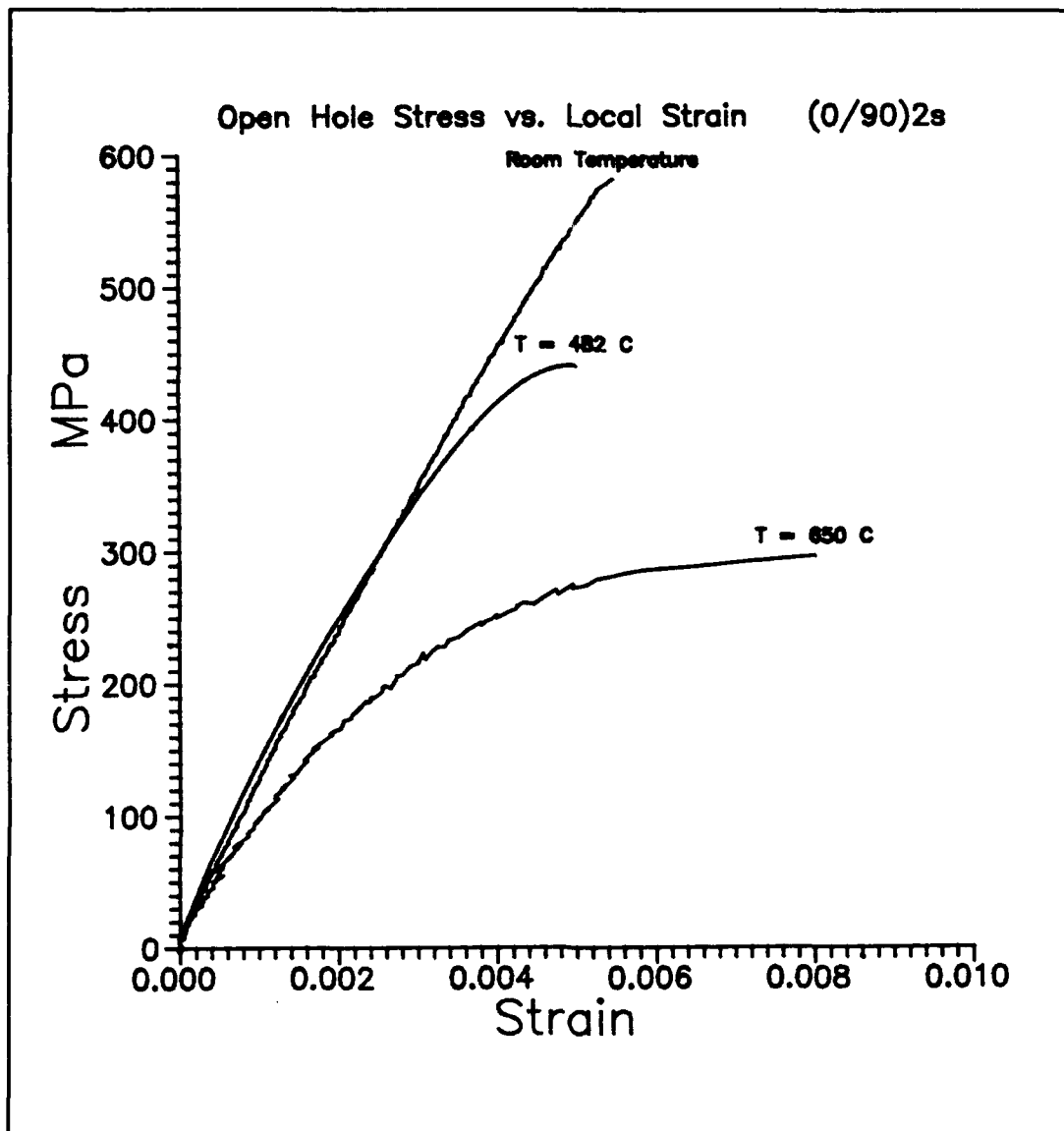
Figure 36 Open Hole Stress vs Local Strain $[0/90]_{2s}$

extensometer stress-strain data. The second linear portion of the $650°C$ tests is obscured in both laminates due to matrix yielding, therefore the secondary modulus for this temperature regime is not very reliable measurement for either laminate. This material behavior has been addressed thoroughly in the
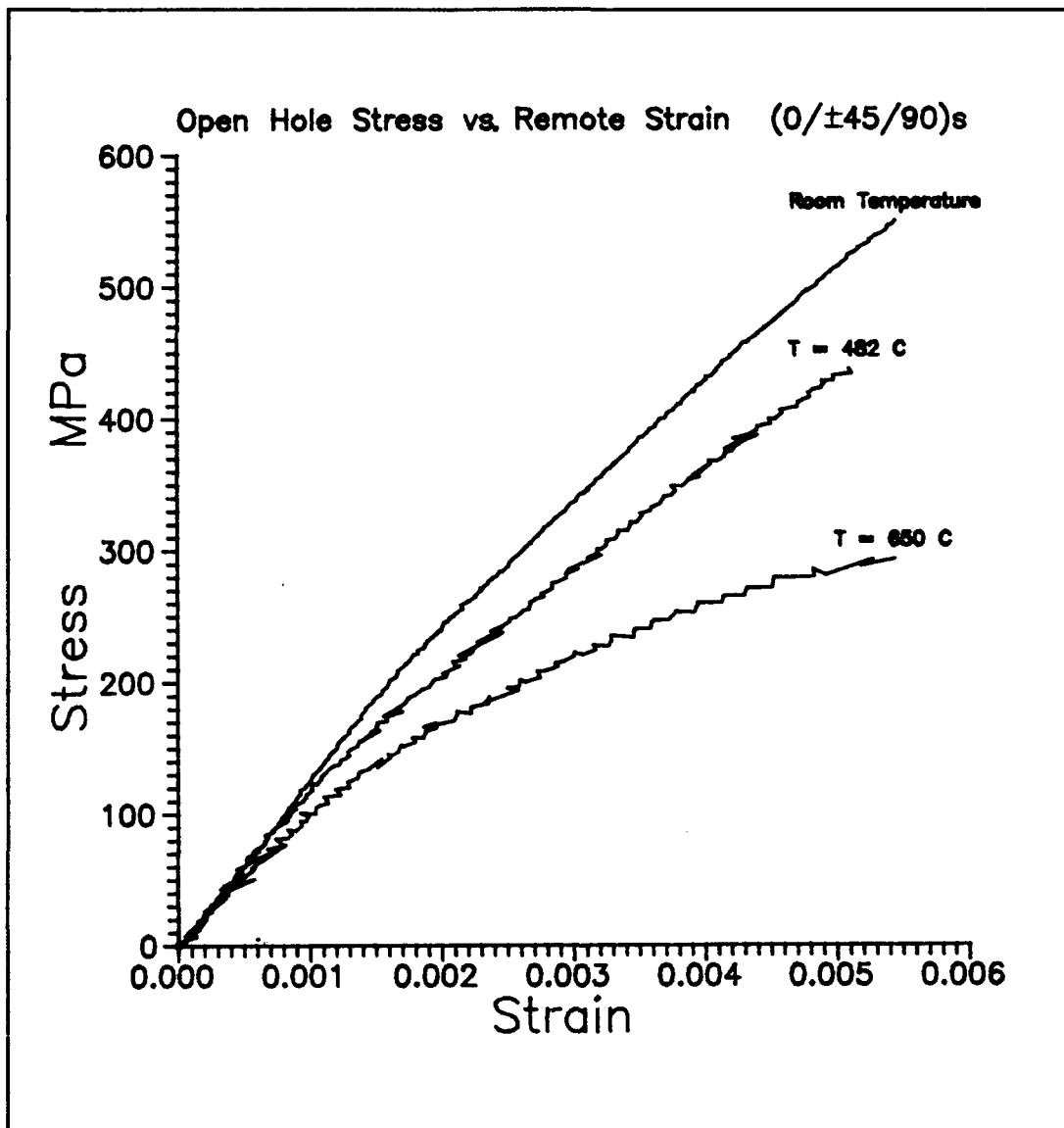
Figure 37 Open Hole Stress vs. Remote Strain $[0/\pm45/90]_s$

unnotched specimen analysis.

The initial modulus from remote data for both laminates is significantly higher then the initial modulus from local data at room temperature; this is due to the existence of a stress concentration at room temperature. It is not possible to draw

84
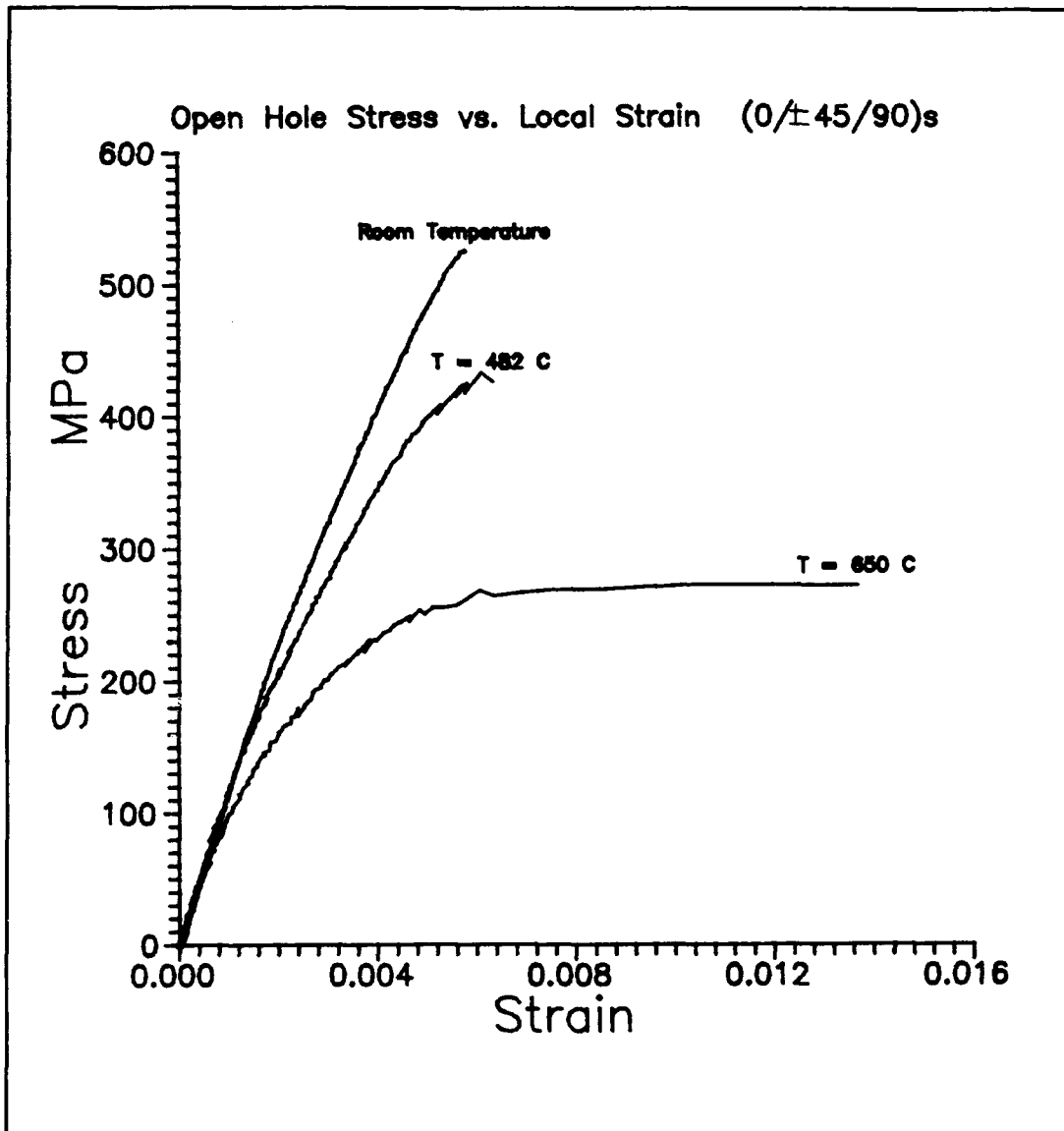
Figure 38 Open Hole Stress vs. Local Strain $[0/\pm45/90]_s$

this conclusion for both laminates at 482°C due to a lack of local stiffness data for the $[0/90]_{2s}$ laminate. At 650°C neither laminate exhibits a decrease in stiffness due to the existence of the hole, suggesting notch insensitivity.

Figures 36 and 38 exhibit large local failure strains by

85

both laminates at the 650°C temperature regime in comparison with the room temperature and 482°C data. This large failure strain is due to the extensive debonding and failure of 0 degree fibers in the net section. No evidence was obtained through acetate replication to prove debonding of 0 degree fibers at room temperature and 482°C; but it can be shown through optical microscopy that debonding of the 0 degree fibers occurs in a very small localized area immediately adjacent to the failure surface. On the other hand, acetate replication technique proves that the debonding of the 0 degree fibers begins to occur at as low as 30 percent of the failure strength of the laminates at 650°C. This is due the relaxation of the residual stresses and the extreme drop in matrix strength at this temperature regime. Figure 39 presents a photograph of a replica taken at 30 percent of the failure strength in a 650°C tensile test. **The load and the 0 degree fiber are in the vertical direction**. Note that both the 90 and 0 degree fibers have been debonded. Recall that the composite was shown, Chapter 3, to contain broken fibers due to the manufacturing process. Once a broken fiber debonds from the matrix it can no longer carry load. Also visual examination of failed specimens displays much fiber pull-out, macroscopic evidence of fiber debonding, at 650°C and little or none at room temperature and 482°C, Figure 40. Figure 41 displays SEM photographs of a $[0/90]_{2s}$ specimen at 650°C loaded to 94 percent of the failure strength. The load is in the
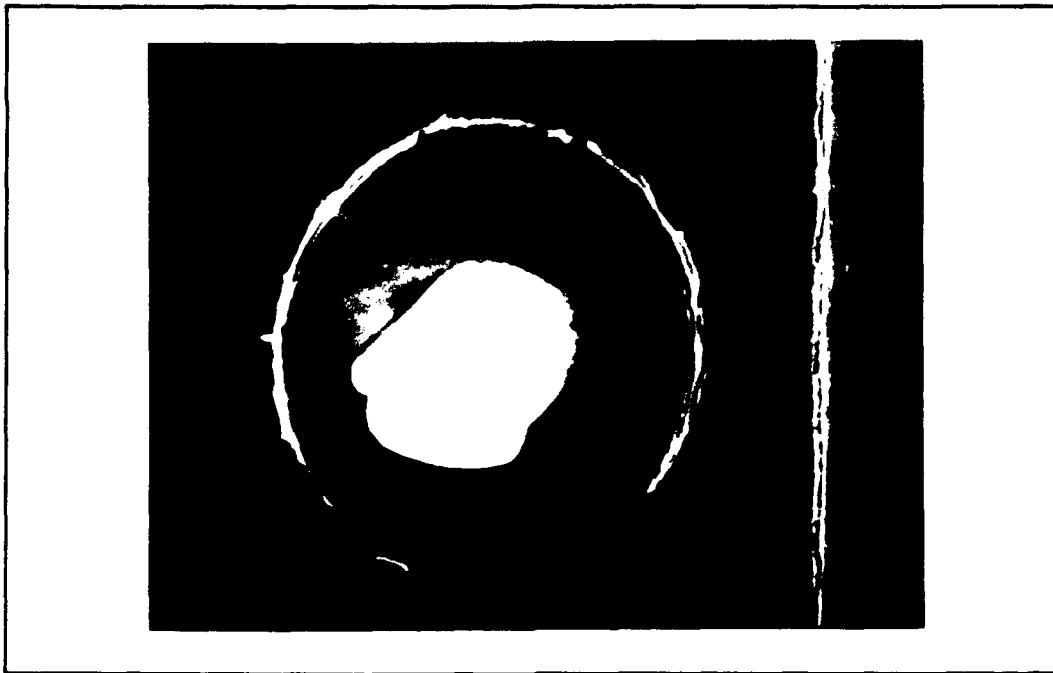
Figure 39 0 Degree Fiber Debonded at 30 Percent Failure
Stress at 650°C

direction of the arrows. The matrix material has been etched
down to the first 0 degree ply using Kroll's etchant. From
this photograph it is seen that practically all the 0 degree
fibers have failed across the net section and are separating
under the tensile load prior to failure of the composite. It
should also be noted that the failure strength of ß21s is 270
MPa at 650°C. This is within 8 percent of the failure
strengths of both the $[0/90]_{2s}$ and $[0/\pm45/90]_s$ specimens at
650°C. The excessive degree of nonlinearity is caused by the
debonding and failure of the 0 degree fibers in the net
section for the 650°C tensile tests. The failed fibers can no
longer assume any of the applied gross stress, causing the

87
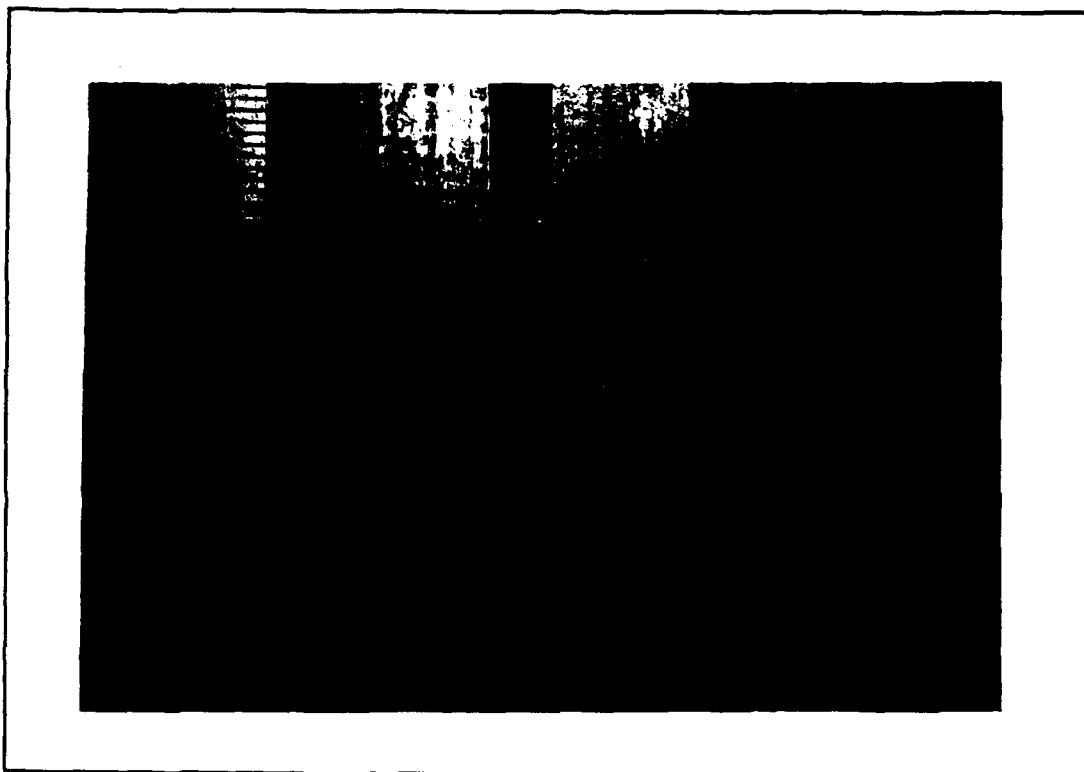
Figure 40 Failed Room Temperature, 482°C, and 650°C
Specimens (From Left to Right)

ultimate strength of both laminates at 650°C to be equivalent, within the experimental deviation, to the ultimate strength of β21s. Young's modulus of β21s at 650°C is 66 MPa while the initial modulus of the cross-ply and quasi-isotropic laminates are greater than 100 MPa. Therefore, the 0 degree fibers are bonded initially and carry load during the initial portion of the stress-strain curve; or heat alone does not cause debonding in the 0 degree plies. The secondary modulus in the 650°C specimens, although obscured by matrix yielding, approaches the modulus of β21s at 650°C.
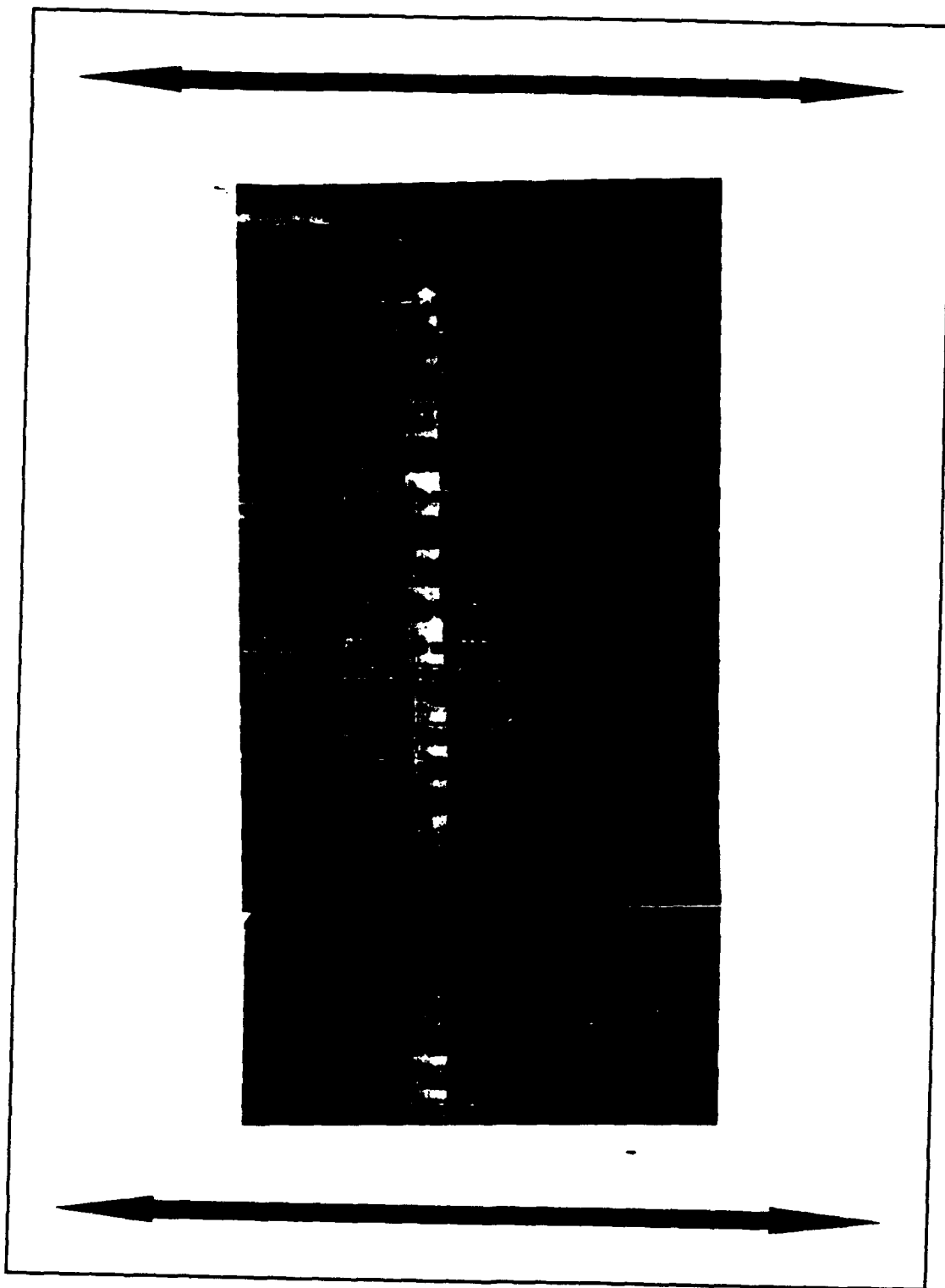
Figure 41 [0/90]$_{2s}$ Laminate at 94 Percent of the Failure
Strength at 650°C

Analyzing the percent failure stress, locally and remotely, where a knee becomes evident implies that the 90 and 45 degree fibers near the hole debond prior to remote debonding in all temperature regimes. Table 11 displays the percent failure stress where the knee occurs for both laminates as a function of temperature and the position of the extensometer, local or remote.

Table 11: Percent Failure Stress for Initiation of Debonding

Laminate	Temp. C	$\%\sigma_{ult}$ Remote	$\%\sigma_{ult}$ Local
$[0/90]_{2s}$	R.T	32	29
$[0/90]_{2s}$	482	24	21
$[0/90]_{2s}$	650	28	22
$[0/\pm45/90]_s$	R.T	29	25
$[0/\pm45/90]_s$	482	20	20
$[0/\pm45/90]_s$	650	28	18

Comparing acetate replication photographs of an unnotched specimen in a 482°C tensile test, Figures 21 through 25, with acetate replication near the hole, Figure 42, also proves that at the same applied gross stress the 90 degree fibers have debonded near the hole prior to any remote debonding. Realize that this stress level, 21 percent of the failure stress, is at the knee in the stress-local strain curve and below the knee in the stress-remote strain curve.

Fracture surfaces exhibit distinct characteristics

The fracture surfaces of the cross-ply and quasi-isotropic laminates were examined via optical and scanning electron
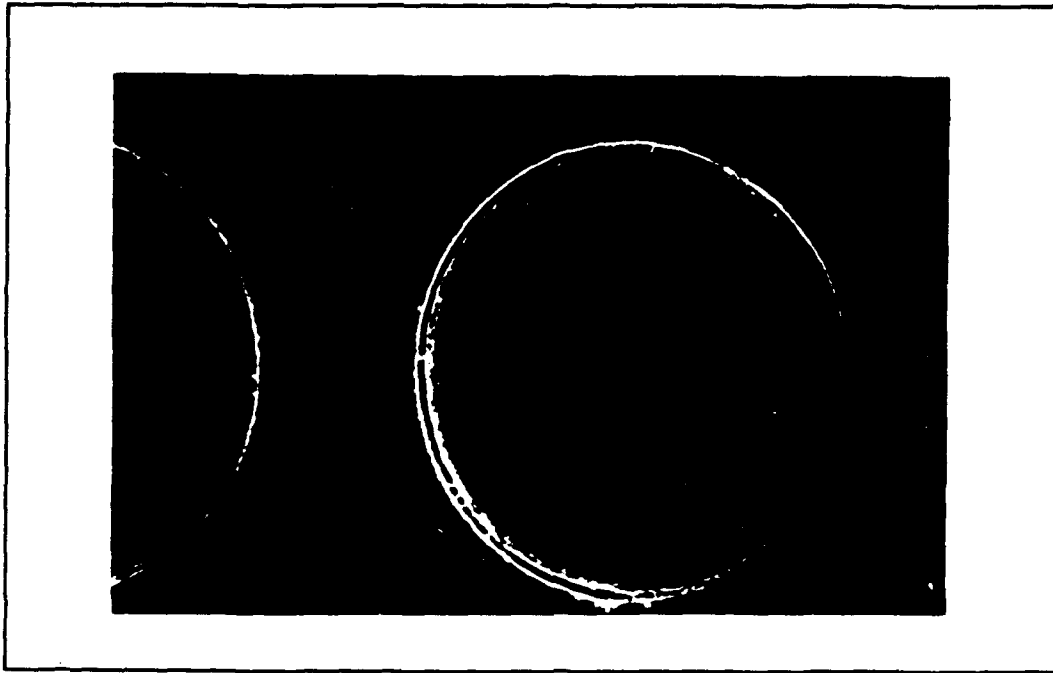
Figure 42 21 % of Failure Stress Near Hole

microscopy. Specimens tested at room temperature and 482°C exhibited little or no matrix cracking near the fracture surface. Figures 43 and 44 are optical photographs of an initially polished edge after failure of a typical [0/90]$_{2s}$ and [0/±45/90]$_s$ specimen tested at room temperature. A few small matrix cracks are evident under higher magnification immediately adjacent to the fracture surface; but in general, there is an absence of large scale matrix cracking. Figures 45 and 46 are photographs of typical [0/90]$_{2s}$ and [0/±45/90]$_s$ specimens tested at 650°C. These specimens exhibit numerous matrix cracks near the fracture surface and obvious debonding of the 0 degree fibers. The cracks can be seen emanating from the interface of the debonded 0 and 90 degree fibers and

91
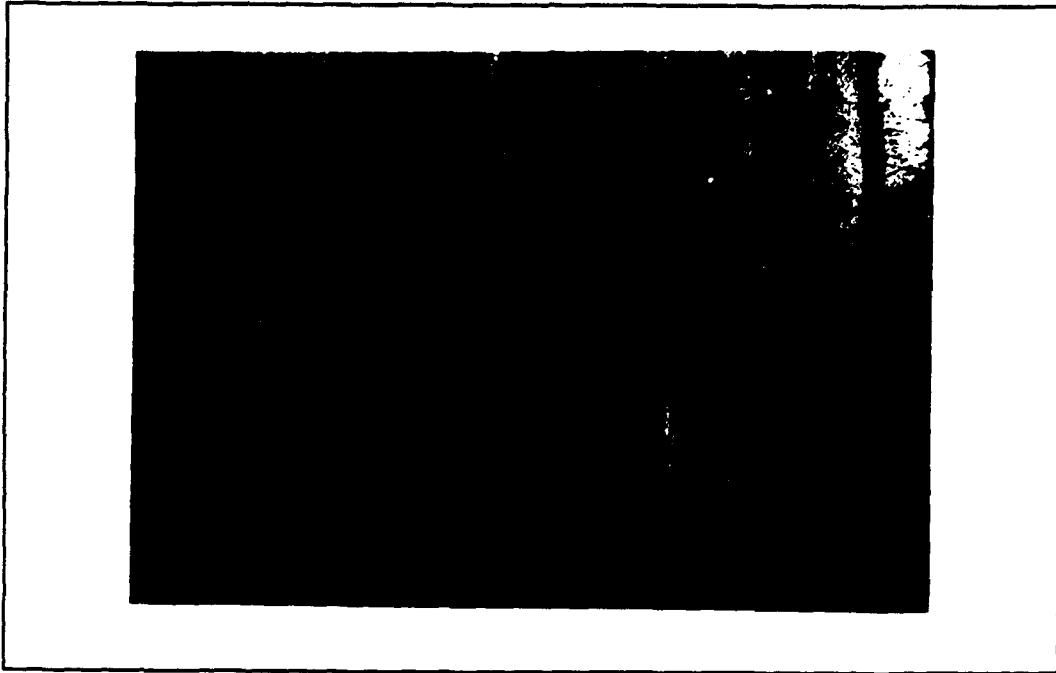
Figure 43 Fracture Edge at Room Temperature $[0/90]_{2s}$

Figure 44 Fracture Edge at Room Temperature $[0/\pm45/90]_s$
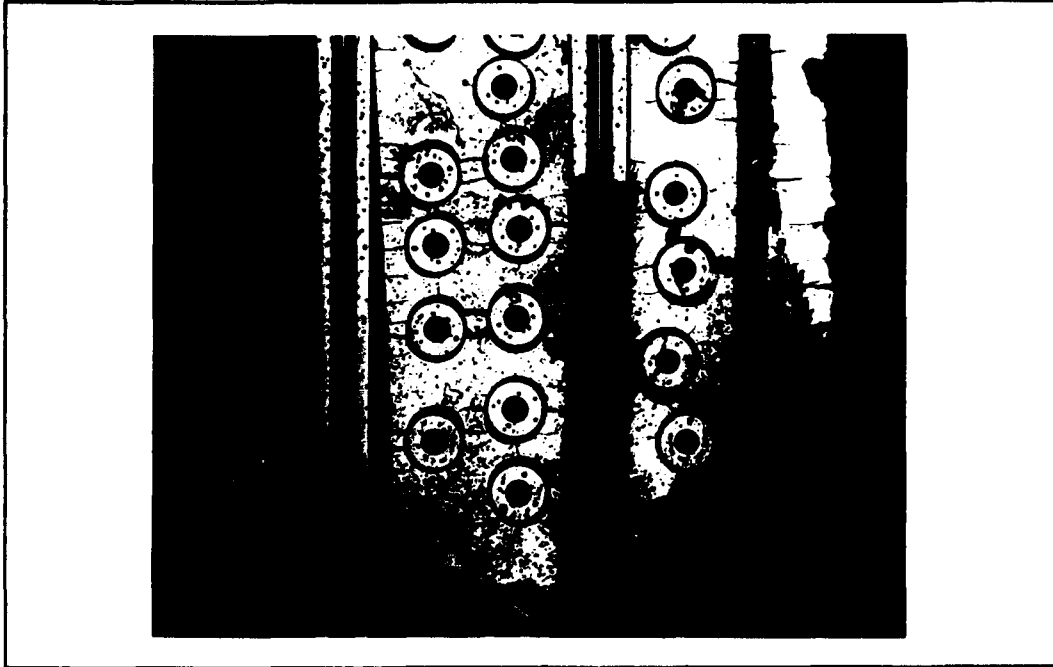
Figure 45 Fracture Edge at 650°C $[0/90]_{2s}$
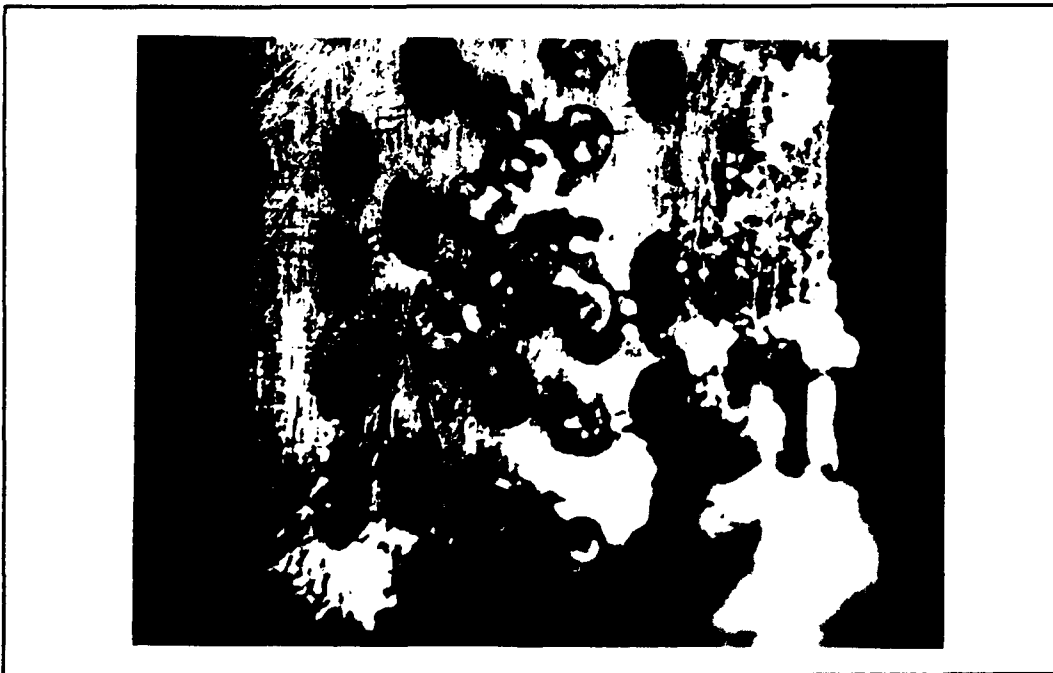
Figure 46 Fracture Edge at 650°C $[0/\pm45/90]_s$

93

growing into the matrix. Figure 47, another optical photograph of a $[0/90]_{2s}$ specimen this time taken approximately five hole diameters away from the fracture surface, proves that the matrix cracking is not locally confined to the fracture surface. Figure 48 shows similar characteristics at approximately one hole diameter away from the fracture surface in the $[0/\pm45/90]_s$ laminate. Since matrix cracking could not be detected during acetate replication it is therefore believed to occur after 85 percent of the failure strength of the laminates. Matrix cracking probably does not occur at room temperature and 482°C because the matrix strength is 4.5 to 3.4 times higher than at 650°C and the 0 degree fibers do not exhibit gross debonding.

Figure 47 $[0/90]_{2s}$ at 650°C Remote
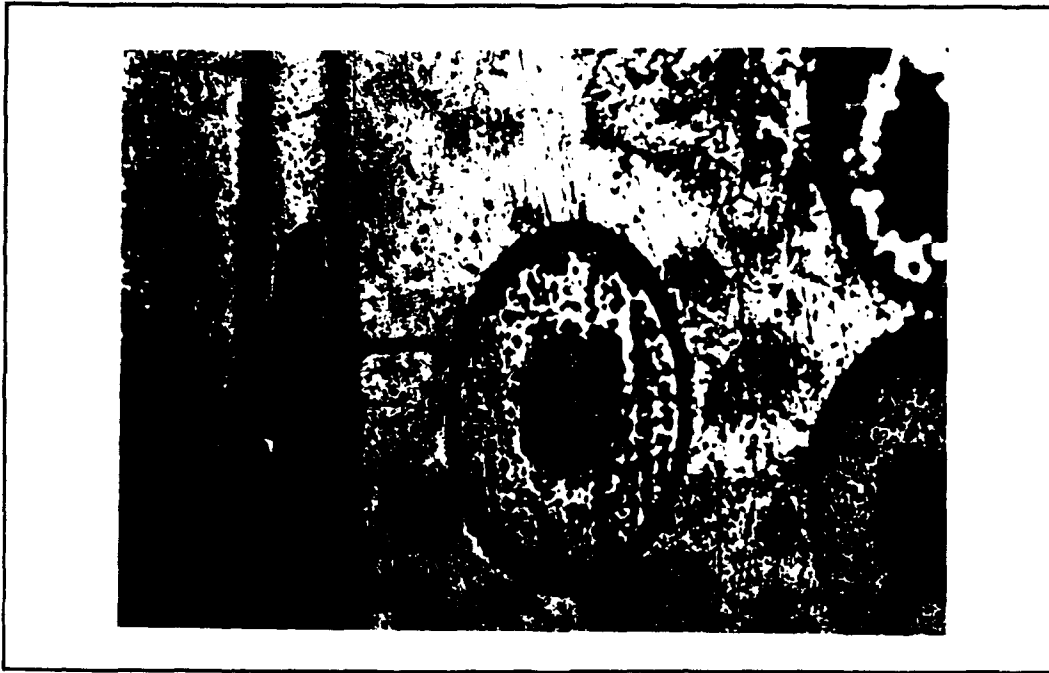
Figure 48 [0/±45/90]$_s$ at 650°C One Hole Diameter Away

Selected specimens were carbon coated and examined by SEM techniques. Figures 49 and 50 are photographs of failed [0/90]$_{2s}$ specimens at room temperature and 650°C. Fracture surfaces for both the cross-ply and quasi-isotropic laminates at all temperature regimes exhibited fracture associated with plastic deformation, which is essentially ductile. ß21s, like typical engineering materials, contains large amounts of second phase particles. These particles, termed alpha, were purposely introduced by means of an appropriate heat treatment to aid in increasing the yield strength. These particles cannot deform as readily as the surrounding matrix and loose coherence when plasticity takes place in their vicinity.

95
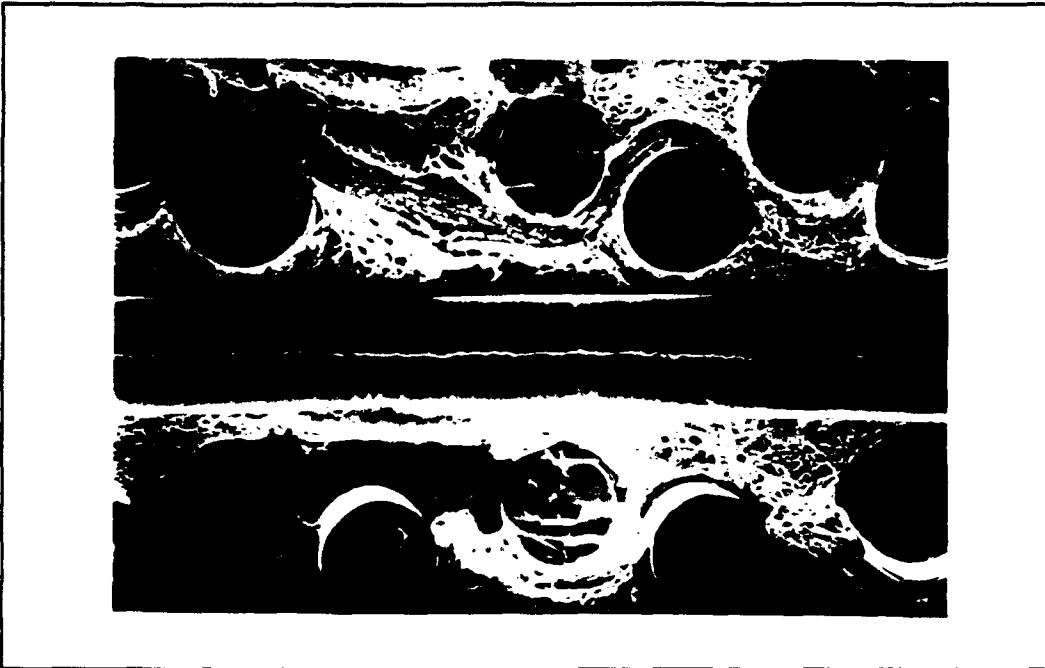
Figure 49 Fracture Surface at Room Temperature $[0/90]_{2s}$
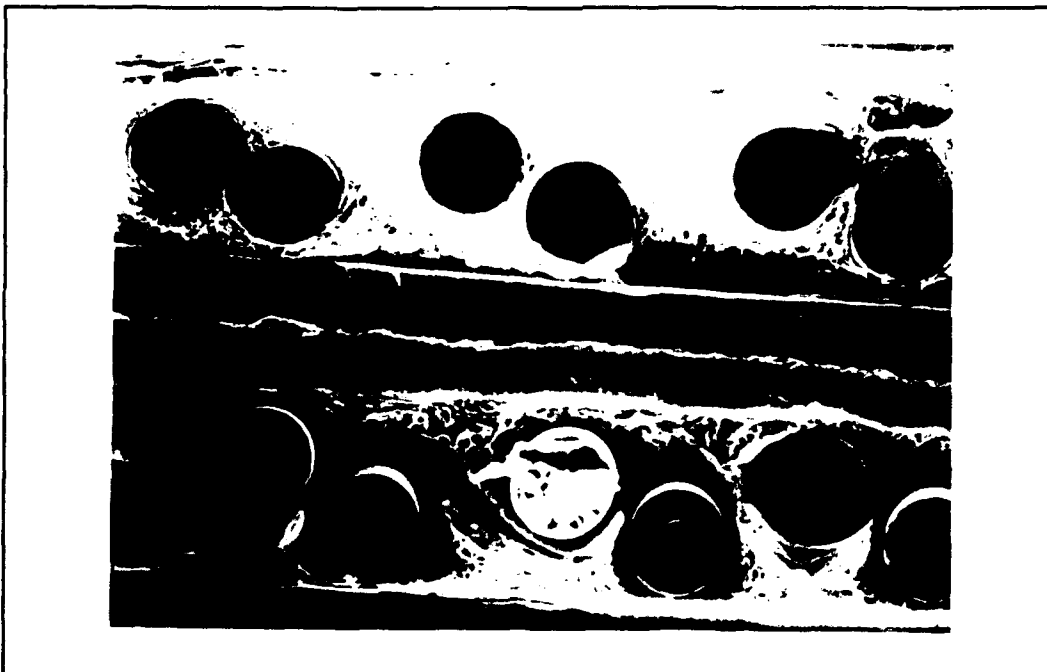
Figure 50 Fracture Surface at $650^{\circ}C$ $[0/90]_{2s}$

96

Tiny voids form, grow by slip, coalesce, and give rise to a characteristic dimpled appearance of the fracture surface. Figure 51 displays the dimpled appearance under higher magnification. Quasi-isotropic specimens also exhibited this dimpled appearance of the fracture surface. The molybdenum ribbon, used to hold fibers in place during the manufacturing process, is evident in both Figures 49 and 50 at the 0 degree fibers, which are oriented out of the page. The majority of fracture surfaces examined exhibited failure occurring along the ribbon in the 0 degree plies. The molybedum ribbon has been shown by others, Chapter 3, to be a weak link in metal matrix composites.
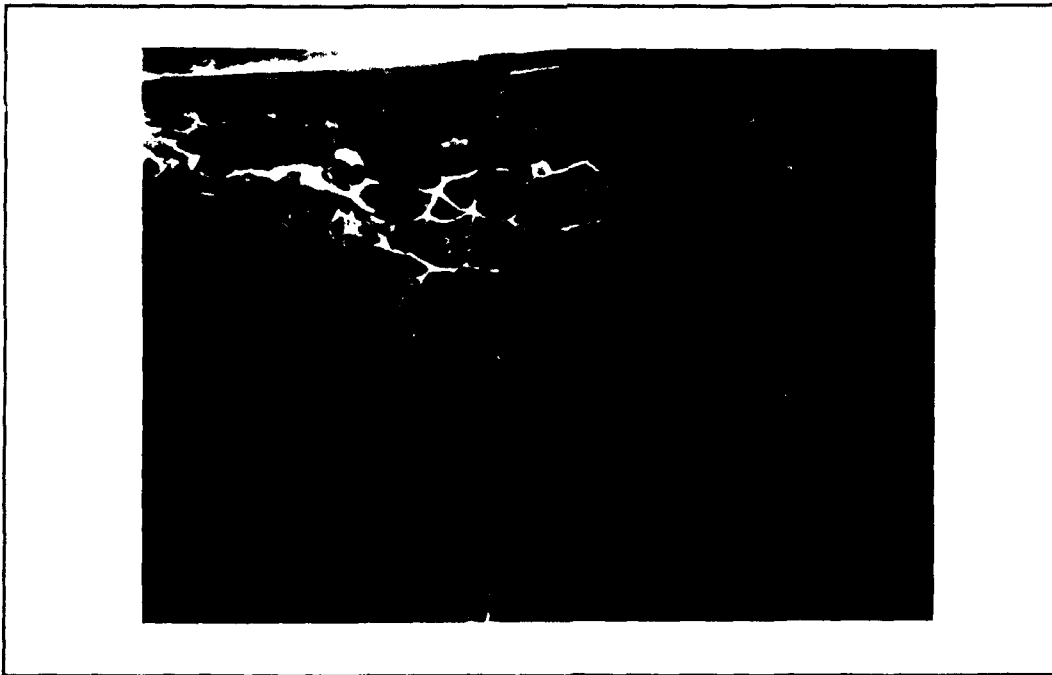
Figure 51 Fracture Surface at 1400 Times Magnification

Notch Sensitivity

A composite is termed notch sensitive when it experiences a reduction in strength above the amount expected solely due to the decrease in the cross-sectional area from a hole or a notch. The net strength of a specimen is obtained by dividing the failure load by the remaining cross-sectional area with the hole area subtracted out, $\sigma_{net} = P_f/((w-d)*t)$. Figure 52 and 53 implement a dimensionless quantity termed the Strength Reduction Factor (SRF). The SRF normalizes the net strength of a notched specimen at any particular temperature by dividing it by an appropriate unnotched laminate strength (Equation 15).

$$SRF = \frac{\text{Unnotched or Notched Net Strength at Temperature}}{\text{Unnotched Strength at Room Temperature}} \quad (15)$$

A cubic spline curve has been drawn through the data at room temperature, 482°C, and 650°C. From Figure 52, the results for the $[0/90]_{2s}$ laminate, it is concluded that the laminate is notch sensitive at room temperature and 482°C. Since the deviation between the unnotched tensile strength and the open hole net strength becomes negligible at 650°C, the cross-ply laminate is defined as notch insensitive at 650°C. The quasi-isotropic laminate, represented in Figure 53, is notch sensitive at room temperature, only slightly notch sensitive at 482°C, and insensitive to the existence of a hole

98
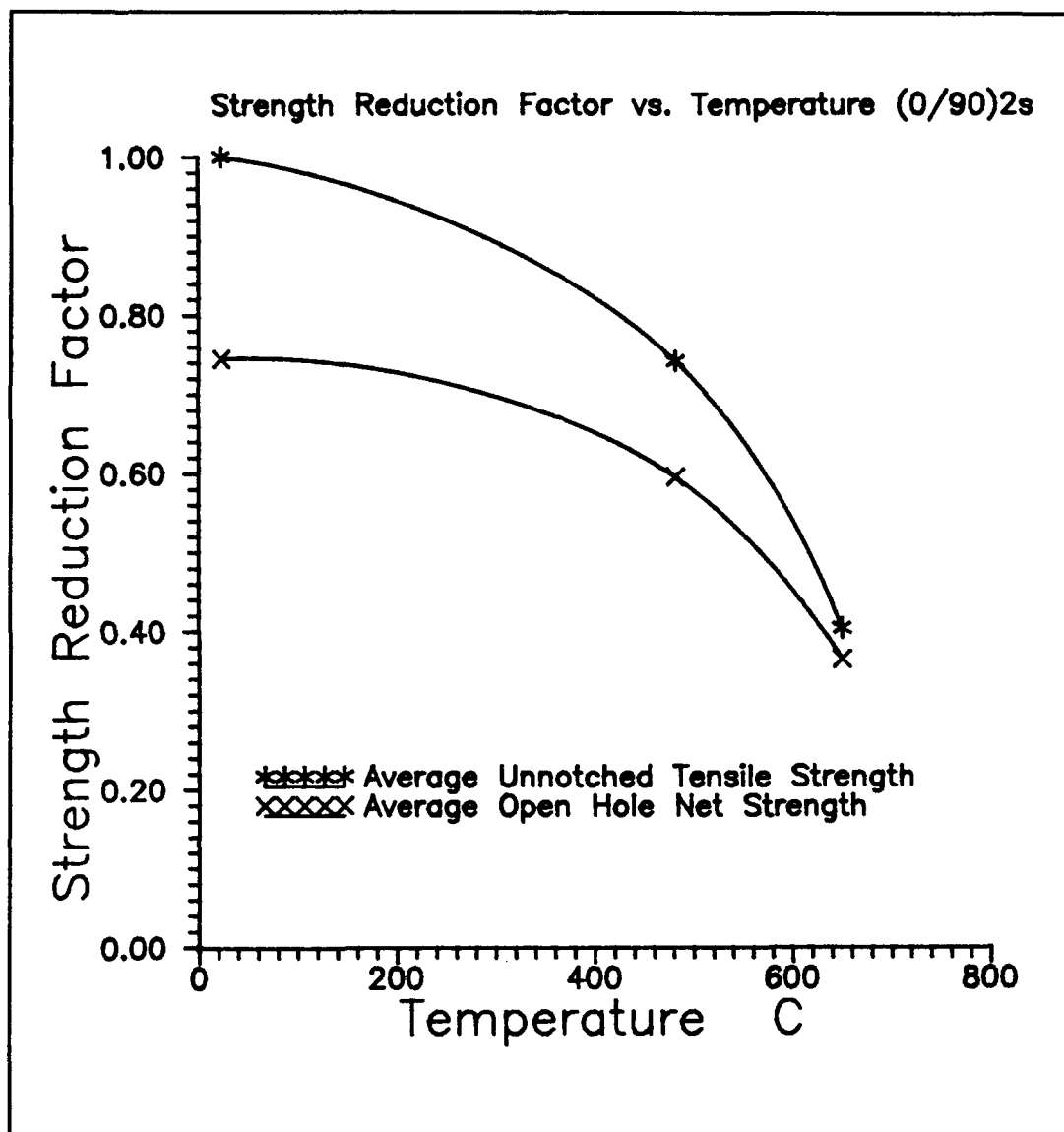
Figure 52 Strength Reduction Factor vs. Temperature

at 650°C. It has been shown by others that damage near a notch such as: plastic deformation, matrix cracking, and fiber-matrix debonding decrease the stress concentration factors associated with a notch. Recall that at the 650°C temperature regime β21s has a very low yield strength and it

99
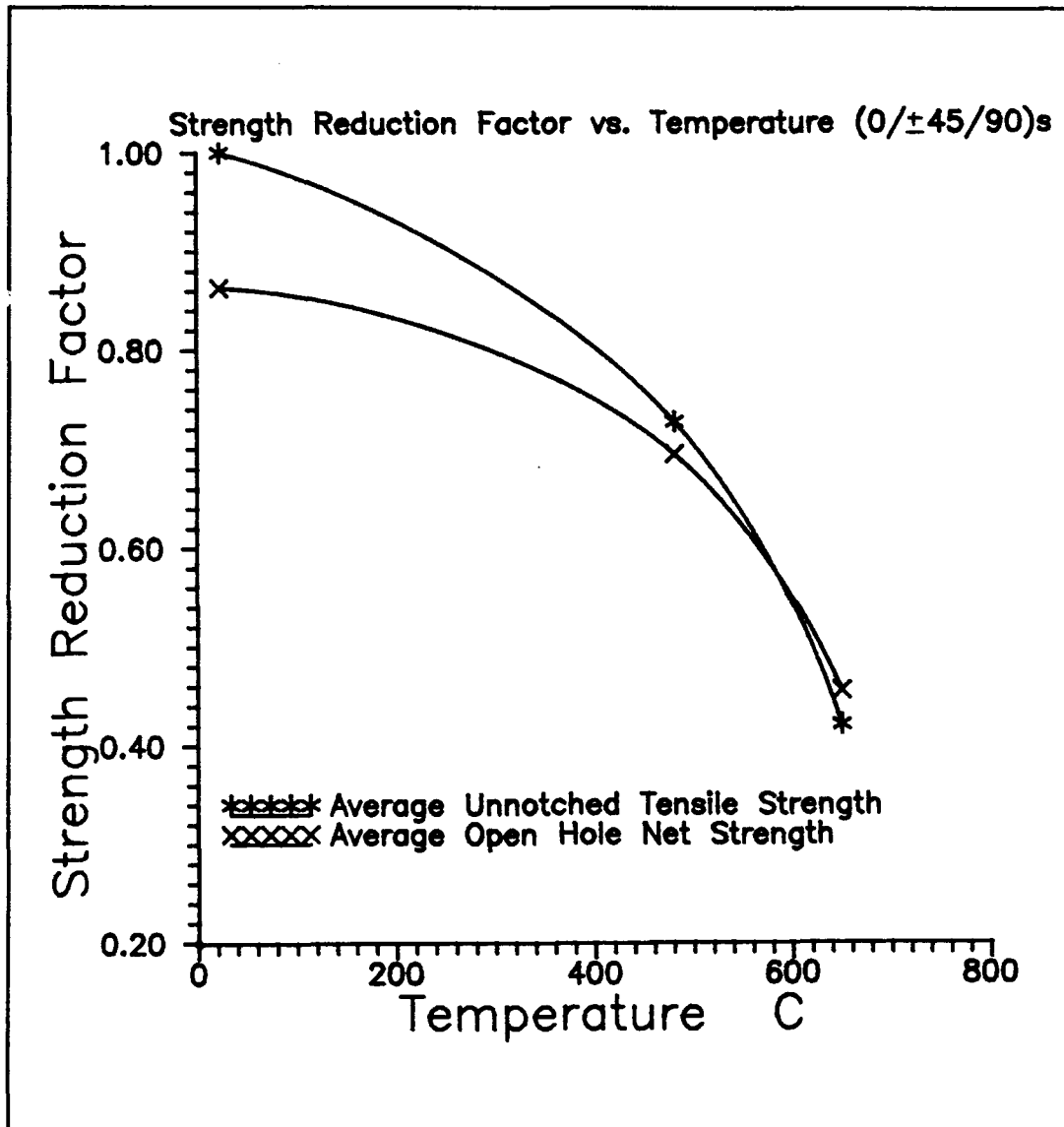
Figure 53 Strength Reduction Factor vs. Temperature

has already been shown that near the hole, the 0 and 90 degree fibers debond, the matrix develops cracks, and plasticity is evident.

Stress Around the Periphery of the Hole

Figure 54 is included to avoid any confusion concerning
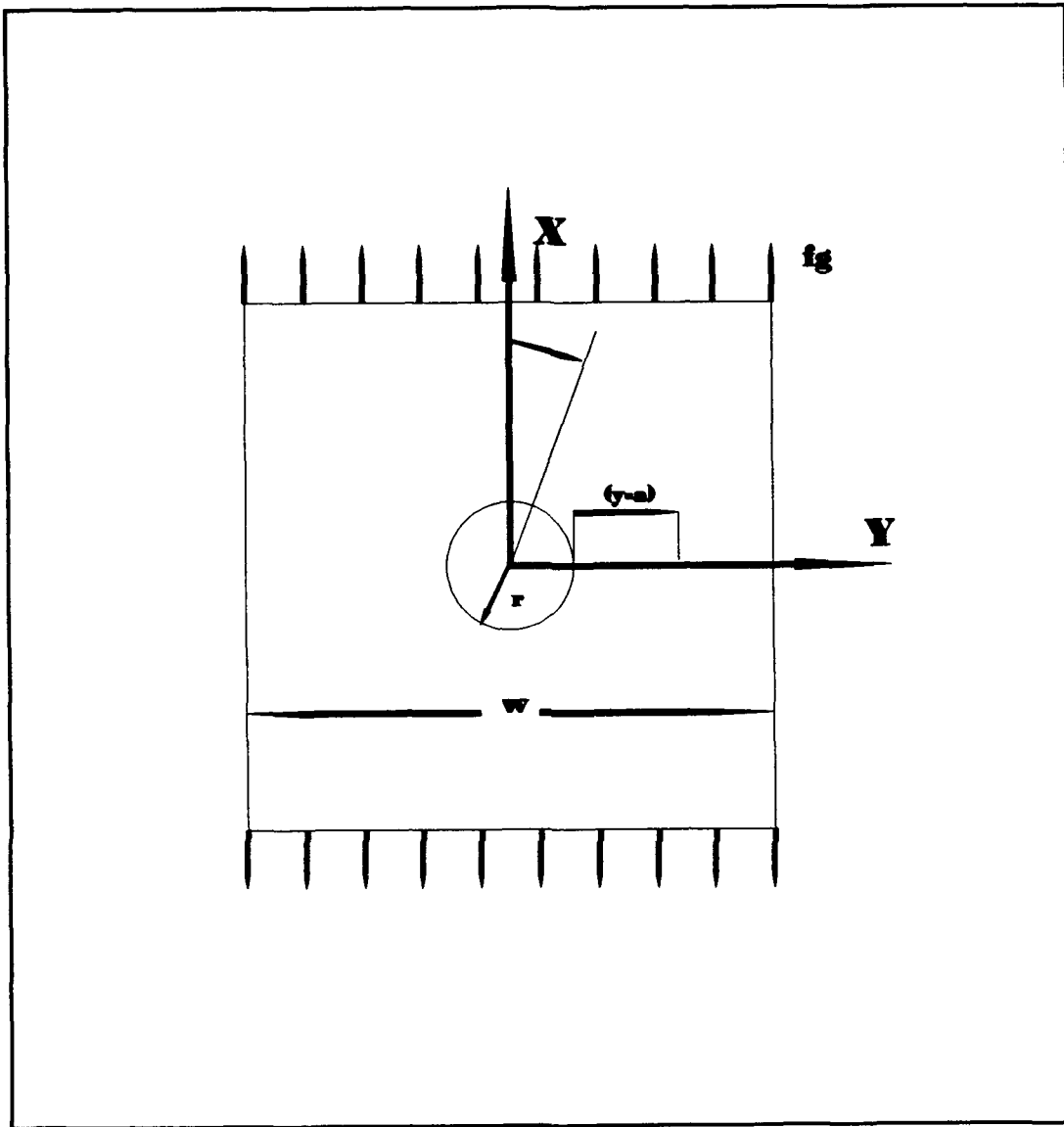
Figure 54 Laminate With Circular Opening

the coordinate frame used throughout this discussion.   The

longitudinal,   transverse,   and   shear   stress   around   the

periphery of a notch are essential quantities for a complete

understanding of the effect of a hole or notch in a laminate.

Lekhnitskii formulated results for the stress distribution in

101

an orthotropic plate with a circular opening (22). Harmon and Saff applied Lekhnitskii's formulations to composite materials (21). The following will be valid for an uniaxially loaded laminate, X is always the load direction and Y is transverse to the load direction. The following nomenclature will apply throughout the following discussion.

```
Ex   = Composite stiffness in the load direction
Ey   = Composite stiffness transverse to load
νxy  = Poisson's Ratio
Gxy  = Composite shear modulus
Et   = Stiffness of the laminate tangent to the notch in
       the θ direction
θ    = Angle taken positive from the X axis, positive
       is clockwise
ft   = Tangential stress at the periphery of the notch
fg   = Applied gross stress in the X direction
η    = Measure or plate orthotropy
Kto  = Stress concentration factor at θ = 0 degrees
Kt   = Stress concentration factor at θ = 90 degrees
Ktnet= Net stress concentration factor at θ = 90 degrees
r    = Radius of hole
w    = Width of laminate
2a   = Major axis of an elliptical notch
2b   = Minor axis of an elliptical notch
beff = to be defined later
σxy  = Shear stress at the periphery of the notch
σx   = Longitudinal stress at the periphery of the notch
σy   = Transverse stress at the periphery of the notch
f1-f6 = Variables necessary for elliptical calculations
A,B,C = Variables necessary for stress gradient
```

Given an infinitely wide, uniaxial loaded laminate with a center notch, the general expressions for tangential stress concentration at any point along the periphery is given by Equations 16, 17, and 18.

$$ft/fg = Et/Ex[.5(1+\eta-\sqrt{Ex/Ey})-.5(1+\eta+\sqrt{Ex/Ey})Cos2\theta] \quad \textbf{(16)}$$

102

$$\eta = \sqrt{Ex/Gxy - 2vxy + 2\sqrt{Ex/Ey}} \qquad (17)$$

$$1/Et = Sin^4\theta/Ex + [1/Gxy - 2vxy/Ex]Sin^2\theta Cos^2\theta + Cos^4\theta/Ey \qquad (18)$$

Realize that with θ equal to zero, Et equals Ey and Equation 16 reduces to stress concentration factor Kto. At θ equal to 90, Et equals Ex and Equation 16 reduces to Kt.

$$Kto = -\sqrt{Ey/Ex} \qquad (19)$$

$$Kt = (1 + \eta) \qquad (20)$$

Equation 16 can then be written in the following form.

$$ft/fg = .5[(Et/Ex)Kt + (Et/Ey)Kto] - .5[(Et/Ex)Kt - (Et/Ey)Kto]Cos2\theta \qquad (21)$$

"If Kt and Kto are computed for finite width plates ...Equation 21... can be used to determine the tangential stress concentration factor for any plate. (21)" In order to account for the finite width effect in notched composite specimens an elliptical approach, Equations 23, in conjunction with Equation 22 is implemented.

$$Kt = Ktnet/(1-2a/w) \qquad (22)$$

$$Ktnet = 2 + f1f2^2 + f1f2^4 + .643f3(1-f4^2) + \tag{23}$$
$$.167f3(1-f4^4) + .218f3f5(a/w)$$

where

$$f1 = (1-\eta a/b)/2 - 1$$
$$f2 = 1 - 2a/w$$
$$f3 = a/b - 1$$
$$f4 = 4a/w - 1$$
$$f5 = 1-(2a/w)^{100}$$

Providing the material properties and geometry of the notch are known, η is an easily calculated value. Kt, the stress concentration factor at 90 degrees, is an obtainable value. Harmon and Saff introduce an effective minor axis dimension, beff, which in effect changes the circular notch into an ellipse in order to account for material orthotropy. When this is done for a circle a different f1 is implemented in the elliptical formulations. Major axis dimension a is simply the radius of the circle. Equations 22, 23, and 24 yield the stress concentration at θ equal to 90 degrees. Equation 25, derived by Harmon and Saff via finite-element and boundary collocation analysis, can then be implemented to generate Kto for a finite width orthotropic plate. These stress concentration factors are then applied in Equation 21 to yield an elastic stress concentration factor, as a function of θ, which takes finite width and material orthotropy into effect.

$$f1 = .5(2a/beff - 1)$$

$$beff = (2b/\eta)[1-(2a/w)]^{.125(\eta/2 - 1)} \tag{24}$$

$$Kto = -[\sqrt{Ey/Ex} + 2.8/(w/2/a)^2] / [1 + .00865/(w/2/a-1)^{2.76}] \tag{25}$$

The stress gradient from a notch at θ equal to 90 degrees can also be estimated assuming an exponential decay.

$$ft/fg = A + B[1+(y-a)a/b^2]^{-C} \qquad (26)$$

A, B, and C are constants obtained through an application of boundary conditions. The origin of the Y axis is at the center of the notch as shown in Figure 54. All the above formulations were incorporated into the Fortran 77 code, STRESS.FOR, which is included in Appendix B. This program calculates the elastic stress concentration factor for infinite and finite width composite plates with elliptical and circular notches. With the tangential stress component calculated as a function of θ, the program then calculates the longitudinal, transverse, and shear stresses along the periphery of the notch for a applied unit gross stress. The program also has the capability of estimating a stress gradient at θ equal to 90 degrees. Inputs: Ex, Ey, Gxy, νxy, notch dimensions, and plate dimensions are entered interactively.

The elastic stress concentration factors at room temperature were calculated to be 3.480 for the $[0/90]_{2s}$ laminate and 3.149 for the $[0/\pm45/90]_s$ laminate. Stress concentration factors were only calculated at room temperatures due to the fact that the material has been shown to be notch insensitive at 650°C and only mildly notch sensitive at 482°C. The elastic stress concentration factor

in the quasi-isotropic laminate proved to be 9.5 percent lower then in the cross-ply laminate with identical notch dimensions. This is due to the fact that the shear modulus of the quasi-isotropic laminate, calculated from Classical Laminate Plate Theory, is essentially equivalent to an isotropic assumption. The degree of material orthotropy is obviously higher in the cross-ply laminate, causing it to possess a higher elastic stress concentration factor.

Figures 55 and 56 display the calculated stresses at the periphery of the notch for θ from 0 to 90 degrees for the cross-ply and quasi-isotropic laminates. It is important to note the angle θ where the composite is experiencing maximum shear at the periphery of the notch. Maximum shear occurs at 66 degrees in the $[0/90]_s$ laminate and at 64 degrees in the $[0/\pm45/90]_s$ laminate. Newaz and Majumdar have found that in unidirectional laminates under fatigue loading cracks initiate at the location of maximum shear (23). Although the laminates investigated in this study did not develop cracks at locations of maximum shear, the elevated stresses in conjunction with debonded fibers could have caused yield in the matrix. Varying the diameter to width ratio of the coupons obviously has substantial effect on the magnitude of these stresses along the periphery; but has little or no effect on the angle where the maximum shear stress occurs.

Figure 57 displays the stress concentration gradient at θ equal to 90 degrees for both laminates. From this figure it
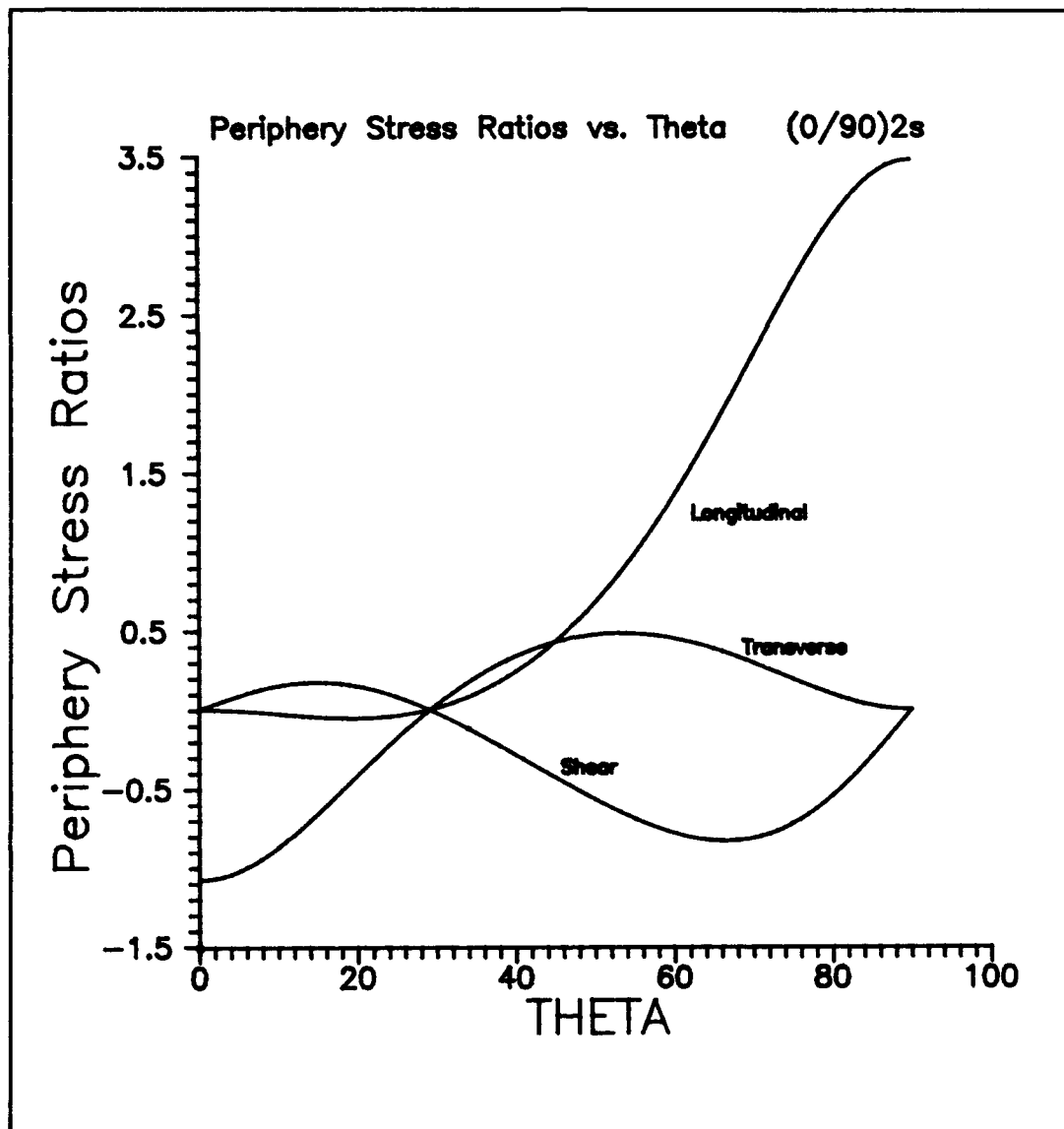
Figure 55 Stresses Along the Periphery of the Hole for the $[0/90]_{2s}$ Laminate

is evident that in a relatively small distance y, from the hole, the stress concentration factor can decrease substantially. The information supplied by this figure in conjunction with experimental results can be used to obtain a

107
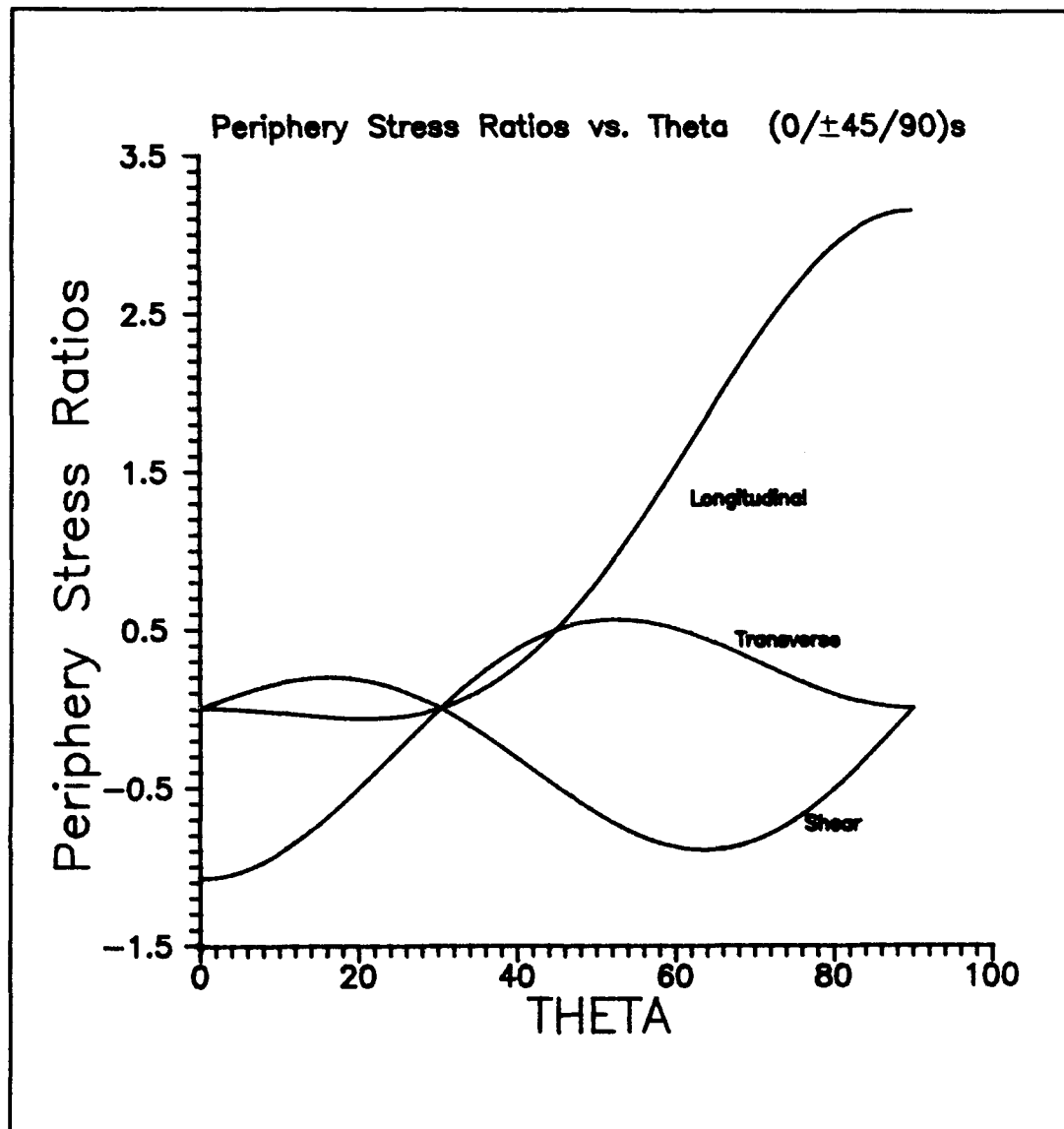
Figure 56 Stresses Along the Periphery of the Hole for the $[0/\pm45/90]_s$ Laminate

variable termed the critical length or critical distance, which is used in attempting to predict the notched strength of composites laminates. This variable can be used as a type of correction for the elastic stress concentration factor which
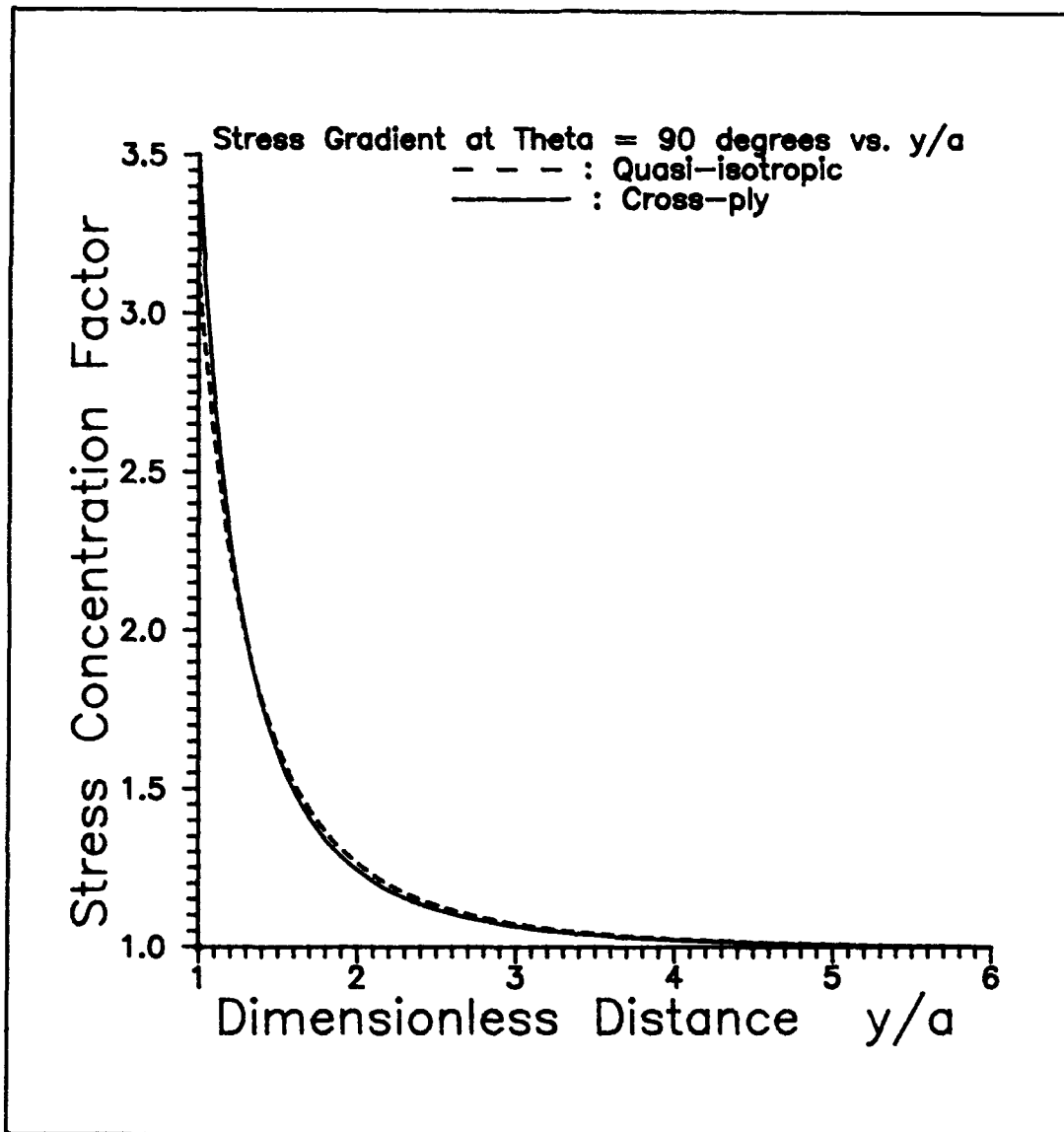
Figure 57 Stress Concentration Gradient at θ=90 degrees

usually underestimates the notched laminate strength when applied to a failure criteria.

Critical Distance Attempt

$[0/90]_{2s}$ and $[0/\pm45/90]_s$ specimens were loaded to a

particular percentage of an average failure stress. This was completed at both room temperature and 650°C. The specimens were then etched with Kroll's etchant down to the first 0 degree ply in an attempt to document the damage progression in the fibers near the notch as a function of the applied stress. An ultimate goal, in such an experiment, would be to get an indication of an appropriate critical distance, which could be implemented to reduce the calculated elastic stress concentration factor which assumes no damage or plasticity. Damage, for a circular notch, would be expected to initiate at the point of maximum stress concentration, θ equal to 90 degrees, or at the point of maximum shear stress. This was not the case for SCS-9/ß21s. Instead, damage around the notch was observed to be random, dependent upon wherever the molybdenum ribbon happen to exist for the particular specimen tested. Recall that the moly-weave has been shown, in Chapter 3, to cause fiber failure during the manufacturing process prior to an applied load, which compounded the problem. Figure 41 displays SEM photographs of a $[0/90]_{2s}$ specimen at 650°C loaded to 94 percent of the failure strength. Virtually all the 0 fibers across the width of the laminate have failed. The angle θ is approximately 45 degrees which corresponds to neither the location maximum shear or maximum stress concentration factor.

Plastic Stress Concentration Factors

Damage and plasticity in metal matrix composites decrease

the stress concentrations induced by a notch. An attempt was made to estimate a plastic stress concentration factor for the 0 degree plies in the laminates by incorporating a shear lag model developed by Harmon and Saff (21). The 90 and 45 degree plies were assumed to behave elastically up to failure. A computer program STRESS.FOR, with its elliptical notch capabilities, was employed.

"The amount of load carried by the matrix at shear yield is the amount of load through the hole that cannot be carried elastically. This load had to be carried by the matrix at shear yield over length L. (21)" Figure 58 displays this shear lag model and Equation 27 is the mathematical expression necessary to calculate L. The circular hole is mathematically transformed to an elliptical notch with its major axis oriented parallel to the load dir~.tion and its minor axis oriented perpendicular to the load direction. The result is a decrease in the stress concentration factor at θ equal to 90 degrees. L initiates at the position of maximum shear around the periphery of the notch. With calculated dimension L, and simple trigonometry, the major axis of the ellipse is obtained. The minor axis remains the diameter of the hole.

$$L = \frac{(P-Po)D}{2\sigma_{mus}A} \qquad (27)$$

D = Notch diameter perpendicular to load direction
P = Applied load
Po = Load at which yielding first occurs in matrix
σ_{mus}= Matrix shear ultimate strength
A = Specimen gross area

111
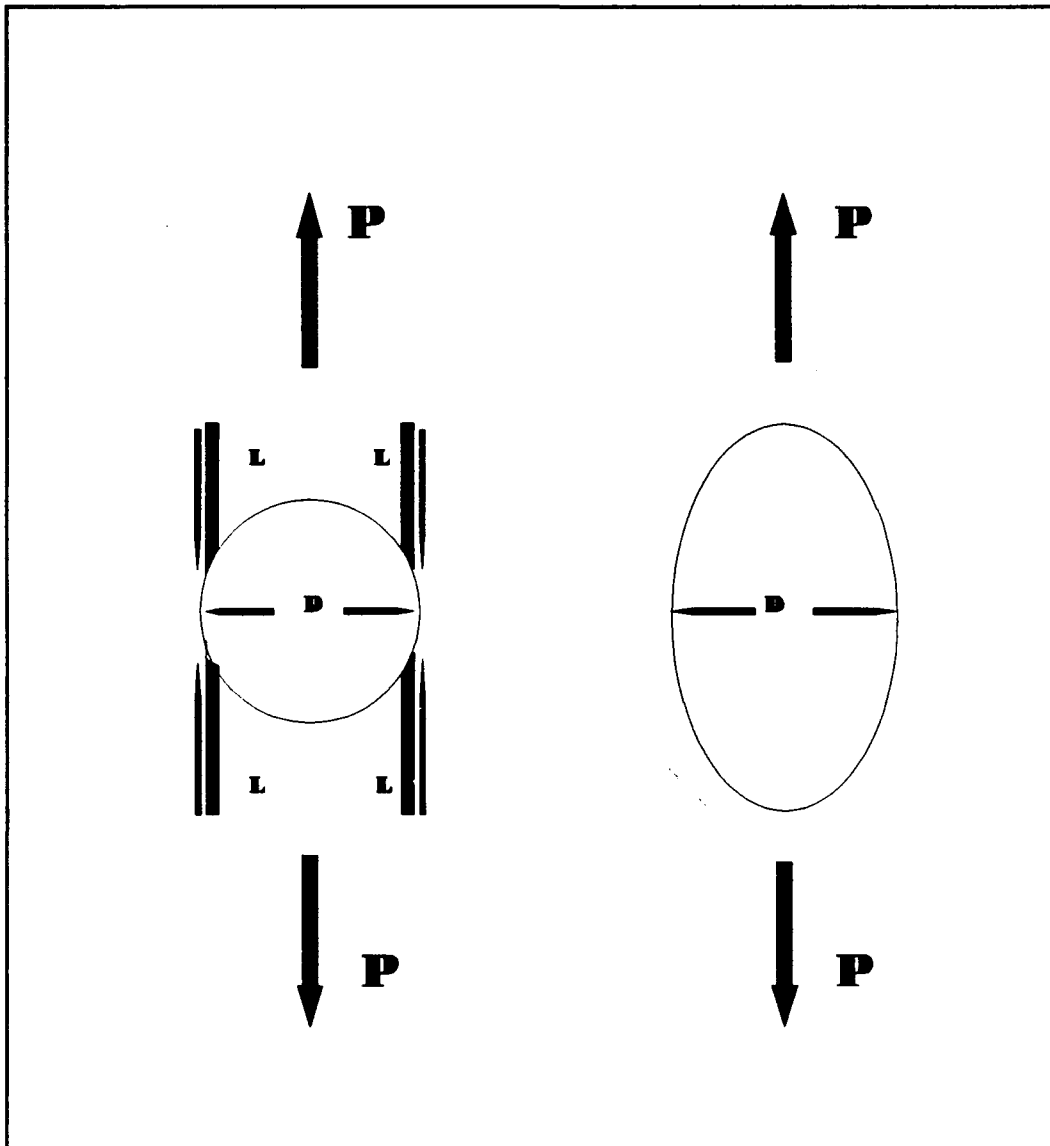
Figure 58 Shear Lag Model Developed by Harmon and Saff

Since shear testing of ß21s has not been completed to date, the ultimate and yield strength of ß21s in shear was estimated for this analysis. Using maximum octahedral shear stress theory the shear strength of an isotropic material can be estimated by dividing the tensile strength by the square

112

root of three. Maximum shear stress theory reveals that the shear strength of an isotropic material should be around one-half the ultimate tensile strength. The average of these two theories yields a value for the ultimate shear strength of ß21s equal to 615 MPa. The yield strength of ß21s in shear will be assumed to be 360 MPa, this will then be incremented to check the effect of this assumption on the analysis. Lissenden from the University of Virginia has completed two preliminary Iosipescu shear tests of ß21s and estimates the yield strength of the material to be between 330 MPa and 410 MPa.

In the $[0/90]_{2s}$ laminate the 90 degree plies basically assume none of the applied gross stress at, or near, failure. The stress in the 0 degree plies was then calculated via total discount method to obtain the largest value that P would reach at failure of the laminate. Recall that the attempt here is to obtain a plastic stress concentration factor for the 0 degree plies and not the laminate. STRESS.FOR was then implemented for a 0 degree laminae with w/d = 6 to obtain the ratio of the shear stress to an applied gross stress and the angle where this becomes a maximum. This was then used to obtain the applied load, Po, where yielding was expected to occur in shear. The value of L was calculated to be 2.3 mm and the major axis of the ellipse was then found to be 6.0 mm. The plastic stress concentration factor at $\theta=90$ degrees for the cross-ply laminate, through an application of the

elliptical formulations in STRESS.FOR, was calculated to be 2.418.

Since the values of shear yield and ultimate shear strength for β21s are not 100 percent reliable, they were varied in order to examine the effect on the stress concentration calculations. By changing the yield stress of β21s in shear from 360 MPa to 450 MPa and maintaining the ultimate shear stress value of 615 MPa; modifying the deviation between the two values by a factor of 1.25, or 25 percent, the plastic stress concentration factor was only effected by 7.3 percent.

This same analysis was completed for the quasi-isotropic laminate for two separate cases. In the first case the 90 and 45 degree plies were assumed to contribute no strength in the laminate just prior to failure. In the second case the 45 degree plies were assumed to carry load until final failure of the composite. Actual specimen failure would be some where in between these two cases. With these two assumptions the stresses in the individual plies could be calculated at the failure strength and the shear lag model could then be applied to the 0 degree plies. In the first case the plastic stress concentration factor was calculated to be 1.728 and in the second case it was found to be 2.218.

Strength Prediction for Notched Specimens

The calculated elastic and plastic stress concentration factors were used in conjunction with maximum stress failure

114

criteria to predict the room temperature strengths of notched specimens. The procedure was identical to unnotched strength predictions with two exceptions. The 90 and 45 degree plies were assumed to behave perfectly elastic to failure and the elastic stress concentration factor was used as a multiplication factor for the stresses. The 0 degree plies were modeled as elastic-plastic, incorporating the plastic stress concentration factor for failure of these plies. Elevated temperature notch strength predictions were not attempted since the material has been shown to be completely notch insensitive at 650°C and only mildly notch sensitive at 482°C. The failure strengths of notched specimens at elevated temperature can be conservatively estimated by simply using the net cross-sectional area to calculate a net stress and assuming that the laminate would then fail when this stress exceeds the unnotched tensile strength.

Table 12 presents the predicted and average experimental failure strength for the notched room temperature $[0/90]_{2s}$ and $[0/\pm45/90]_s$ laminates. The predicted failure strength of the

Table 12:Predicted Notched Room Temperature Strengths

Laminate	Predicted σ_{ult} MPa	Experimental σ_{ult} MPa	% Error
$[0/90]_{2s}$	367.5	553.3	34% low
$[0/\pm45/90]_s$ (1)	299.2	537.6	44% low
$[0/\pm45/90]_s$ (2)	384.3	537.6	29% low

room temperature $[0/90]_{2s}$ laminate is approximately 34 percent lower then the average notched experimental failure strength at room temperature. The result obtained for the notched quasi-isotropic room temperature laminate with the 45 degree plies assuming load up to failure, (1 in table), is approximately 44 percent lower than experimental results. Implementing the plastic stress concentration, developed under the assumption that the 90 and 45 degree plies attribute negligible strength during the later part of the stress-strain response (2 in table), yielded a predicted failure strength result that was approximately 28 percent lower then the experimental results.

The predictions invariably underestimate the notched laminate strength. Assuming the 90 and 45 degree plies to behave elastically to failure is probably the major source of error in this analysis. Damage is known to occur, fiber/matrix debonding, and plasticity is plausible. This damage and plasticity would lower the applied elastic stress concentration factor in the 90 and 45 degree plies, increasing the predicted strength of the laminate considerably.

Filled Hole Specimen Evaluation

Room temperature SCS-9/ß21s specimens, of orientations $[0/90]_{2s}$ and $[0/\pm45/90]_s$ and width to diameter ratios of six, were characterized with pins inserted into the holes. Two different pin materials were employed at room temperature, namely: the aluminum alloy 7075-T6, and the nickel alloy Mar-

116

m-246. The tolerance between the pins and the holes did not exceed 0.0254 mm. Both cross-ply and quasi-isotropic laminates were also tested at 482°C and 650°C using only the Mar-m-246 pin material. The intent of filled hole testing was to analyze the effect of the pin on stiffness, strength, and failure progression in comparison with open hole specimen data.

Pin material 7075-T6 was chosen because its stiffness is considerable lower than ß21s, 35 percent, and its strength is 50 percent lower than ß21s at room temperature. As a result of this lower stiffness and strength, the pin could deform to accommodate the deformation of the hole during loading. This type of plug has been shown to have advantageous effects on the stiffness and strength of some notched homogeneous and composite materials. Mar-m-246 pins were chosen for completely different reasons. The stiffness of these pins is 46 percent higher than ß21s and its strength is compatible with ß21s, causing the pin to remain completely rigid during coupon loading. Also Mar-m-246 retains 83 percent of its stiffness and all of its strength at temperatures up to 650°C.

Room Temperature

Table 13 contains the results of this testing completed at room temperature. In some tests data for both a remote strain, from either a remote strain gauge or a remote extensometer, and a local strain, from a local extensometer, could be obtained. It has been shown during open hole

117

Table 13: Room Temperature Filled Hole Static Tensile Data

Spec.	Laminate	Pin	ϵ_{ult}	σ_{ult} MPa	Ei GPa	Es GPa
52	$[0/90]_{2s}$	Mar	R=.0049	606.5	143.9	116.3
53	$[0/90]_{2s}$	Mar	R=.0044	552.0	141.1	116.8
55	$[0/90]_{2s}$	Mar	R=.0044	544.8	137.5	114.9
57	$[0/90]_{2s}$	Mar	L=.0044	513.6	137.4	114.3
58	$[0/90]_{2s}$	7075	L=.0046 R=.0045	547.1 -----	140.4 133.9	116.9 114.4
59	$[0/90]_{2s}$	7075	L=.0050 R=.0046	571.2 -----	134.0 145.4	112.4 116.6
65	$[0/\pm45/90]_s$	Mar	L=.0069 R=.0065	532.3 -----	119.4 114.3	78.6 76.4
66	$[0/\pm45/90]_s$	7075	L=.0069 R=.0062	513.4 -----	116.8 118.3	75.3 75.0
67	$[0/\pm45/90]_s$	Mar	L=.0067 R=.0064	518.1 -----	121.0 121.0	74.5 75.7
68	$[0/\pm45/90]_s$	Mar	R=.0063	535.1	120.3	79.5
69	$[0/\pm45/90]_s$	7075	L=.0066	501.7	120.3	75.7

specimen evaluation that the remote extensometer and the remote strain gauge yield the same results. Local strain gauge data is not presented but available upon request for room temperature testing. The ultimate stress given in Table 13 is a gross stress. Ultimate strain is given for remote data (R=...) and for local extensometer data (L=...).

Prior to a comparison, concerning the effect of the pin, between open and filled hole data the initial remote modulus of the open and filled hole specimens must be examined. They should be, within experimental deviation, equivalent. As expected, the average $[0/90]_{2s}$ laminates open hole remote modulus was within one percent of the average filled hole

remote modulus. The effect of the pin on the notched laminate can therefore be investigated by comparing local filled hole data with local open hole data. On the other hand, the average $[0/\pm45/90]_s$ laminates open hole remote modulus was eighteen percent higher than the average filled hole remote modulus. This is beyond any percent error expected due to panel to panel deviation. The difference in remote moduli is believed to manifest from a problem that must have been introduced during the heat treatment of the quasi-isotropic filled hole specimens. No effect of the pin can be made by comparing these specimens with open hole data presented previously. Instead, the remaining four specimens from this heat treatment batch were tested with open holes; two tested at room temperature and two tested at elevated temperature. The data from these tests are presented in Table 14. The deviation in remote modulus for these $[0/\pm45/90]_s$ open hole coupons in comparison with filled hole remote modulus was within three percent at room temperature. The effect of the

Table 14: Open Hole Specimen Data from Panel B910584

Spec.	Laminate	Temp C	ϵ_{ult}	σ_{ult} MPa	Ei GPa	Es GPa
74	$[0/\pm45/90]_s$	R.T	L=.0063 R=.0060	487.4 -----	110.5 119.5	75.5 74.0
77	$[0/\pm45/90]_s$	R.T	L=.0060 R=.0057	486.6 -----	116.9 118.1	75.4 76.6
75	$[0/\pm45/90]_s$	482	L=.0066	380.8	102.8	70.0
76	$[0/\pm45/90]_s$	650	L=.0169	246.5	91.8	38.9

pin on the stiffness, strength, and failure progression for the quasi-isotropic laminates can be examined by implementing this new open hole data.

Figure 59 presents the open and filled hole stress verses local strain, extensometer, for the $[0/90]_{2s}$ laminate employing both the 7075-T6 and Mar-m-246 pins at room temperature. Neither pin had any effect on the ultimate strength of the notched laminate. The local stiffness was increased by approximately fifteen percent using either pin material. Figure 60 displays the open and filled hole stress verses local strain for the $[0/\pm45/90]_{s}$ laminate using both pin materials at room temperature. This laminate experienced a small increase in strength, approximately four percent employing the 7075-T6 pin and 8 percent employing the Mar-m-246 pin. Pins had no effect on the stiffness of the notched $[0/\pm45/90]_{s}$ laminate at room temperature. This is visually obvious by noting that all the stress-strain curves fall directly on top of each other in Figure 60.

Elevated Temperature

SCS-9/β21s notched specimens with orientations $[0/90]_{2s}$ and $[0/\pm45/90]_{s}$ and a width to diameter ratio of six were analyzed with Mar-m-246 pins inserted in the holes at $482^{\circ}C$ and $650^{\circ}C$. 7075-T6 pin material was not used because the material has a melting range around 500 to $650^{\circ}C$. The effect of inserting a plug on the stiffness, strength, and damage progression at elevated temperatures can then be addressed. Table 15 presents
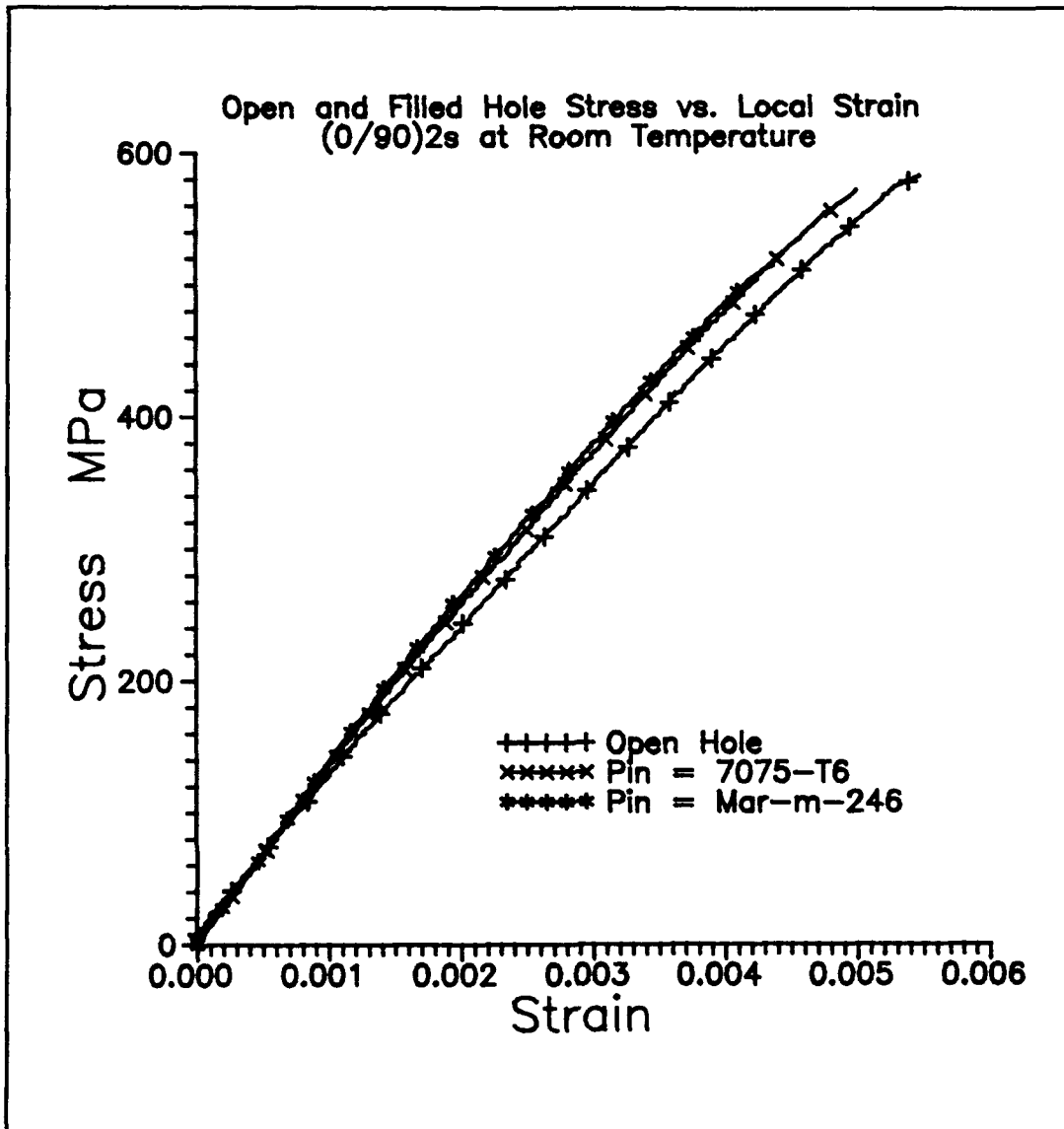
Figure 59 Open and Filled Hole Stress vs. Local Strain
for $[0/90]_{2s}$ at Room Temperature

the elevated temperature filled hole (Mar-m-246) static

tensile testing of cross-ply and quasi-isotropic laminates.

The ultimate strain given (R=remote extensometer, L= local

extensometer) is a mechanical strain. The insertion of the
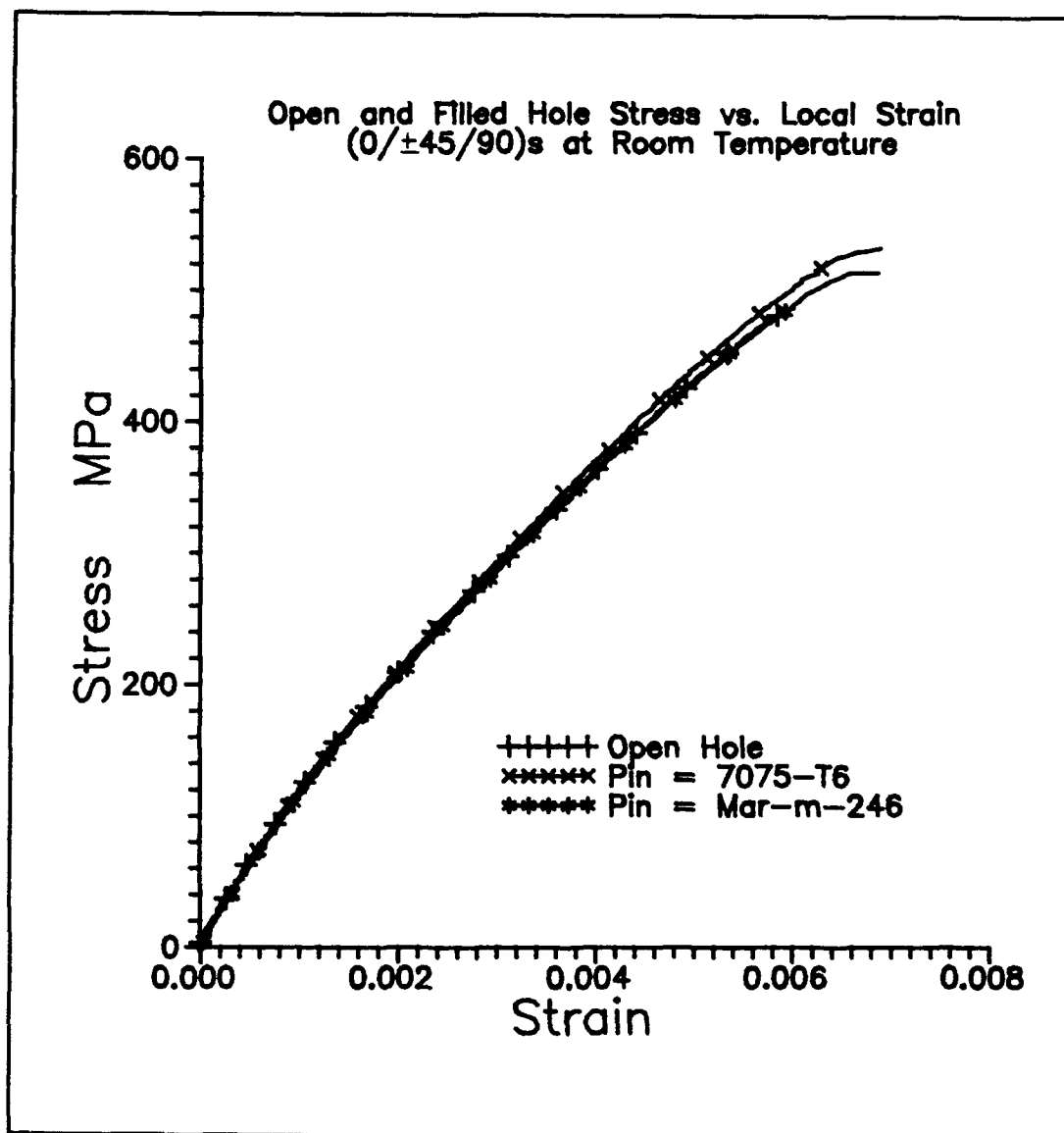
Figure 60 Open and Filled Hole Stress vs. Local Strain for [0/±45/90]$_s$ at Room Temperature

pin has no effect on the stiffness or strength of either laminate at elevated temperatures. Figures 61 and 62 display open and filled hole data at elevated temperature for [0/90]$_{2s}$ and [0/±45/90]$_s$ laminates respectively.

Table 15: Elevated Temperature Filled Static Tensile Data

Spec.	Laminate	Temp. C	ϵ_{ult}	σ_{ult} MPa	Ei GPa	Es GPa
54	$[0/90]_{2s}$	482	L=.0043	433.5	123.7	91.4
56	$[0/90]_{2s}$	482	R=.0034	370.4	125.5	102.3
60	$[0/90]_{2s}$	650	L=.0090	271.0	107.2	78.8
61	$[0/90]_{2s}$	650	R=.0048	309.6	114.6	72.2
70	$[0/\pm45/90]_{s}$	482	L=.0067	384.2	116.8	69.0
71	$[0/\pm45/90]_{s}$	482	R=.0055	393.8	116.7	71.5
72	$[0/\pm45/90]_{s}$	650	L=.0153	237.8	84.6	71.7
73	$[0/\pm45/90]_{s}$	650	R=.0053	246.0	96.4	63.0

Failure Progression

The failure progression of the filled hole cross-ply and quasi-isotropic laminates is analogous to open hole. Both laminates at all temperatures exhibit two linear regions, although the second linear region at 650°C is somewhat obscured by plasticity. In the first linear region the stress-strain response is governed by elastic behavior in the fiber and matrix without damage. Using the data from the local strain gauge and the acetate replication technique, it is concluded that the debonding of the off-axis plies occurs at a lower stress level near the hole then away from the hole. The amount of strain near the hole is also extensive relative to the remote failure strain. The debonding of the off-axis plies in conjunction with a release in residual stresses manifest as a knee in the stress-strain curves between the two
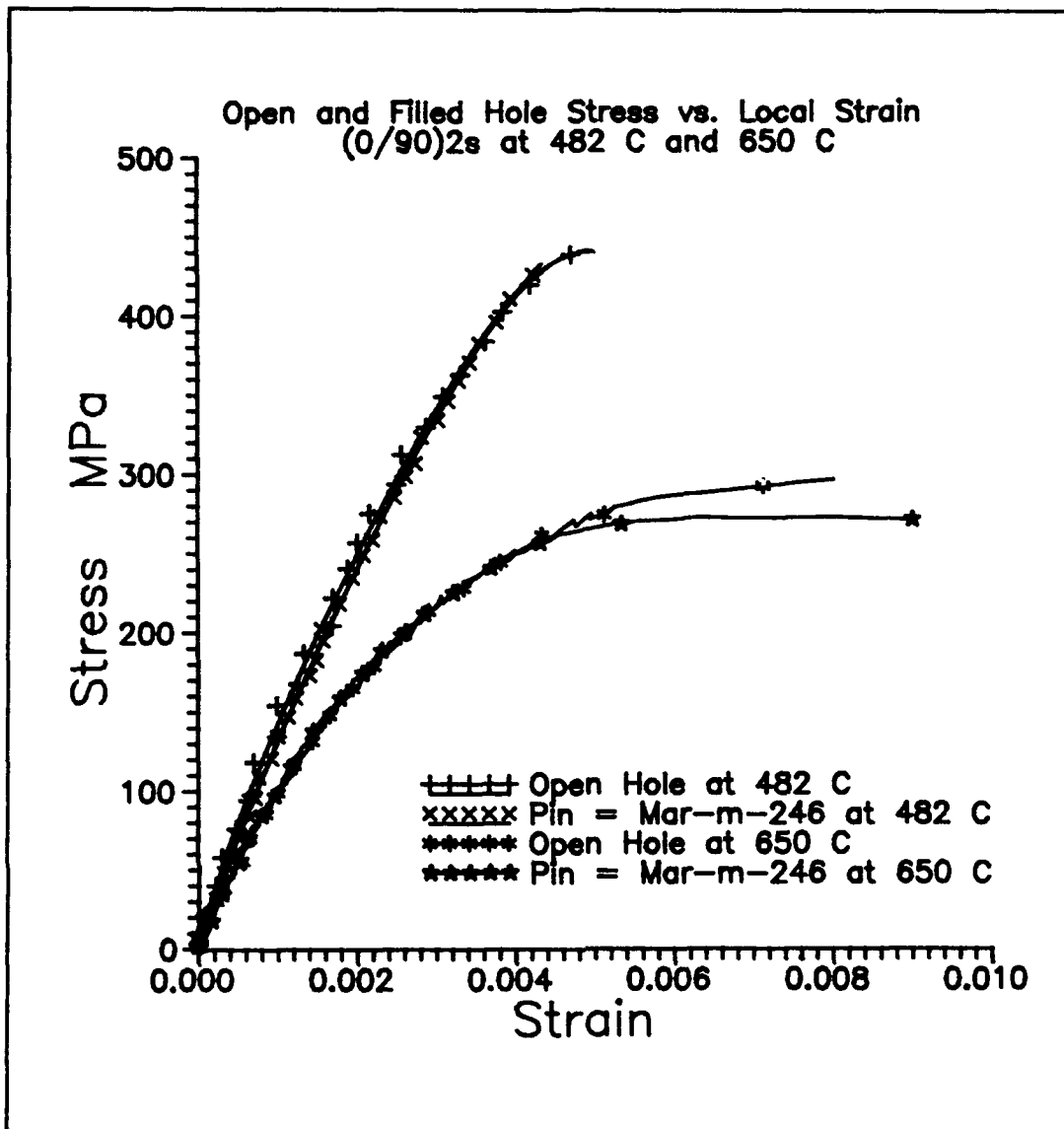
Figure 61 Open and Filled Hole Stress vs. Local Strain for [0/90]$_{2s}$ at 482°C and 650°C

linear regions. In the second linear region the constituents

still behave elastically with damage in the form of off-axis

ply interfacial failures. Nonlinearity is evident in all

tensile tests, excessive in the local strain gauge data and in
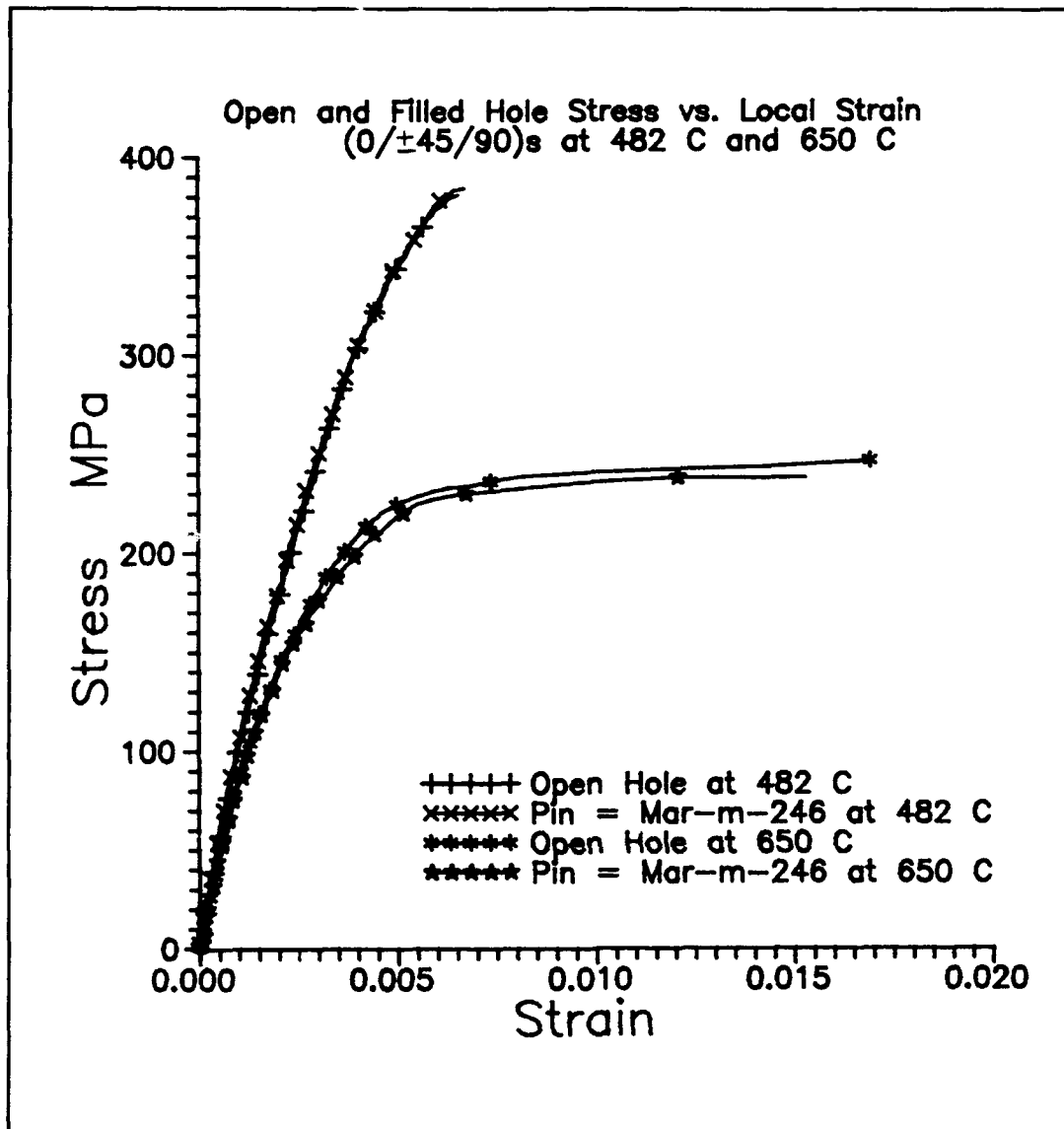
Figure 62 Open and Filled Hole Stress vs. Local Strain for $[0/\pm45/90]_s$ at 482°C and 650°C

the 650°C local extensometer data, and is caused by debonding and failure of the 0 degree plies in conjunction with plasticity in the matrix material. There exists a stress concentration factor at room temperature and the laminates are

125

notch sensitive. All fracture surfaces exhibited ductile failure due to tensile overload. The 650°C specimens exhibited matrix cracking near the fracture surface while room temperature and 482°C specimens were void of this phenomena.

Conclusions and Recommendations

The purpose of this study was to characterize the tensile behavior of metal matrix composite SCS-9/ß21s with open and filled holes of laminate orientations $[0/90]_{2s}$ and $[0/\pm45/90]_{s}$. In order for this to be accomplished, unnotched tensile behavior also had to be investigated. Static tensile testing was completed for $[16]_{16}$ and $[\pm45]_{2s}$ laminates in order to obtain necessary material properties for a thorough analysis. Testing was completed at three temperature regimes: room temperature, $482^{\circ}C$, and $650^{\circ}C$.

Conclusions

1. A characteristic bi-linear stress-strain curve, in both notched and unnotched tensile testing at all temperature regimes, results from the release of residual stresses and failure of off-axis plies, not from micro-plasticity

2. Final laminate response is governed by nonlinear behavior caused by debonding and failure of the 0 degree plies in conjunction with plasticity in the matrix material.

3. All fracture surfaces exhibited ductile fracture due to tensile overload. Failure surfaces of the $650^{\circ}C$ tensile specimens exhibited matrix cracking while the room temperature and $482^{\circ}C$ specimens were void of this matrix cracking. Through acetate replicating techniques, it was shown that the laminates were free from the development of matrix cracks up to 85 percent of the failure strength. Therefore, these matrix cracks in the $650^{\circ}C$ tensile testing occurred after 85

127

percent of failure load.

4. Unnotched laminate strength predictions were completed at all temperature regimes using a limited discount method in conjunction with Tsai-Hill and Maximum Stress Failure Theory. The strength predictions were within ten percent of experimental data except for the quasi-isotropic prediction at 650°C which was about twenty percent low.

5. Both $[0/90]_{2s}$ and $[0/\pm 45/90]_s$ laminates are notch sensitive at room temperature, mildly notch sensitive at 482°C, and completely insensitive to the existence of a hole at 650°C.

6. Elastic and plastic stress concentration factors were calculated and applied in a strength prediction attempt for notched laminates. The predicted values were invariably low due to modeling the off-axis plies as elastic to failure without damage incorporated.

7. The local stiffness of the cross-ply laminate was increased by approximately fifteen percent by inserting a pin into the open hole at room temperature. The pin had no effect on the failure strength of $[0/90]_{2s}$ at room temperature. The $[0/\pm 45/90]_s$ laminate experienced a small increase in strength at room temperature by inserting a pin into the open hole, approximately four percent employing the 7075-T6 pin and 8 percent employing the Mar-m-246 pin. Pins had no effect on the stiffness of the notched $[0/\pm 45/90]_s$ laminate at room temperature. The insertion of the pin has no effect on the stiffness or the strength of either laminate at elevated

temperatures.

Recommendations

1. Metal matrix composite SCS-9/ß21s, of orientations $[0/90]_{2s}$ and $[0/\pm45/90]_s$, needs to be characterized with open and filled holes subject to static compressive loads.

2. Bearing testing of SCS-9/ß21s under tensile and compressive static loads has not been completed to date.

3. Open hole tensile tests of 0 degree SCS-9/ß21s specimens should be completed as a final check on the shear lag model used to evaluate the plastic stress concentration factors.

Bibliography

1. Weeton, John W. <u>Engineers' Guide to Composite Materials.</u> Ohio: Carnes Publication Services, Inc., 1988.

2. Mittnick, M. A. and McElman, J. "Continuous Silicon Carbide Fiber Reinforced Metal Matrix Composites," Proceedings of 3rd Technical Conference on Composite Materials at Seattle, WA, 395-403 26-29 September, 1988.

3. Griffith, A. A. "The Phenomena of Rupture Flow in Solids," Phil. Trans. Royal Society of London, 163-197 1921.

4. Castelli, Mike and Lerch, Brad. "Preliminary Heat Treatment Study of Ti-ß21-S." NASA Lewis Research Center report to the Materials Laboratory, Wright Patterson Air Force Base, Dayton, Ohio 45433, May 1991.

5. Newaz, G. M. and Majumdar, B. S. "Deformation and Failure Mechanisms in Metal Matrix Composites," Battelle Memorial Institute, Columbus, OH. Presented at ASME Winter Annual Meeting, Atlanta, GA, December 1991.

6. Park, H. S., Zong, G. S., Brown, L. D., Rabenberg, L., and Marcus, H. L. "Fiber-Matrix Interface Failures," <u>Metal Matrix Composites: Testing, Analysis, and Failure Modes</u>. ASTM STP 1032, Johnson, W. S. Ed., American Society for Testing and Materials, Philadelphia, 270-279 1989.

7. Santhosh, U., Ahmad, J. and Nagar, A. "Non-linear Micromechanics Analysis Prediction of the Behavior of Titanium-Alloy Matrix Composites," To be Presented at ASME Winter Annual Meeting, Anaheim, Ca, December 1992.

8. Bakuckas, J. G., Johnson, W. S., and Bigelow, C. A. "Fatigue Damage in Cross-Ply Titanium Metal Matrix Composites Containing Center Holes," NASA Langley Research Center, Hampton, VA 23665. Presented at ASME Winter Annual Meeting, Atlanta, GA, December 1991.

9. Jones, Robert M. <u>Mechanics of Composite Materials</u>, New York, Hemisphere Publishing Corporation, 1975.

10. Hopkins, D. A., and Chamis, C. C., "A Unique Set of Micromechanics Equations for High Temperature Metal Matrix Composites," <u>Testing Technology of Metal Matrix Composites</u>, ASTM STP 964, P.R. DiGiovanni and N.R. Adsit, Eds., American Society for Testing and Materials,

Philadelphia, 1988.

11.   ----- and Murthy, P. L., Users Guide for Metal Matrix
       Composite Analyzer, NASA Lewis Research Center,
       Cleveland, OH 44135 Version 3.0 Prepared December 1991.

12.   Gayda, J. and Gabb, T. P. "Effect of Heating Mode and
       Specimen Geometry on Fatigue Properties of a Metal Matrix
       Composite," NASA Lewis Research Center, Cleveland, OH,
       Unpublished.

13.   Pindera, M-J, "Shear Testing of Fiber Reinforced Metal
       Matrix Composites," Metal Matrix Composites: Testing,
       Analysis, and Failure Modes, ASTM STP 1032, W.S. Johnson,
       Ed., American Society for Testing and Materials,
       Philadelphia, 19-42 1989.

14.   Lerch, B. A. and Saltsman, J. F. "Tensile Deformation of
       SiC/Ti-15-3 Laminates," NASA Lewis Research Center,
       Cleveland, OH 44135. Presented at ASTM Symposium on
       Composite Materials, Indianapolis, IN, May 1991.

15.   Newaz, G. M. and Majumdar, B. S. "Inelastic Deformation
       of Metal Matrix Composites: Plasticity and Damage
       Mechanisms," Battelle Memorial Institute, Columbus, OH.
       Submitted to Philosophical Magazine, June, 1991.

16.   Johnson, W. S. "Fatigue Testing and Damage Development
       in Continuous Fiber Reinforced Metal Matrix Composites,"
       NASA TM-100628, June, 1988.

17.   ----- and Pollock, W. D. "Characterization of Unnotched
       SCS-6/Ti-15-3 Metal Matrix Composites at 650°C," NASA TM-
       102699, September, 1990.

18.   -----, Bakuckas, J. G., and Bigelow, C. A. "Fatigue
       Damage in Cross-Ply Titanium Metal Matrix Composites
       Containing Center Holes," NASA Langley Research Center,
       Hampton, VA 23665. Presented at ASME Winter Annual
       Meeting, Atlanta, GA, December 1991.

19.   -----, and Naik, R. A. "Observations of Fatigue Crack
       Initiation and Damage Growth in Notched Titanium Matrix
       Composites," Proceedings of the Third Symposium on
       Composite Materials: Fatigue and Fracture. November 1989.

20.   Rattray, Captain Jeff. Tensile Characterization of a
       Metal Matrix Composite with Circular Holes. MS Thesis,
       AFIT/GAE/ENY/91D-24. School of Engineering, Air Force
       Institute of Technology, Wright-Patterson AFB OH,
       December, 1990.

21. Harmon, D. M., Saff, C. R., and Graves, D. L. "Strength Predictions for Metal Matrix Composites," Metal Matrix Composites: Testing, Analysis, and Failure Modes, ASTM STP 1032, W.S. Johnson, Ed., American Society for Testing and Materials, Philadelphia, 222-236 1989.

22. Lekhnitskii, S. G. Anisotropic Plates. Translated from the Second Russian Edition by Tsai, S. W. and Cheron, T. New York: Gordon and Breach, Science Published Inc., 1968.

23. Newaz, G. M. and Majumdar, B. S. "Crack Initiation Around Holes in a Unidirectional MMC Under Fatigue Loading," Battelle Memorial Institute, Columbus, OH. Submitted to Engineering Fracture Mechanics, August 1991. (in press)

24. Lee, J. H. and Mall, S. "Experimental Investigation of Quasi-Isotropic Graphite/Epoxy Laminate with a Reinforced Hole," Proceedings of 3rd Technical Conference on Composite Materials 384-391, Seattle, WA, September, 1988.

25. Grant, Bill. "Development of a 3-Mil Silicon Carbide Fiber For Titanium Matrix Composites." Electronic Message. Textron Specialty Materials, Lowell, MA 01851 April 1992.

26. Grant, Bill. Manufacturing Process, ß21s Preliminary Properties, Textron SCS-9/ß21s Panel Fabrication. Electronic Messages. Textron Specialty Materials, Lowell, MA, 01851 May 1992.

27. Larson, J. M. and Russ, S. M. Director and Assistant Director of the NIC Steering Committee, Machining and Heat Treatment Guidelines for NIC ß21s Composite Specimens. Wright Laboratory, Wright-Patterson Air Force Base, Dayton, OH 45433 (Meeting Summary) September 25, 1991.

28. McDonnell Douglas Corporation and United States Air Force "Consortium Testing Specifications (CTS) Materials & Structures Augmentation Program," (unpublished) Government Guidelines available through Wright Laboratory, Wright-Patterson Air Force Base, Dayton, OH 45433.

29. Ahmad, Jalees. "ß21s Material Characterization Data," AdTech Systems Research, Inc. Presented to the NIC Steering Committee. Wright Laboratory, Wright-Patterson Air Force Base, Dayton, OH 45433 (unpublished) January, 28-29, 1992.

30. Bearden, Keith. and Mall S. <u>Behavior of a Titanium Matrix Composite Under Quasi-Static Tensile and Compressive Loading</u>. MS Thesis, AFIT/GAE/ENY/92D- . School of Engineering, Air Force Institute of Technology, Wright-Patterson AFB OH, December, 1990.

APPENDIX A

Laminate properties of [0/90]2s SCS-9/Beta21-S

$Ef := 324.054 \cdot 10^9$ Pa

$Em := 111.6 \cdot 10^9$ Pa

$Vf := .385$

$Vm := .615$

Using the rule of mixtures

$E1 := Ef \cdot Vf + Em \cdot Vm$

$E1 = 1.934 \cdot 10^{11}$ Pa

Using Halpin-Tsai Equations

$Xi := 2$

$$Eta := \frac{\left[\dfrac{Ef}{Em}\right] - 1}{\left[\dfrac{Ef}{Em}\right] + Xi} \qquad Eta = 0.388$$

$$E2 := Em \cdot \left[\frac{1 + Xi \cdot Eta \cdot Vf}{1 - Eta \cdot Vf}\right] \qquad E2 = 1.704 \cdot 10^{11} \quad Pa$$

Comparing E2 with values obtained from McDonnel Douglas testing of [90]4 proves that Halpin Tsai predictions are much too high. Therefore an experimental value for E2 will be implemented

$E2 := 1.16981 \cdot 10^{11}$ Pa

Poissons Ratio based on bulk SiC and C core

$nuef := .26$

The matrix is considered isotropic and poisson's ratio will be assumed to be that of Ti-15-3

$nuem := .3$

$nue12 := nuef \cdot Vf + nuem \cdot Vm$

$nue12 = 0.285$

134

$$gm := \frac{Em}{2 + 2 \cdot nuem}$$

$$gm = 4.292 \cdot 10^{10} \quad Pa$$

Information for the S**3 company for the Shear Modulus of SCS-9

$$gf := 137.9 \cdot 10^{9} \quad Pa$$

Therefore G12 can now be calculated by Halpin-Tsai Equation

$$Xi2 := 1$$

$$Eta2 := \frac{\left[\dfrac{gf}{gm}\right] - 1}{\left[\dfrac{gf}{gm}\right] + Xi2}$$

$$Eta2 = 0.525$$

$$g12 := gm \cdot \left[\frac{1 + Xi2 \cdot Eta2 \cdot Vf}{1 - Eta2 \cdot Vf}\right]$$

$$g12 = 6.468 \cdot 10^{10} \quad Pa$$

Halpin Tsai also over-estimates the value for g12. Therefore the following experimental value for g12 will be used

$$g12 := 3.75 \cdot 10^{10}$$

Calculate the S matrix

$$S := \begin{bmatrix} \dfrac{1}{E1} & \dfrac{-nue12}{E1} & 0 \\ \dfrac{-nue12}{E1} & \dfrac{1}{E2} & 0 \\ 0 & 0 & \dfrac{1}{g12} \end{bmatrix}$$

$$S = \begin{bmatrix} 5.171 \cdot 10^{-12} & -1.472 \cdot 10^{-12} & 0 \\ -1.472 \cdot 10^{-12} & 8.548 \cdot 10^{-12} & 0 \\ 0 & 0 & 2.667 \cdot 10^{-11} \end{bmatrix}$$

135

Calculate the Q matrix, the inverse of S

$$Q := S^{-1}$$

$$Q = \begin{bmatrix} 2.034 \cdot 10^{11} & 3.501 \cdot 10^{10} & 0 \\ 3.501 \cdot 10^{10} & 1.23 \cdot 10^{11} & 0 \\ 0 & 0 & 3.75 \cdot 10^{10} \end{bmatrix}$$

Calculate the transformation matrix for the 90 ply

$$\theta := \frac{\pi}{2}$$

$$T(\theta) := \begin{bmatrix} \cos(\theta)^2 & \sin(\theta)^2 & 2 \cdot \sin(\theta) \cdot \cos(\theta) \\ \sin(\theta)^2 & \cos(\theta)^2 & -2 \cdot \sin(\theta) \cdot \cos(\theta) \\ -\sin(\theta) \cdot \cos(\theta) & \sin(\theta) \cdot \cos(\theta) & \cos(\theta)^2 - \sin(\theta)^2 \end{bmatrix}$$

Calculate Qbar for 0 amd 90 ply

$$Qbar0 := Q$$

$$Qbar90 := T(\theta)^{-1} \cdot Q \cdot \left[T(\theta)^{T^{-1}} \right]$$

$$Qbar90 = \begin{bmatrix} 1.23 \cdot 10^{11} & 3.501 \cdot 10^{10} & -7.963 \cdot 10^{-7} \\ 3.501 \cdot 10^{10} & 2.034 \cdot 10^{11} & 5.718 \cdot 10^{-6} \\ -7.963 \cdot 10^{-7} & 5.718 \cdot 10^{-6} & 3.75 \cdot 10^{10} \end{bmatrix}$$

Q16, Q26, are in reality equal to zero

Calculate values for distnaces z1 through z8

$$thickness := .0009525 \quad m$$

$$z0 := \frac{-thickness}{2} \qquad z0 = -4.763 \cdot 10^{-4}$$

$$z1 := z0 + \frac{thickness}{8} \qquad z1 = -3.572 \cdot 10^{-4}$$

136

$$z2 := z1 + \frac{\text{thickness}}{8} \qquad z2 = -2.381 \cdot 10^{-4}$$

$$z3 := z2 + \frac{\text{thickness}}{8} \qquad z3 = -1.191 \cdot 10^{-4}$$

$$z4 := z3 + \frac{\text{thickness}}{8} \qquad z4 = 0$$

$$z5 := z4 + \frac{\text{thickness}}{8} \qquad z5 = 1.191 \cdot 10^{-4}$$

$$z6 := z5 + \frac{\text{thickness}}{8} \qquad z6 = 2.381 \cdot 10^{-4}$$

$$z7 := z6 + \frac{\text{thickness}}{8} \qquad z7 = 3.572 \cdot 10^{-4}$$

$$z8 := z7 + \frac{\text{thickness}}{8} \qquad z8 = 4.763 \cdot 10^{-4}$$

Calculate values for matrix A

$$A := (z8 - z7) \cdot (4 \cdot Qbar0 + 4 \cdot Qbar90)$$

$$A = \begin{bmatrix} 1.554 \cdot 10^{8} & 3.335 \cdot 10^{7} & -3.792 \cdot 10^{-10} \\ 3.335 \cdot 10^{7} & 1.554 \cdot 10^{8} & 2.723 \cdot 10^{-9} \\ -3.792 \cdot 10^{-10} & 2.723 \cdot 10^{-9} & 3.572 \cdot 10^{7} \end{bmatrix} \qquad \text{Pa-m}$$

Actually A16 and A26 are zero

The inverse of A is necesary

$$AI := A^{-1}$$

$$AI = \begin{bmatrix} 6.744 \cdot 10^{-9} & -1.447 \cdot 10^{-9} & 0 \\ -1.447 \cdot 10^{-9} & 6.744 \cdot 10^{-9} & 0 \\ 0 & 0 & 2.8 \cdot 10^{-8} \end{bmatrix}$$

The force and moment vector

$$NM := \begin{bmatrix} 150 \cdot 10^6 \cdot thickness \\ 0 \\ 0 \end{bmatrix} \qquad NM = \begin{bmatrix} 1.429 \cdot 10^5 \\ 0 \\ 0 \end{bmatrix}$$

The resultant strains for this particular force/unit width

$$\epsilon := AI \cdot NM$$

$$\epsilon = \begin{bmatrix} 9.636 \cdot 10^{-4} \\ -2.067 \cdot 10^{-4} \\ 0 \end{bmatrix}$$

Youngs modulus in the load direction

$$Ex := \frac{NM_0}{\epsilon_0 \cdot thickness} \qquad Ex = 1.557 \cdot 10^{11}$$

Poisson's Ratio

$$nuexy := \frac{-\epsilon_1}{\epsilon_0} \qquad nuexy = 0.215$$

Modulus in the transverse direction

$$NM := \begin{bmatrix} 0 \\ 150 \cdot 10^6 \cdot thickness \\ 0 \end{bmatrix} \qquad NM = \begin{bmatrix} 0 \\ 1.429 \cdot 10^5 \\ 0 \end{bmatrix}$$

$$\epsilon := AI \cdot NM$$

$$\epsilon = \begin{bmatrix} -2.067 \cdot 10^{-4} \\ 9.636 \cdot 10^{-4} \\ 0 \end{bmatrix}$$

$$Ey := \frac{NM_1}{\epsilon_1 \cdot thickness} \qquad Ey = 1.557 \cdot 10^{11}$$

As expected

138

Shear Modulus

$$NM := \begin{bmatrix} 0 \\ 0 \\ 150 \cdot 10^6 \cdot thickness \end{bmatrix} \qquad NM = \begin{bmatrix} 0 \\ 0 \\ 1.429 \cdot 10^5 \end{bmatrix}$$

$$\epsilon := AI \cdot NM$$

$$\epsilon = \begin{bmatrix} 0 \\ 0 \\ 0.004 \end{bmatrix}$$

$$Gxy := \frac{NM_2}{\epsilon_2 \cdot thickness}$$

$$Gxy = 3.75 \cdot 10^{10}$$

Laminate properties of [0, 45,90]s SCS-9/beta21-S

$Ef := 324.054 \cdot 10^9$ Pa

$Em := 111.6 \cdot 10^9$ Pa

$Vf := .385$

$Vm := .615$

The following is an attempt to model the laminate with the 90
degree, and/or 45 degree fibers bonded and debonded. For bonded
laminae simply use the appropriate Qbar matrices; for debonded
laminae Qbar**d should be implemented. Properties Ef, Gf, and nuef
will all be set to zero for the debonded lamina. In the following
analysis the following nomenclature will apply:

E1: modulus in fiber direction for the 0 degree laminae
E2: modulus transverse to fiber direction
g12: shear modulus
nue12: Poisson's ratio
E1d: modulus in fiber direction for debonded laminae
E2d: modulus in transverse direction for debonded laminae
nue12d: Poisson's ratio of debonded laminae
g12d: shear modulus of debonded laminae
f: fiber
m: matrix

Using the rule of mixtures for bonded laminae
$E1 := Ef \cdot Vf + Em \cdot Vm$

$E1 = 1.934 \cdot 10^{11}$ Pa

Using Halpin-Tsai Equations

$Xi := 2$

$$Eta := \frac{\left[\dfrac{Ef}{Em}\right] - 1}{\left[\dfrac{Ef}{Em}\right] + Xi} \qquad Eta = 0.388$$

$$E2 := Em \cdot \left[\frac{1 + Xi \cdot Eta \cdot Vf}{1 - Eta \cdot Vf}\right] \qquad E2 = 1.704 \cdot 10^{11} \text{ Pa}$$

140

Comparing E2 with values obtained from McDonnel Douglas
testing of [90]4 proves Halpin Tsai predictions are much
too high. Therefore experimental values for E2 will be
implemented

$$E2 := 1.16981 \cdot 10^{11} \quad Pa$$

Poissons Ratio based on bulk SiC and C core

nuef := .26

The matrix is considered isotropic and poisson's ratio will be
assumed to be that of Ti-15-3

nuem := .3

nue12 := nuef·Vf + nuem·Vm

nue12 = 0.285

$$gm := \frac{Em}{2 + 2 \cdot nuem} \qquad gm = 4.292 \cdot 10^{10} \quad Pa$$

Information for the S**3 company for the Shear Modulus of SCS-9

$$gf := 137.9 \cdot 10^{9} \quad Pa$$

Therefore G12 can now be calculated by Halpin-Tsai Equation

Xi2 := 1

$$Eta2 := \frac{\left[\dfrac{gf}{gm}\right] - 1}{\left[\dfrac{gf}{gm}\right] + Xi2} \qquad Eta2 = 0.525$$

$$g12 := gm \cdot \left[\frac{1 + Xi2 \cdot Eta2 \cdot Vf}{1 - Eta2 \cdot Vf}\right] \qquad g12 = 6.468 \cdot 10^{10} \quad Pa$$

Halpin Tsai also grossly over-estimates an appropriate value for g12
Use experimental value would be

$$g12 := 3.75 \cdot 10^{10}$$

141

Calculate the S matrix

$$S := \begin{bmatrix} \dfrac{1}{E1} & \dfrac{-nue12}{E1} & 0 \\ \dfrac{-nue12}{E1} & \dfrac{1}{E2} & 0 \\ 0 & 0 & \dfrac{1}{g12} \end{bmatrix}$$

m**2/N

$$S = \begin{bmatrix} 5.171 \cdot 10^{-12} & -1.472 \cdot 10^{-12} & 0 \\ -1.472 \cdot 10^{-12} & 8.548 \cdot 10^{-12} & 0 \\ 0 & 0 & 2.667 \cdot 10^{-11} \end{bmatrix}$$

Calculate the Q matrix, the inverse of S

$$Q := S^{-1}$$

$$Q = \begin{bmatrix} 2.034 \cdot 10^{11} & 3.501 \cdot 10^{10} & 0 \\ 3.501 \cdot 10^{10} & 1.23 \cdot 10^{11} & 0 \\ 0 & 0 & 3.75 \cdot 10^{10} \end{bmatrix}$$

Now for debonded laminae properties

$E1d := Em \cdot Vm + 0 \cdot Vf$

$E1d = 6.863 \cdot 10^{10}$ Pa

$Etad := -.5$

$E2d := Em \cdot \dfrac{1 + Xi \cdot Etad \cdot Vf}{1 - Etad \cdot Vf}$

$E2d = 5.755 \cdot 10^{10}$ Pa

$nue12d := 0 \cdot Vf + nuem \cdot Vm$

$nue12d = 0.185$

142

Eta2d := -.5

$$g12d := gm \cdot \frac{1 + Xi2 \cdot Eta2d \cdot Vf}{1 - Eta2d \cdot Vf} \qquad g12d = 2.907 \cdot 10^{10} \qquad Pa$$

Halpin Tsai proved inadequate for bonded properties therefore the above values will be assumed incorrect. Instead the following debonded formulations will be used

E2d := .615· Em

$$E2d = 6.863 \cdot 10^{10}$$

g12d := .615· gm

$$g12d = 2.64 \cdot 10^{10}$$

Calculate the S matrix for the debonded laminae

$$Sd := \begin{bmatrix} \dfrac{1}{E1d} & \dfrac{-nue12d}{E1d} & 0 \\ \dfrac{-nue12d}{E1d} & \dfrac{1}{E2d} & 0 \\ 0 & 0 & \dfrac{1}{g12d} \end{bmatrix}$$

$$Sd = \begin{bmatrix} 1.457 \cdot 10^{-11} & -2.688 \cdot 10^{-12} & 0 \\ -2.688 \cdot 10^{-12} & 1.457 \cdot 10^{-11} & 0 \\ 0 & 0 & 3.788 \cdot 10^{-11} \end{bmatrix}$$

$$Qd := Sd^{-1}$$

$$Qd = \begin{bmatrix} 7.105 \cdot 10^{10} & 1.311 \cdot 10^{10} & 0 \\ 1.311 \cdot 10^{10} & 7.105 \cdot 10^{10} & 0 \\ 0 & 0 & 2.64 \cdot 10^{10} \end{bmatrix}$$

143

Calculate the transformation matrix for the 90 and 45 degree laminae

$$T(\theta) := \begin{bmatrix} \cos(\theta)^2 & \sin(\theta)^2 & 2\cdot\sin(\theta)\cdot\cos(\theta) \\ \sin(\theta)^2 & \cos(\theta)^2 & -2\cdot\sin(\theta)\cdot\cos(\theta) \\ -\sin(\theta)\cdot\cos(\theta) & \sin(\theta)\cdot\cos(\theta) & \cos(\theta)^2 - \sin(\theta)^2 \end{bmatrix}$$

Calculate Qbar for 0, 90, and debonded 90 laminae

Qbar0 := Q

$$\theta := \frac{\pi}{2}$$

$$Qbar90 := T(\theta)^{-1}\cdot Q\cdot\left[T(\theta)^{T^{-1}}\right]$$

$$Qbar90d := T(\theta)^{-1}\cdot Qd\cdot\left[T(\theta)^{T^{-1}}\right]$$

$$Qbar90 = \begin{bmatrix} 1.23\cdot10^{11} & 3.501\cdot10^{10} & -7.963\cdot10^{-7} \\ 3.501\cdot10^{10} & 2.034\cdot10^{11} & 5.718\cdot10^{-6} \\ -7.963\cdot10^{-7} & 5.718\cdot10^{-6} & 3.75\cdot10^{10} \end{bmatrix}$$

Q16, Q26, are in reality equal to zero

$$Qbar90d = \begin{bmatrix} 7.105\cdot10^{10} & 1.311\cdot10^{10} & -3.154\cdot10^{-7} \\ 1.311\cdot10^{10} & 7.105\cdot10^{10} & 3.154\cdot10^{-7} \\ -3.154\cdot10^{-7} & 3.154\cdot10^{-7} & 2.64\cdot10^{10} \end{bmatrix}$$

$$\theta := \frac{\pi}{4}$$

$$Qbar45 := T(\theta)^{-1}\cdot Q\cdot\left[T(\theta)^{T^{-1}}\right]$$

144

$$\text{Qbar45} = \begin{bmatrix} 1.366 \cdot 10^{11} & 6.16 \cdot 10^{10} & 2.009 \cdot 10^{10} \\ 6.16 \cdot 10^{10} & 1.366 \cdot 10^{11} & 2.009 \cdot 10^{10} \\ 2.009 \cdot 10^{10} & 2.009 \cdot 10^{10} & 6.409 \cdot 10^{10} \end{bmatrix}$$

$$\theta := \frac{-\pi}{4}$$

$$\text{Qbarn45} := T(\theta)^{-1} \cdot Q \cdot \left[T(\theta)^T{}^{-1} \right]$$

$$\text{Qbarn45} = \begin{bmatrix} 1.366 \cdot 10^{11} & 6.16 \cdot 10^{10} & -2.009 \cdot 10^{10} \\ 6.16 \cdot 10^{10} & 1.366 \cdot 10^{11} & -2.009 \cdot 10^{10} \\ -2.009 \cdot 10^{10} & -2.009 \cdot 10^{10} & 6.409 \cdot 10^{10} \end{bmatrix}$$

$$\theta := \frac{\pi}{4}$$

$$\text{Qbar45d} := T(\theta)^{-1} \cdot Qd \cdot \left[T(\theta)^T{}^{-1} \right]$$

$$\text{Qbar45d} = \begin{bmatrix} 6.848 \cdot 10^{10} & 1.568 \cdot 10^{10} & -2.047 \cdot 10^{-6} \\ 1.568 \cdot 10^{10} & 6.848 \cdot 10^{10} & -1.768 \cdot 10^{-6} \\ 3.675 \cdot 10^{-6} & 1.394 \cdot 10^{-7} & 2.897 \cdot 10^{10} \end{bmatrix}$$

$$\theta := \frac{-\pi}{4}$$

$$\text{Qbarn45d} := T(\theta)^{-1} \cdot Qd \cdot \left[T(\theta)^T{}^{-1} \right]$$

$$\text{Qbarn45d} = \begin{bmatrix} 6.848 \cdot 10^{10} & 1.568 \cdot 10^{10} & 2.047 \cdot 10^{-6} \\ 1.568 \cdot 10^{10} & 6.848 \cdot 10^{10} & 1.768 \cdot 10^{-6} \\ -3.675 \cdot 10^{-6} & -1.394 \cdot 10^{-7} & 2.897 \cdot 10^{10} \end{bmatrix}$$

145

Calculate values for distances z1 through z8

$$\text{thickness} := .0009525 \ m$$

$$z0 := \frac{-\text{thickness}}{2}$$
$$z0 = -4.763 \cdot 10^{-4} \quad m$$

$$z1 := z0 + \frac{\text{thickness}}{8}$$
$$z1 = -3.572 \cdot 10^{-4} \quad m$$

$$z2 := z1 + \frac{\text{thickness}}{8}$$
$$z2 = -2.381 \cdot 10^{-4} \quad m$$

$$z3 := z2 + \frac{\text{thickness}}{8}$$
$$z3 = -1.191 \cdot 10^{-4} \quad m$$

$$z4 := z3 + \frac{\text{thickness}}{8}$$
$$z4 = 0 \quad m$$

$$z5 := z4 + \frac{\text{thickness}}{8}$$
$$z5 = 1.191 \cdot 10^{-4} \quad m$$

$$z6 := z5 + \frac{\text{thickness}}{8}$$
$$z6 = 2.381 \cdot 10^{-4} \quad m$$

$$z7 := z6 + \frac{\text{thickness}}{8}$$
$$z7 = 3.572 \cdot 10^{-4} \quad m$$

$$z8 := z7 + \frac{\text{thickness}}{8}$$
$$z8 = 4.763 \cdot 10^{-4} \quad m$$

Calculate values for matrix A

$$A := (z8 - z7) \cdot 2 \cdot (Qbar0 + Qbar90 + Qbar45 + Qbarn45)$$

$$A = \begin{bmatrix} 1.428 \cdot 10^{8} & 4.601 \cdot 10^{7} & 0 \\ 4.601 \cdot 10^{7} & 1.428 \cdot 10^{8} & 9.084 \cdot 10^{-10} \\ 0 & 9.084 \cdot 10^{-10} & 4.838 \cdot 10^{7} \end{bmatrix} \quad \text{Pa-m}$$

Actually A16 and A26 are zero

146

The inverse of A is necesary

$$AI := A^{-1}$$

$$
AI = \begin{bmatrix}
7.816 \cdot 10^{-9} & -2.519 \cdot 10^{-9} & 0 \\
-2.519 \cdot 10^{-9} & 7.816 \cdot 10^{-9} & 0 \\
0 & 0 & 2.067 \cdot 10^{-8}
\end{bmatrix}
$$

The force and moment vector

$$
NM := \begin{bmatrix}
150 \cdot 10^{6} \cdot \text{thickness} \\
0 \\
0
\end{bmatrix}
\qquad
NM = \begin{bmatrix}
1.429 \cdot 10^{5} \\
0 \\
0
\end{bmatrix}
$$

The resultant strains for this particular force/unit width

$$
\epsilon := AI \cdot NM
$$

$$
\epsilon = \begin{bmatrix}
0.001 \\
-3.599 \cdot 10^{-4} \\
0
\end{bmatrix}
$$

Youngs modulus in the load direction

$$
Ex := \frac{NM_0}{\text{thickness} \cdot \epsilon_0}
\qquad\qquad
Ex = 1.343 \cdot 10^{11}
$$

$$
nuexy := \frac{-\epsilon_1}{\epsilon_0}
\qquad\qquad
nuexy = 0.322
$$

Youngs modulus in transverse direction

$$
NM := \begin{bmatrix}
0 \\
150 \cdot 10^{6} \cdot \text{thickness} \\
0
\end{bmatrix}
\qquad\qquad
NM = \begin{bmatrix}
0 \\
1.429 \cdot 10^{5} \\
0
\end{bmatrix}
$$

147

$$\epsilon := AI \cdot NM$$

$$Ey := \frac{NM_1}{thickness \cdot \epsilon_1} \qquad Ey = 1.343 \cdot 10^{11}$$

$$nueyx := \frac{-\epsilon_0}{\epsilon_1} \qquad nueyx = 0.322$$

Shear Modulus

$$NM := \begin{bmatrix} 0 \\ 0 \\ 150 \cdot 10^6 \cdot thickness \end{bmatrix} \qquad NM = \begin{bmatrix} 0 \\ 0 \\ 1.429 \cdot 10^5 \end{bmatrix}$$

$$\epsilon := AI \cdot NM$$

$$\epsilon = \begin{bmatrix} 0 \\ 0 \\ 0.003 \end{bmatrix}$$

$$Gxy := \frac{NM_2}{\epsilon_2 \cdot thickness} \qquad Gxy = 5.079 \cdot 10^{10}$$

PROGRAM STRESS
     This Program perform the following functions for analysis
of unidirectionally loaded metal matrix composites
     1.Calculate stress concentration factors for a hole or
       ellipse accounting for material orthotropy and finite
       width.
     2.Calculate the shear stresses, tranverse stresses, and
       longitudinal stresses around the perifery of the hole
       as a function of theta from 0 to 90 degrees.
     3.Determine coefficients necessary to obtain a stress
       gradient at theta equal to 90 degrees.
The program will be throughly commented so potential users
will be aware of its strengths and limitations.

Jacob T. Roush
Air Force Institute of Technology
Wright Patterson Air Force Base
(513) 255-4616
```
       INTEGER I,J,L
       REAL f1,f2,f3,f4,f5,ft,fg,Et,Ex,Ey,Z,theta,Gxy,nuexy,Kto,Kt,a,b
      +w,r,Ktnet,beff,X,k1(90),PIE,K2(90),shear(90),C,C1,A1,B1
      +,bi,bj,bk,bl,k3,INC,CS,LONG(90),TRAN(90)
       CHARACTER*8 OUTPUT
C      ****************************************************************
C      Ex: composite stiffness in load direction
C      theta: angle taken positive from load direction where = zero
C      Ey: composite stiffness in transverse direction
C      Gxy: shear modulus
C      nuexy: Poisson's Ratio
C      f1,f2,f3,f4,f5: parameters used in elliptical analysis
C      ft: stress of the laminate tangent to the notch at the periphery
C         of the notch
C      fg: gross load
C      fnet: net load
C      Et: stiffness of the laminate tangent to the notch in the theta
C         direction
C      Z: a parameter used in analysis to be defined later
C      Kto: stress concentration factor at the top of a hole where
C           theta equals zero
C      Kt: stress concentration factor at theta equals 90 degrees
C      Ktnet: stress concentration factor using the net cross-sectional
C           area, ft/fnet
C      2a: major axis of ellipse
C      2b: minor axis of ellipse
C      w: width of laminate
C      r: radius of circle
C      beff: an effective dimension used to convert a circle into an
C           ellipse to account for material orthotropy
C      shear: shear stresses in the loading direction around a hole
C           or ellipse normalized for a unit applied stress
C      A1,B1,C1,C,bi,bj,bk,bl: Coefficients necessary to obtain stress
C                       gradient
C      ****************************************************************
       WRITE(*,*)' What is the output file name in apostrophes'
       READ(*,*)OUTPUT
       OPEN(UNIT=7,FILE=OUTPUT,STATUS='NEW')
       WRITE(*,*)' Enter Ex in Pa'
       READ(*,*)Ex
       WRITE(*,*)' Enter Ey in Pa'
       READ(*,*)Ey
```

```
      WRITE(*,*)' Enter nuexy'
      READ(*,*)nuexy
      WRITE(*,*)' Enter Gxy in Pa'
      READ(*,*)Gxy
      WRITE(7,1)
      FORMAT(/,X,'OUTPUT FOR STRENGTH.FOR')
      WRITE(7,2)
      FORMAT(/,X,'ECHO OF INPUT DATA')
      WRITE(7,3)Ex
      FORMAT(/,X,'Ex=',E9.4)
      WRITE(7,4)Ey
      FORMAT(X,'Ey=',E9.4)
      WRITE(7,5)Gxy
      FORMAT(X,'Gxy=',E9.4)
      WRITE(7,6)nuexy
      FORMAT(X,'nuexy=',F5.3)
      WRITE(7,7)
      FORMAT(/,6X,'This portion calculates the stress concentration
     + factor for an',/,X,' infinitely long and wide uniaxially loaded
     + laminate with a hole')
      This portion will calculate the stress concentration factor
      for an infinitely long and wide uniaxially loaded laminate
      with a hole for theta from 0 to 90 degrees.
      PIE=3.141592654
      Z=(Ex/Gxy-2.0*NUEXY+2*(Ex/EY)**.5)**.5
      Kto=-(Ey/Ex)**.5
      Kt=1.0+Z
      WRITE(7,*)'  THETA        Et              K1'
      DO 10 I=1,91
      J=I-1
      THETA=REAL(I-1.0)*PIE/180.0
      Et=1./(SIN(THETA)**4/Ex+(1.0/Gxy-2.0*nuexy/Ex)*SIN(THETA)**2*
     +COS(THETA)**2+COS(THETA)**4/Ey)
      K1(I)=Et/Ex*(.5*(1.+Z-(Ex/Ey)**.5)-.5*(1.+Z+(Ex/Ey)**.5)*COS(
     +2.*THETA))
      K2(I)=.5*(Et*Kt/Ex+Et*Kto/Ey)-.5*(Et*Kt/Ex-Et*Kto/Ey)*
     +COS(2.*THETA)
      WRITE(7,8)J,Et,K2(I)
      FORMAT(3X,I2,3X,E9.4,3X,F8.5)
      CONTINUE
      The following analysis is for a finite width plate with
      material orthotropy.
      WRITE(7,11)
      WRITE(*,11)
      FORMAT(/,6X,'"In metal matrix composites the fibers typically
     + have a higher',/,X,' stiffness than the matrix material. The
     + higher stifness fibers will',/,X,' increase the stress conc
     +entration at the edge of the hole when they ',/,X,' are orien
     +ted parallel to the fibers (0 degrees) in a notched specimen.'
     +,/,X,' Similarily the stress concentration in an isotropic
     + material can be',/,X,' increased by changing the circular hole
     + into an ellipse with',/,X,' its major axis perpendicular to
     + the loading.  In order to calculate',/,X,' the stress concent
     +rations in notched metal matrix composites, an',/,X,' effective
     + notch dimension beff is defined, which accounts for the',/,X,'
     + material orthotropy"',/,X,' "Strength Predictions for Metal
     + Matrix Composites", Harmon, Saff, and Graves',//)
      WRITE(*,*)'ENTER 0 FOR CIRCULAR OR 1 FOR ELLIPTICAL NOTCH'
      READ(*,*)L
      IF(L.EQ.1)THEN
      WRITE(*,*)' Enter dimension a in mm'
      READ(*,*)a
      WRITE(*,*)' Enter dimension b in mm'
```

150

```
      READ(*,*)b
      WRITE(*,*)' Enter dimension w in mm'
      READ(*,*)w
      WRITE(7,*)' '
      WRITE(7,*)' Elliptical notch chosen'
      WRITE(7,12)a
      WRITE(7,13)b
      WRITE(7,14)w
      FORMAT(2X,'a=',f9.4)
      FORMAT(2X,'b=',f9.4)
      FORMAT(2X,'w=',f12.4)
      f1=(1.+Z*a/b)/2.-1.
     ELSE
      WRITE(*,*)' Enter radius of circle in mm'
      READ(*,*)r
      WRITE(*,*)' Enter dimension w in mm'
      READ (*,*)w
      WRITE(7,15)r
      FORMAT(2X,'r=',f9.4)
      WRITE(7,16)w
      FORMAT(2X,'w=',f12.4)
      a=r
      e=.125*(Z/2.-1.)
      beff=2.*a/Z*(1-2*a/w)**e
      b=beff
      WRITE(7,*)' Elliptical dimensions used for inputed circle'
      WRITE(7,17)a
      WRITE(7,18)beff
      FORMAT(2X,'a=',f9.4)
      FORMAT(2X,'beff=',f9.4)
      f1=.5*(2.*a/beff-1.)
     ENDIF
      f2=1.-2.*a/w
      f3=a/b-1.
      f4=4.*a/w-1.
      f5=1.-(2.*a/w)**100
      Ktnet=2.+f1*f2**2+f1*f2**4+.643*f3*(1-f4**2)+
     +        .167*f3*(1-f4**4)+.109*f3*f5*2.*a/w
      Kt=Ktnet/(1-2*a/w)
      Kto=-((Ey/Ex)**.5+2.8/(w/2./a)**2)/(1.+.00865/(w/2./a-1.)**2.76)
      WRITE(7,19)Z
      WRITE(7,20)Kto
      WRITE(7,21)Ktnet
      WRITE(7,22)Kt
      FORMAT(2X,'Eta='f7.4)
      FORMAT(2X,'Kto=',F8.5)
      FORMAT(2X,'Ktnet=',F8.5)
      FORMAT(2X,'Kt=',F8.5)
      WRITE(7,111)
      FORMAT(2X,' Theta     Et         K     (SigXL/Gross) (SigYL/Gross)
     + (SigXYL/Gross)')
      WRITE(7,112)
      FORMAT(2X,'**********************************************************
     +*******************')
      DO 30 I=1,91
       J=I-1
       THETA=REAL(I-1.0)*PIE/180.0
       Et=1./(SIN(THETA)**4/Ex+(1.0/Gxy-2.0*nuexy/Ex)*SIN(THETA)**2*
     + COS(THETA)**2+COS(THETA)**4/Ey)
       K2(I)=.5*(Et*Kt/Ex+Et*Kto/Ey)-.5*(Et*Kt/Ex-Et*Kto/Ey)*
     + COS(2.*THETA)
       THE SHEAR, TRANSVERSE, AND LOGITUDIANL STRESSES AS A FUNCTION
       OF THETA AROUND THE PERIFERY OF THE HOLE FOR AN APPLIED UNIT
       GROSS STRESS
```

151

```
      SHEAR(I)=-.5*SIN(2.*THETA)*K2(I)
      LONG(I)=SIN(THETA)**2*K2(I)
      TRAN(I)=COS(THETA)**2*K2(I)
      WRITE(7,25)J,Et,K2(I),LONG(I),TRAN(I),SHEAR(I)
      FORMAT(3X,I2,3X,E9.4,3X,F8.5,3X,F8.5,5X,F8.5,6X,F8.5)
    CONTINUE

Calculation of constants necessary to obtain the stress gradient
C1=(.5+5./3.*(b/a)**.5)*(1.-2.*a/w)**.5
C=C1*Kt/(Kt-1.)
 bi=1.-Kt*(1.-2.*a/w)
 bj=2.*b**2/(a*w*(1-c))
 bk=(a*w/(2.*b**2)+1.-(a/b)**2)**(1-c)-1.
 bl=1.-2.*a/w
B1=bi/(bj*bk-bl)
A1=Kt-B1
WRITE(7,*)' '
WRITE(7,*)'    Stress gradient coefficients'
WRITE(7,31)C1
WRITE(7,32)C
WRITE(7,33)B1
WRITE(7,34)A1
FORMAT(3X,'C1=',F10.5)
FORMAT(3X,'C=',F10.5)
FORMAT(3X,'B=',F10.5)
FORMAT(3X,'A=',F10.5)
WRITE(*,*)' Would you like to find some values of Kt, the stress'
WRITE(*,*)' concentration at 90 degrees, with respect to x?'
WRITE(*,*)' If so enter 1, if not enter 0'
READ(*,*)I
IF(I.EQ.1)THEN
 WRITE(*,*)' Enter the number of equally spaced values of x at'
 WRITE(*,*)' which you would Kt calculated, depending upon what'
 WRITE(*,*)' resolution of the gradient you desire'
 READ(*,*)J
 WRITE(7,*)' '
 WRITE(7,*)'       x          x/a         Kt'
 aprime=a
 x=a
 cs=(w-2.*a)/2.
 INC=cs/REAL(J)
 WRITE(*,*)'J=',J
 WRITE(*,*)'INC=',INC
 roe=b**2/a
 xprime=x/aprime
 k3=A1+B1*(1.+(x-a)/roe)**-C
 write(7,37)x,xprime,k3
 format(x,f10.4,3x,f10.4,3x,f8.5)
 DO 40 N=1,J
  x=x+inc
  xprime=x/aprime
  k3=A1+B1*(1.+(x-a)/roe)**-C
  write(7,38)x,xprime,k3
  format(x,f10.4,3x,f10.4,3x,f8.5)
 CONTINUE
 ELSE
  GO TO 41
 ENDIF
X=A
END
```

Vita

Jacob T. Roush was born on 5 February 1967 in Buffalo, New York. He graduated from Hamburg High School in Hamburg, New York in 1985 and attended the State University of New York at Buffalo (UB), graduating with a Bachelor of Science in Aeronautical Engineering in May 1990. Upon graduation he accepted the position of Mechanical Estimator at the mechanical company Bosch Mechanical Inc. in Buffalo, New York. In September 1990 he was accepted into The Air Force Civilian Intern Program, Palace Acquire Internship. His first position was a part time student / part time staff at the School of Engineering, Air Force Institute of Technology, WPAFB.

Permanent Address: 842-D Edinboro Ct
Dayton, OH 45431

REPORT DOCUMENTATION PAGE

Public reporting burden for this collection of information is estimated to average 1 hour per response, including the time for reviewing instructions, searching existing data sources, gathering and maintaining the data needed, and completing and reviewing the collection of information. Send comments regarding this burden estimate or any other aspect of this collection of information, including suggestions for reducing this burden, to Washington Headquarters Services, Directorate for Information Operations and Reports, 1215 Jefferson Davis Highway, Suite 1204, Arlington, VA 22202-4302, and to the Office of Management and Budget, Paperwork Reduction Project (0704-0188), Washington, DC 20503

1. AGENCY USE ONLY (Leave blank)	2. REPORT DATE	3. REPORT TYPE AND DATES COVERED
	December 1992	Masters Thesis

4. TITLE AND SUBTITLE
Open and Filled Hole Static Tensile Strength Characterization of Metal Matrix Composite SCS-9/β21s

5. FUNDING NUMBERS

6. AUTHOR(S)

Jacob Thomas Roush, Palace Acquire Intern

7. PERFORMING ORGANIZATION NAME(S) AND ADDRESS(ES)

School of Engineering
Air Force Institute of Technology
WPAFB, OH 45433-6583

8. PERFORMING ORGANIZATION REPORT NUMBER

AFIT/GAE/ENY/92D-12

9. SPONSORING/MONITORING AGENCY NAME(S) AND ADDRESS(ES)

Materials Behavior Branch (MLLN)
Metals and Ceramics Division
Materials Directorate
Wright Laboratory
Wright-Patterson AFB, OH 45433-6583

10. SPONSORING/MONITORING AGENCY REPORT NUMBER

11. SUPPLEMENTARY NOTES

12a. DISTRIBUTION/AVAILABILITY STATEMENT

Approved for public release;
distribution unlimited

12b. DISTRIBUTION CODE

13. ABSTRACT (Maximum 200 words)

   SCS-9/β21s has a reduced gauge thickness, in comparison with other metal matrix composites, due to a smaller diameter fiber. This reduced gauge thickness makes it an attractive candidate for the skin of hypersonic vehicles. Tensile testing of $[0/90]_{2s}$ and $[0/\pm45/90]_s$ laminates was performed at room temperature, 482°C, and 650°C. Both notched and unnotched specimens were tested. Notched specimens, open and filled hole, had a width-to-diameter ratio of six. Materials 7075-T6 and Mar-m-246 were used as pins in the filled hole tensile testing. Analytical work was completed to predict material properties, elastic and plastic stress concentration factors, residual stresses, and failure strengths. Damage was documented in the form of fiber-matrix debonding, matrix cracking, fiber failure, and plasticity.

14. SUBJECT TERMS
SCS-9, β21s, Open Hole, Filled Hole, Metal Matrix Composite, Notch, Static Tensile

15. NUMBER OF PAGES
163

16. PRICE CODE

17. SECURITY CLASSIFICATION OF REPORT	18. SECURITY CLASSIFICATION OF THIS PAGE	19. SECURITY CLASSIFICATION OF ABSTRACT	20. LIMITATION OF ABSTRACT
Unclassified	Unclassified	Unclassified	